

# The Breaching of Temporary Open/Closed Estuaries

Michael Parkinson

Submitted in fulfilment of the academic requirements for the degree of  
Masters of Science in Engineering  
School of Civil Engineering, Surveying and Construction Management  
University of KwaZulu-Natal

March 27, 2007

## Abstract

Intermittent breaching of sand barriers at temporary open estuaries plays a key role in the functioning of these systems. Breaching events lead to large and rapid changes in the physico-chemical environment which in turn triggers major biological responses. The breaching process can cause significant morphological changes as strong breach outflows can scour large quantities of accumulated sediments from an estuary. Simple laboratory experiments are reported that investigate the temporal evolution of the breach and the scaling of the breach characteristics namely the breach width  $W$ , volume  $V_b$ , formation time  $T_F$  and peak outflow  $Q_P$ . The experiments were specifically designed to investigate the influence of the outflow volume  $S$ , the hydraulic head  $H$  and the barrier breadth  $B$  on the breach characteristics. The breach width  $W$  was found to be proportional to  $S^{1/3}$ , whilst the breach volume  $V_b$  was found to be proportional to  $HBS^{1/3}$ . The breach formation time  $T_F$  was found to be proportional to  $(g/S^{1/3})^{-1/2} (H/S^{1/3})^{-3/2} (B/S^{1/3})^1$  and the peak outflow  $Q_P$  was found to be proportional to  $(g S^{5/3})^{1/2} (H/S^{1/3})^{3/2} (B/S^{1/3})^{-1}$ . These scalings are also shown to be consistent with observed breach characteristics for actual estuaries and earth dam failures where outflow volumes are typically six orders of magnitude larger than for the models.

**Preface**

I, Michael Gerald Parkinson hereby declare that the whole of this dissertation is my own work and has not been submitted in part, or in whole to any other University. Where use has been made of the work of others, it has been duly acknowledged in the text. The research work was carried out in the Department of Civil Engineering, Surveying and Construction, University of KwaZulu-Natal, Howard College, Durban, under the supervision of Professor Derek Stretch.

Signature: .....

Date: .....

---

## ACKNOWLEDGEMENTS

---

- I would like to thank the Centre for Research in Environmental, Coastal, and Hydrological Engineering (CRECHE), the National Research Foundation (NRF) and the World Wildlife Fund (WWF) for without their funding this project would not have been possible.
- I would like to thank Prof. Derek Stretch and the Post Graduate team for without their guidance and support this project would never have been completed.
- I would also like to thank my family and friends for their continuous support.

---

# TABLE OF CONTENTS

---

<b>1</b>	<b>Introduction</b>	<b>2</b>
1.1	What is an estuary? . . . . .	2
1.2	Perched temporary open/closed estuaries . . . . .	2
1.3	Motivation for the study . . . . .	3
1.3.1	Management Strategies . . . . .	4
1.4	Aims . . . . .	5
1.5	Outline of the dissertation . . . . .	5
<b>2</b>	<b>Literature Review</b>	<b>7</b>
2.1	Perched temporary open estuaries . . . . .	7
2.1.1	Ecological functioning of Perched TOCE . . . . .	8
2.2	Formation of the sand barrier . . . . .	9
2.2.1	Mechanism 1: interaction between inlet current and the long shore sediment transport process . . . . .	9
2.2.2	Mechanism 2: interaction between inlet current and the cross-shore sediment transport . . . . .	10
2.2.3	Supratidal barriers . . . . .	11
2.3	Estuary breaching . . . . .	11
2.3.1	Breach mechanism 1: overtopping from the impound- ment . . . . .	11
2.3.2	Breach mechanism 2: seepage and liquefaction . . . . .	12
2.3.3	Artificial breaching . . . . .	12
2.3.4	Breaching of coastal barriers . . . . .	13
2.4	Dam breaks . . . . .	14
2.4.1	Previous investigations into dam breaks . . . . .	15
2.4.2	Breach parameters . . . . .	15
2.4.3	Breach width . . . . .	16
2.4.4	Breach formation time and peak outflow . . . . .	17
2.5	Existing models for perched TOCEs . . . . .	18
2.6	Previous model investigations . . . . .	19
2.7	Summary . . . . .	21

<b>3</b>	<b>Methodology</b>	<b>23</b>
3.1	Scaling analysis . . . . .	23
3.1.1	Breach width, $W$ and volume of sediment removed, $V_b$	24
3.1.2	Breach formation time, $T_F$ and peak outflow, $Q_P$ . . .	25
3.2	Pilot study . . . . .	26
3.3	Model investigation . . . . .	27
3.3.1	Experimental setup . . . . .	27
3.3.2	Data acquisition . . . . .	28
3.4	Summary of experimental procedure . . . . .	30
3.5	Data Processing . . . . .	30
<b>4</b>	<b>Results</b>	<b>36</b>
4.1	Observed breaching process . . . . .	36
4.2	Quantitative features of the breach process . . . . .	40
4.3	Scaling results from model data . . . . .	44
4.3.1	Breach widths . . . . .	44
4.3.2	Breach development with time . . . . .	46
4.3.3	Breach volumes . . . . .	47
4.3.4	Breach formation times and peak outflows . . . . .	50
4.4	Obtaining full scale data . . . . .	56
4.4.1	Estuary data: breach widths and volumes . . . . .	56
4.4.2	Estuary Data: breach formation times and peak outflows	56
4.4.3	Earth dam data . . . . .	57
4.5	Scaling results from full scale data . . . . .	58
4.5.1	Breach widths and volumes . . . . .	58
4.5.2	Breach formation times and peak outflows . . . . .	62
4.6	Discussion . . . . .	65
4.6.1	Breach widths and volumes . . . . .	65
4.6.2	The effects of floods . . . . .	67
4.6.3	Breach formation times and peak outflows . . . . .	67
4.6.4	Management implications . . . . .	69
<b>5</b>	<b>Conclusion</b>	<b>71</b>
<b>A</b>	<b>Experimental Data</b>	<b>77</b>
<b>B</b>	<b>Journal Articles</b>	<b>79</b>

---

## LIST OF FIGURES

---

1.1	Photos of the Mhlanga estuary (a) before a breaching of the mouth (b) after a breaching of the mouth. The difference in water level in the estuary before and after the breach is evident.	3
2.1	Photo of the Mhlanga estuary on the right and the adjacent ocean on the left. The difference in water levels, the closed mouth state, and the barrier breadth are evident. . . . .	8
2.2	(a) estuary inlet closure by mechanism 1 (b) estuary inlet closure by mechanism 2 (adapted from Ranasinghe and Pattiaratchi (2003)). . . . .	10
2.3	Photograph of the Mhlanga estuary in its closed state. The overwash fans caused by wave overtopping at spring high tide are evident. . . . .	11
2.4	Photo of the down stream face of the Mhlanga estuary sand barrier shortly before a breach. The rate of seepage through the sand barrier is evident as well as the volume of sediment being removed from the barrier. . . . .	13
2.5	Barrier schematic representing the relevant barrier and breach parameters. The final breach width is denoted $W$ , $H$ is the difference between the initial and final water levels, and $S$ is the volume of water that has flowed out through the breach. .	16
2.6	Breach schematic for Eqs. (2.9), (2.10) and (2.11)( adapted from Kraus (2003)). . . . .	19
2.7	Schematic of the breach process as described by Coleman et al. (2002) for a sand barrier under a constant head. . . . .	20
2.8	Schematic of the breach process for a dike burst as described by Visser (1998). . . . .	21
3.1	Photo of the pilot study experimental setup. The sand barrier is shown on the left with the impoundment on the right. A vertical measuring stick was placed in the impoundment so that the depth of the water could easily be recorded at any time.	27

3.2 Photo of the leveled base of the model and the three concrete side walls. . . . . 28

3.3 Photographs showing the outcome of a model breaching experiment (a) An elevation photograph with the sand barrier in the foreground with the storage basin in the background. The hourglass shape of the breach in elevation is evident (b) A plan photograph showing a close up view from upstream showing the curved half ellipse shaped upstream crest of the breach and the irregular sidewalls with small vertical overhangs. 29

3.4 A captured video image showing how and where the water levels and breach widths were obtained for this time step ( $t_i$ ). 31

3.5 Graphical representation of the parameters  $s_i$ ,  $H_i$ ,  $A_i$  and  $A_f$ . . 31

3.6 The non-dimensional breach width (solid triangles) and water level (solid squares) data for model B2,  $H_0 = 0.15\text{m}$ ,  $S_0 = 0.9\text{m}^3$  fitted with both the Log Normal (solid black line) and Gaussian (dashed black line) sigmoidal curves. The 5<sup>th</sup>, 50<sup>th</sup> and 95<sup>th</sup> percentile levels are shown as horizontal dashed lines for reference. . . . . 32

3.7 The time history of the non-dimensional breach width (solid triangle), water level (solid squares), outflow volume (solid diamonds) and flow rate (dash dot **dash line**) data for model B2,  $H_0 = 0.15\text{m}$ ,  $S_0 = 0.9\text{m}^3$ . The breach width, water level and outflow volume data are fitted with Log-Normal sigmoidal functions. The 5<sup>th</sup>, 50<sup>th</sup>, and 95<sup>th</sup> percentile levels are shown as horizontal dashed lines for reference. . . . . 33

3.8 The visually estimated breach formation times,  $T_{F_{visual}}$  plotted against the timescale estimated from the fitted LN sigmoidal curves  $T_F = (T_{95} - T_{05})$ . Symbols refer to different barrier shapes (see Table 1). . . . . 35

4.1 Photo sequence of a breaching experiment (berm B2,  $H_0 = 0.15\text{m}$ , bay area of  $3\text{m} \times 2\text{m}$ ). The berm is in the foreground with the rectangular storage basin behind. (a) and (b) show the breach in its *initiation* phase while (c), (d), (e) and (f) show the breach in its *formation* phase. . . . . 38

4.2 Photo of the berm B2,  $H_0 = 0.15\text{m}$ ,  $S_0 = 0.9\text{m}^3$  at the end of the breach formation phase. The berm is in the foreground with the rectangular storage basin behind. . . . . 40



- 4.3 Breach width measurements presented in non-dimensional form: breach widths are normalized by the final breach width, and time is normalized by the breach formation timescale  $T_F = (T_{95} - T_{05})$  with the median time  $T_{50}$  as the time origin. Symbols refer to different barrier shapes as indicated in Table 1. The 5<sup>th</sup>, 50<sup>th</sup> and 95<sup>th</sup> percentile levels are shown as horizontal dashed lines for reference. . . . . 41
- 4.4 Combined measurements of water levels and outflow volumes for all the experiments, plotted in non-dimensional form. The computed outflow hydrographs are also shown, non-dimensionalised by the peak outflows  $Q_P$ . Time is non-dimensionalised by the timescale  $(T_{95} - T_{05})$  inferred from sigmoidal curves fitted to the outflow volumes. Symbols refer to different barrier shapes as indicated in Table 1. The 5<sup>th</sup>, 50<sup>th</sup> and 95<sup>th</sup> percentile levels are shown as horizontal dashed lines for reference. . . . . 42
- 4.5 A non-dimensional composite plot constructed from averaging the time-histories of the breach widths (heavy solid line), outflow volumes (dash-dotted line), water levels (dash-dot-dot line), and outflow hydrographs (dashed line). The 5<sup>th</sup>, 50<sup>th</sup> and 95<sup>th</sup> percentile levels are shown as horizontal dashed lines for reference. . . . . 43
- 4.6 Comparison of the timescales for breach width development  $T_F$  and for the water level variations (or outflow volumes). In both cases the time differences  $(T_{95} - T_{05})$  inferred from the respective fitted sigmoidal curves are used. The line shown has a slope of 3/2. . . . . 43
- 4.7 Non-dimensional breach widths from the model experiments, plotted against (a)  $H/S^{1/3}$ , and (b)  $B/S^{1/3}$ . The horizontal dashed line represents the average value of the model data and is equal to the scaling co-efficient  $C_W = 0.38$ . The symbols correspond to different berm shapes as listed in Table 1. . . . 45
- 4.8 The non-dimensional breach width plotted against the non-dimensional outflow volume. The solid line represents a 1/3 power law while the red dashed line is Eq. 4.2 with  $k = 6$ . The symbols correspond to different berm shapes as listed in Table 1. . . . . 46
- 4.9 Breach volumes from the model experiments non-dimensionalised by  $S$ , plotted against (a)  $H/S^{1/3}$ , and (b)  $B/S^{1/3}$ . The symbols correspond to different berm shapes as listed in Table 1. . . 48

- 4.10 Breach volumes from the model experiments non-dimensionalised by  $HBS^{1/3}$ , plotted against (a)  $H/S^{1/3}$ , and (b)  $B/S^{1/3}$ . The horizontal dashed line represents the average value of the model data and is equal to the scaling co-efficient  $C_v = 0.26$ . The symbols correspond to different berm shapes as listed in Table 1. 49
- 4.11 The breach formation times non-dimensionalised by the timescale given by Eq. 3.3 with  $\alpha = -1.0$ ,  $\gamma = 0$  plotted against (a)  $H/S^{1/3}$  and (b)  $B/S^{1/3}$ . The symbols correspond to different berm shapes as listed in Table 1. . . . . 51
- 4.12 The Peak outflows non-dimensionalised by the outflow scale given by Eq. 3.14 with  $\alpha = -1.0$ ,  $\gamma = 0$  plotted against (a)  $H/S^{1/3}$  and (b)  $B/S^{1/3}$ . The symbols correspond to different berm shapes as listed in Table 1. . . . . 52
- 4.13 The breach formation times plotted against the timescale given by Eq. 3.12 with  $\alpha = -1.5$ ,  $\gamma = 1$  plotted against (a)  $H/S^{1/3}$  and (b)  $B/S^{1/3}$ . The horizontal dashed line represents the average value of the model data and is equal to the scaling co-efficient  $C_T = 13$ . The symbols correspond to different berm shapes as listed in Table 1. . . . . 54
- 4.14 The Peak outflows non-dimensionalised by the outflow scale given by Eq. 3.14 with  $\alpha = -1.5$ ,  $\gamma = 1$  plotted against (a)  $H/S^{1/3}$  and (b)  $B/S^{1/3}$ . The horizontal dashed line represents the average value of the model data and is equal to the scaling co-efficient  $C_Q = 0.067$ . The symbols correspond to different berm shapes as listed in Table 1. . . . . 55
- 4.15 Recorded water levels for a natural breaching event at the Mhlanga estuary, plotted in nondimensional form. The fitted Log-Normal sigmoidal curve is shown (thin solid black line) together with the associated outflow hydrograph (thick solid black line). . . . . 58
- 4.16 Non-dimensional breach widths plotted against (a) the hydraulic head  $H$ , and (b) the barrier breadth  $B$ . The horizontal dashed line represents the average value of all of the data and is equal to the scaling co-efficient  $C_W = 0.33$ . Data from homogeneous earth dam failures (Wahl, 1998) are plotted as circles. Data from actual estuaries are plotted as large filled circles. Data from the model experiments are shown as solid symbols. The symbols correspond to different berm shapes as listed in Table 1. . . . . 60

4.17 Non-dimensional breach volume plotted against (a) the hydraulic head  $H$ , and (b) the barrier breadth  $B$ . The horizontal dashed line represents the average value for all of the data and is equal to the scaling co-efficient  $C_V = 0.21$ . Data from homogeneous earth dam failures (Wahl, 1998) are plotted as circles. Data from actual estuaries are plotted as large filled circles. Data from the model experiments are shown as solid symbols. The symbols correspond to different berm shapes as listed in Table 1. . . . . 61

4.18 The breach formation times non-dimensionalised by the time scales given by Eq. 3.12 with  $\alpha = -1.5$ ,  $\gamma = 1$  plotted against (a)  $H/S^{1/3}$  and (b)  $B/S^{1/3}$ . The horizontal dashed line represents the average value of all of the data and is equal to the scaling co-efficient  $C_T = 16$ . Data from homogeneous earth dam failures (Wahl, 1998) are plotted as circles. Data from actual estuaries are plotted as large filled circles. Data from the model experiments are shown as solid symbols. The symbols correspond to different berm shapes as listed in Table 1. . . . . 63

4.19 The peak outflows non-dimensionalised by the time scales given by Eq. 3.12 with  $\alpha = -1.5$ ,  $\gamma = 1$  plotted against (a)  $H/S^{1/3}$  and (b)  $B/S^{1/3}$ . The horizontal dashed line represents the average value for all of the data and is equal to the scaling co-efficient  $C_Q = 0.058$ . Data from homogeneous earth dam failures (Wahl, 1998) are plotted as circles. Data from actual estuaries are plotted as large filled circles. Data from the model experiments are shown as solid symbols. The symbols correspond to different berm shapes as listed in Table 1. . . . . 64

4.20 Dimensional plot of the measured breach widths versus the breach widths predicted by Eq. 4.8 with  $C_W = 0.33$ . . . . . 66

4.21 Dimensional plot of the measured breach volumes versus the breach volumes predicted by Eq. 4.9 with  $C_V = 0.21$ . . . . . 66

4.22 Dimensional plot of the measured breach formation times versus the breach formations times predicted by Eq. 4.10 with  $C_T = 16$ . . . . . 68

4.23 Dimensional plot of the measured peak outflows versus the peak outflows predicted by Eq. 4.11 with  $C_Q = 0.058$ . . . . . 69

---

# LIST OF TABLES

---

3.1	Experimental Parameters. . . . .	29
4.1	Comparison of co-efficients of variation . . . . .	53
4.2	Breach parameters for natural lagoons and estuaries . . . . .	57
A.1	Collected experimental data . . . . .	78

---

# CHAPTER 1

## INTRODUCTION

---

### 1.1 What is an estuary?

Most people understand what is meant by the term estuary. Barnes (1974) loosely describes it as the region through which a river discharges into the sea. Attempting to formulate a definition that accounts for all of the variability amongst estuaries is beyond the scope of this investigation. A definition of an estuary, adequate for this study is “A partially enclosed coastal body of water which is either permanently or periodically open to the sea and within which there is a measurable variation of salinity due to the mixture of sea water and fresh water derived from land drainage” (Day, 1980).

### 1.2 Perched temporary open/closed estuaries

Whitfield (1980) classified South African estuaries according to their morphological structure. Estuaries are initially distinguished by their connection to the sea. This divides estuaries into two main categories, open estuaries and temporarily open/closed estuaries (TOCE). Open estuaries are permanently open to the sea and TOCEs become separated from the sea by a wave built sand barrier or berm that may form across the mouth of the estuary for a period of time.

When the water level in the impoundment behind the sand barrier reaches a critical level (which is not necessarily above the level of the sand barrier) the estuary breaches. During a breaching event the water in the impoundment scours a channel through the sand barrier creating a connection with the sea. The majority of estuaries on the South African Coast (approximately 70%) are TOCEs (Whitfield, 1980).



Fig. 1.1: Photos of the Mhlanga estuary (a) before a breaching of the mouth (b) after a breaching of the mouth. The difference in water level in the estuary before and after the breach is evident.

Perched TOCEs are those estuaries where the base level of the impoundment is above mean sea level. Therefore, when a perched TOCE breaches it essentially empties. Fig. 1.1 shows the perched Mhlanga estuary (a) before a breach and (b) after a breach. The difference in the water levels in the estuary before and after the breach is evident.

### 1.3 Motivation for the study

Estuaries are considered amongst the most fertile natural areas in the world. They provide a sheltered area from the sea where nutrient and sediment rich water from land drainage may mix with salty sea water. In terms of biomass estuaries are up to 7 times as productive as a typical wheat field and 20 times more productive than the open ocean (Barnes, 1977).

As one of their primary functions, estuaries act as a nursery ground for many marine species, including fish, prawns and crabs and are considered critical in terms of their contribution to marine fish stocks (Cooper, 2001). Therefore, it is clear that **preserving** the ecological functioning of our estuaries is essential for sustaining the biodiversity of our seas and oceans.

Humans have always used estuaries as a resource for food and settlement. More recently estuaries have been utilized for industrial developments, waste disposal and recreation. As the use of these systems has increased so too has the impact on the natural functioning of these systems. Loss of inter-tidal and flood plain area due to construction, constriction of flow due to bridge piers and canalization, dredging activities and manipulation of the mouth to

suit recreational or commercial purposes are examples of local development that may alter the natural functioning of these systems (Begg, 1978; Morant and Quinn, 1999). Since estuaries receive freshwater from land drainage, the factors that impact on the functioning of estuaries are not confined to the immediate area of the estuary. Any developments within the catchment area that alters the volume or quality of fresh water inflow, such as dams, storm water outlets and waste water treatment plants have the potential to alter the natural functioning of these systems.

In particular the alteration of flow patterns into many estuaries has effected their mouth dynamics i.e. breaching patterns and so in an attempt to maintain the ecological functioning of these estuaries it has become necessary to manage these scarce resources.

### 1.3.1 Management Strategies

Management strategies include artificially breaching estuaries, timed releases from upstream dams and increased or decreased abstraction allowances from the estuary's tributaries.

Estuaries may be artificially breached at a predetermined water level or season by digging a pilot channel across the berm to a level below the water level in the impoundment. This allows the water in the impoundment to flow through the pilot channel and scour a free connection to the sea. Estuaries may be artificially breached during a predetermined season in order allow the recruitment or migration of a specific fish species into or out of the estuary. Estuaries may be artificially breached at a predetermined water level to prevent the flooding of adjacent farm lands or property. Estuaries may also be artificially breached, to improve the water quality in the estuary, by flushing (Kraus, 2003).

Timed releases from upstream dams can be used to reduce the salinity levels in the estuary by increasing the freshwater input. However large releases may be sufficient to raise the water level in the impoundment to above the level of the sand barrier, triggering a breach. The high flows associated with breaching cause scour, and in this way large releases may be used to remove a build up of sediment within the estuary. Controlling the amount of water that is abstracted from tributaries by industry such as farming, or added to tributaries by industry such as waste water treatment plants, can also be managed so as to control the impact on an estuary in a similar manner to timed releases from an upstream dam (Perissinotto et al., 2004).

Unfortunately, existing models for predicting the consequences of alterations in freshwater flows on estuaries are inadequate (Slinger, 1996). Without accurate models, the impact of management strategies on an estuary can

not be accurately assessed before implementation. Therefore the need for accurate predictive models to estimate the effect of management strategies on the ecological functioning of perched TOCEs is evident.

The single most important factor that drives the ecology of a perched TOCEs is the mouth dynamics (Perissinotto et al., 2004) therefore, the overall objective of this study is to improve the understanding of the mouth dynamics of perched TOCEs. This understanding may then be incorporated into predictive models to more accurately mimic the physical dynamics of perched TOCEs. Such models may be used as decision support tools for management teams that are charged with the task of maintaining these productive ecosystems and sustaining the biodiversity in our oceans.

## 1.4 Aims

The objective of this investigation was to improve the understanding of the mouth dynamics of perched TOCEs, a key element in the functioning of these systems. Therefore, the specific aims of this study were:

- to investigate the breaching process
- to understand the key parameters that influence the breach characteristics, namely the size of the breach channel, the volume of sediment removed from the sand barrier, the length of time taken for the breach channel to develop and the peak outflow.

It is envisaged that the outcomes of this research may be incorporated into models to be used as decision support tools in the assessment of strategies for maintaining the ecological functionality of perched TOCEs.

## 1.5 Outline of the dissertation

In Chapter 2 the ecological importance and functioning of perched TOCEs is outlined. The similarities between a dam break and an estuary breach are discussed and the investigations by dam researchers are reviewed. Previous model studies and their outcomes are also reviewed in this chapter. From this chapter several key questions emerged.

In Chapter 3 a simple scaling analysis is outlined that provides the background for interpreting the experimental results. An initial pilot study that was undertaken is outlined followed by a description of the experimental procedure including how the data was collected and processed.



The results of this investigation are presented in Chapter 4 beginning with a discussion of the breach process. Existing scaling relationships are compared with proposed relationships. The proposed scaling relationships are then subjected to a rigorous test by comparing the model results with field observations of breaching at full scale estuaries and dams.

Finally in Chapter 5 the achievement of the aims and objectives of this dissertation are reviewed and conclusions concerning the key questions raised in Chapter 2 are presented.

---

## CHAPTER 2

# LITERATURE REVIEW

---

In this chapter the functioning of perched TOCEs is briefly explored including how a perched TOCE is formed and the importance of the mouth dynamics for these systems (section 2.1). The mechanisms by which the sand barrier is built up (section 2.2) and breached (section 2.3) is also reviewed in order to gain insight into the breaching process and the key parameters that influence the breach characteristics.

In section 2.4 the similarities and differences between an estuary breach and a dam break are examined in order to explore the research done into dam breaks and its relevance to estuary breaching.

In section 2.5 existing estuarine models developed as decision support tools for the management of perched TOCEs are reviewed, in order to assess how the breaching events were modeled. Existing numerical breach models are also explored.

Finally in section 2.6 previous model studies on the breaching of sand barriers are reviewed.

### 2.1 Perched temporary open estuaries

In an estuary the maintenance of an open mouth state depends on the interaction between sediment removal by scouring and sediment deposition by wave action.

Temporary open/closed estuaries (TOCEs) do not have a permanently open link to the sea. Their inlets are unstable due to a combination of low or intermittent riverflows, small tidal prism and energetic wave climate (with associated sediment transport) (Ranasinghe and Pattiaratchi, 2003). TOCEs are not unique to South Africa and are found in Australia, on the west coast of the USA, South America and India (Ranasinghe et al., 1999); (Ranasinghe and Pattiaratchi, 2003); (Kraus, 2003). They are sometimes referred to as

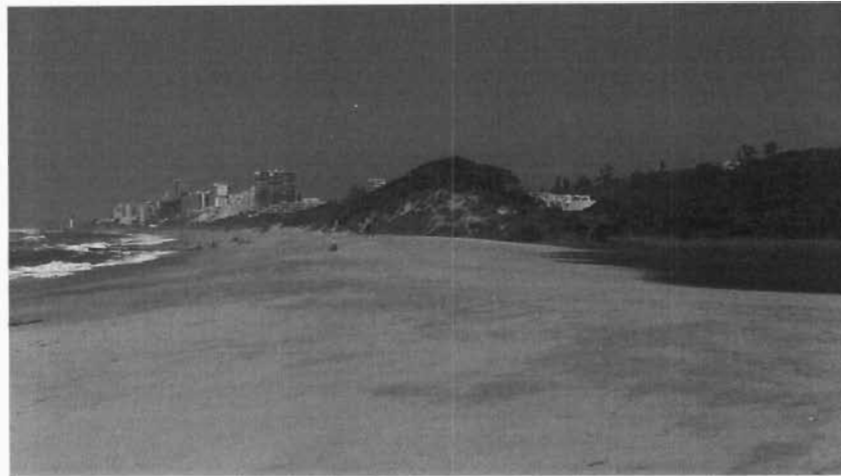


Fig. 2.1: Photo of the Mhlanga estuary on the right and the adjacent ocean on the left. The difference in water levels, the closed mouth state, and the barrier breadth are evident.

“blind”, “intermittently open” or “seasonally open” estuaries.

Perched TOCEs tend to occur on coastlines that are associated with coarse sediments in addition to situations where there are low or intermittent flows, small tidal prism, and energetic wave climate. Coarse sediments are typically associated with steep beach profiles (eg Bascom 1951) which are in turn associated with high wave run-up. The wave run-up can build sand barriers to a level 2-3m above mean sea level (MSL), even in the micro-tidal context of South Africa where the tidal range is less than about 2m.

During the closed phase of a perched TOCE, the base level of the impoundment is graded to a level above sea level (Cooper, 2001). Fig 2.1 shows the difference in vertical water level between the perched Mhlanga estuary and the adjacent ocean.

### 2.1.1 Ecological functioning of Perched TOCE

Key to the functioning of any ecosystem is the area of available habitat. As a perched TOCE essentially empties during a breach, it is clear that a major factor influencing the available habitat is the mouth state. The mouth state does not only effect the area of available habitat. The mouth state also influences the water quality of the estuary impacting either directly or indirectly on the temperature, salinity, light penetration, oxygen concentration

and nutrient availability of the water (Perissinotto et al., 2004). For example when the mouth is closed, the water level in the impounded estuary increases and the velocity of the flow within the impoundment decreases. Therefore, there is little mixing in the water body which may give rise to a stratified water column as the less dense fresh water floats on the more dense salt water. A continuous flow from the tributaries into the impoundment may lead to a build up of available nutrients in the impoundment and depending on the amount of fresh water flow entering the impoundment and the rate of evaporation the salinity levels can either increase or decrease.

When the mouth is open tidal influence can cause high velocities within the estuary exposed to the sea. The high velocities are associated with turbulence and scour. Turbulence ensures the water column is well mixed while scour raises sediment into suspension, increasing the turbidity of the water. Continuous flow through the estuary also prevents a build up of nutrients. Tidal inflow can also either increase or decrease the salinity levels in the estuary depending on the salinity level in the estuary impoundment before the mouth opened.

The mouth state therefore impacts on the available habitat and water quality of the estuary, so that the formation and breaching of the sand barrier are key to the ecological functioning of perched TOCE ecosystems. Although this study focuses on breaching, the formation of the sand barrier is an obvious starting point for this investigation.

## **2.2 Formation of the sand barrier**

There are two main mechanisms by which supratidal barriers may form, with each mechanism associated with a distinct sediment transport process.

### **2.2.1 Mechanism 1: interaction between inlet current and the long shore sediment transport process**

During the long shore sediment transport process sediment is moved parallel to the coastline. Breaking waves suspend sediment in the surf zone that is moved parallel to the coast by long-shore currents. The currents are generated by waves traveling at an oblique angle to the coastline. The tidal exchange flow at the mouth of an open TOCE interrupts the long-shore sediment transport process, causing sediment to accumulate and a spit begins to form on the updrift side of the estuary mouth. The size and rate of growth of the spit will depend on the amount of available sediment and the intensity of the flow and associated scour in the mouth channel. During periods

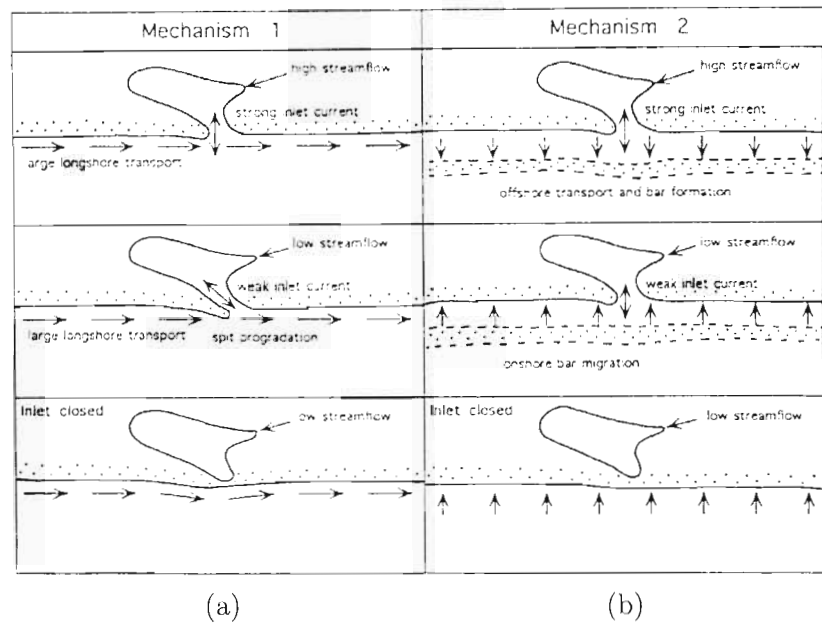


Fig. 2.2: (a) estuary inlet closure by mechanism 1 (b) estuary inlet closure by mechanism 2 (adapted from Ranasinghe and Pattiaratchi (2003)).

of low scour, a continuous supply of sediment to the updrift spit can result in the growth of the spit across the estuary mouth. This process is shown schematically in Fig. 2.2 (a) (after Ranasinghe and Pattiaratchi (2003)).

### 2.2.2 Mechanism 2: interaction between inlet current and the cross-shore sediment transport

During the cross-shore sediment transport process sediment is moved perpendicular to the coastline. Breaking waves suspend sediment in the surf zone. The sediment is then moved perpendicular to the coast due to near normal wave incidence. Depending on the wave characteristics, such as steepness, wave action can cause sediment to be transported on-shore or off-shore (U.S. Army Corps of Engineers, 2002). Periods of continuous on-shore transport and low scour in the estuary mouth, can result in the closure of an inlet. This process is shown schematically in Fig. 2.2 (b) (after Ranasinghe and Pattiaratchi (2003)).

### 2.2.3 Supratidal barriers

Once the estuary mouth is closed, wave run up may continue to deposit sediment onto the sand barrier. This can build the barrier to a height above the water level of spring high tide. Although the barrier may reach a height of 2-3m above MSL, wave overtopping may still occur at spring high tide and it is common at perched South African estuaries. The overwash fans shown in Fig. 2.3 are created by wave overtopping.

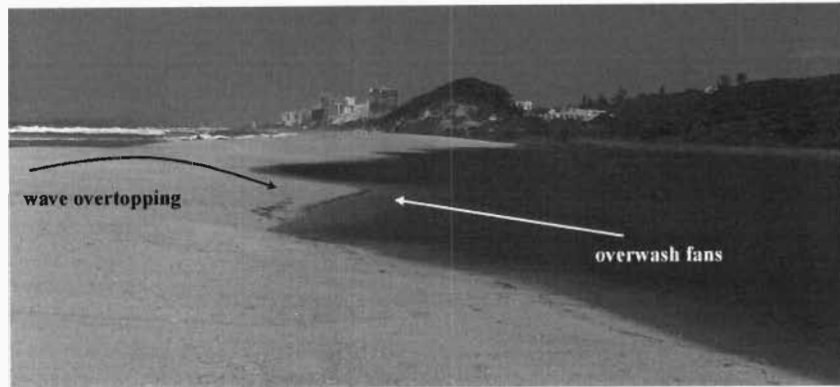


Fig. 2.3: Photograph of the Mhlanga estuary in its closed state. The overwash fans caused by wave overtopping at spring high tide are evident.

## 2.3 Estuary breaching

Estuaries breach naturally by two main mechanisms and can also be artificially breached. These breaching mechanisms are well documented in qualitative case studies, (Kraus and Wamsley, 2003, 2005; Kraus, 2003; Kraus et al., 2002; Zietsman, 2004) although there is a lack of detailed quantitative information on the sand barrier breaching processes (Kraus, 2003; Kraus et al., 2002).

### 2.3.1 Breach mechanism 1: overtopping from the impoundment

Failure due to overtopping is associated with high inflows that increase the water level in the estuary impoundment. Once the water level within the

impoundment rises above the crest of the sand barrier, the water will overtop the sand barrier. The over-topping flow gradually scours a channel across the sand barrier. Running surface water within the channel ultimately scours a free connection through the sand barrier from the impoundment to the sea. The presence of a pre-existing localized area of low elevation in the sand barrier can promote breaching by confining the initial overtopping flow and intensifying the scour (Kraus and Wamsley, 2003).

### 2.3.2 Breach mechanism 2: seepage and liquefaction

Seepage through the porous sand barrier is driven by the hydraulic gradient between the impoundment and the sea. The rate of seepage may be increased due to a narrowing sand barrier or an increasing head difference. Wave action may erode large volumes of sediment from the beach face. This can cause a dramatic narrowing of the sand barrier. The elevated water table in the barrier reduces the effective stresses between sand particles and allows increased erosion due to wave action (Turner and Leatherman, 1997). The berm may also be narrowed by a reduction in the amount of sediment supplied to the beach by the sediment transport processes.

At a sufficiently high rate of seepage through the sand barrier, soil stability is lost. This allows large volumes of sediment to be removed quickly from the sand barrier as a slurry, this is known as sand piping. Fig. 2.4 shows the Mhlanga estuary sand barrier shortly before a breach. The seepage through the sand barrier is removing sediment from the downstream face of the sand barrier. The loss of sediment can cause the sand barrier to slump and lower the elevation of the berm crest below the water level in the impoundment. Once the crest is overtopped, surface water flow can then scour a free connection between the impoundment and the sea as with an overtopping type failure. It is important to note that this breach mechanism does not require the initial water level to be above the level of the sand barrier (Kraus and Wamsley, 2003).

### 2.3.3 Artificial breaching

It is common practice to artificially breach closed estuaries. Artificial breaching involves digging a channel across the crest of the sand barrier. The base of the channel is dug to a level below the water level in the impoundment. This artificially lowers a portion of the sand barrier below the water level in the impoundment creating an overtopping flow. Running surface water confined within the channel can then ultimately scour a free connection between the impoundment and the sea.



Fig. 2.4: Photo of the down stream face of the Mhlanga estuary sand barrier shortly before a breach. The rate of seepage through the sand barrier is evident as well as the volume of sediment being removed from the barrier.

This is sometimes done as part of a management strategy to address the effects of reduced inflows due to dams and abstraction schemes for crop irrigation. Reduced inflows alter the natural rate at which the impoundment will fill thus changing the breaching frequency. This may cause a TOCE to remain closed for longer periods of time than if the inflows were unaltered. Artificial breaching is also undertaken (1) to prevent flooding of farm lands and developments due to high water levels in the impoundment, (2) to improve the water quality in the impoundment by flushing or (3) to facilitate the migration of marine organisms.

A drawback of artificial breaching is that it is often done at a lower estuary water level than that at which the estuary would naturally breach. This reduces the amount and velocity of the water passing through the breach, which in turn reduces the amount of scour that takes place during a breach. This can cause an increase in the rate of sedimentary infilling in the impoundment (van Niekerk et al., 2005; Beck et al., 2004; Schumann, 2003).

#### 2.3.4 Breaching of coastal barriers

Kraus (2003) reviews several articles describing observed breaches of coastal barriers such as those found on the East coast of North America. From these articles Kraus describes a typical coastal barrier breaching process: the



breach initially opens rapidly, then gradually widens and deepens to some equilibrium dimensions. The breach widens by a process of under cutting and collapse referred to as notching, leaving the channel with near vertical side slopes.

Clearly this description is lacking in quantitative features and cannot be considered complete.

## 2.4 Dam breaks

Estuary breaching is conceptually similar to the failure of earth-fill dams. The basic mechanisms of an earth-fill dam failure are similar to the mechanisms of estuary breaching as discussed in sections 2.3.1 and 2.3.2. This raises the question of whether the knowledge gained from the considerable research effort into dam failures (motivated by the potentially catastrophic effects of dam failures) is applicable to estuary breaching.

There are some differences in the failure of earth-fill dams and estuaries that should be noted. The breaching of earth dams is often driven by large hydraulic gradients (due to narrow, high barriers), whereas for coastal barrier breaching these gradients are typically smaller and can vary due to changes in tide and waves. The breaching of coastal barriers may be affected by longshore and cross shore sediment transport which are absent in the case of dam failures.

There are some physical differences between earth-fill dams and coastal sand barriers that should be noted:

- earth dams typically have a well defined, regular cross sectional geometry which is not the case for natural wave built sand barriers
- earth dams are usually constructed with relatively well graded sediments, whereas natural coastal sand barriers are uniformly graded due to the sorting action of waves. In some cases, earth dams incorporate cohesive sediments (e.g. in the form of clay core-walls) which are very different to the cohesionless sandy sediments of coastal barriers.
- earth dams typically have a well defined foundation that is relatively impervious and immobile. Natural sand barriers are more variable and may be founded on additional sandy material that is both pervious and erodible.

However, despite these differences, the conceptual similarities between the failure of coastal sand barriers and earth-fill dams justifies a review of past investigations into dam break analysis.

### 2.4.1 Previous investigations into dam breaks

Predictions of the discharges and downstream flood levels resulting from a dam failure require an estimate of the breach outflow hydrograph. The characteristics of the breach including the outflow hydrograph can be predicted statistically or by using a numerical model that incorporates sediment transport. Sediment transport models typically rely on semi-empirical results that are not applicable to, or are untested for, the regime of flow conditions occurring during a dam break. Therefore, in current practice for dam break flood routing simulations the breach characteristics must first be estimated and provided as inputs to dam break and flood routing simulation models (Coleman et al., 2002).

There are a number of existing models for predicting the breach characteristics of an earth dam failure based on regression analysis of historical dam break data.

### 2.4.2 Breach parameters

Consider the sketch of an idealized barrier in Fig. 2.5. Let  $S_0$  represent the volume of the impoundment and  $S$ , the outflow volume, that is the total volume of water that flows out of the impoundment during a breaching event. Let  $H_0$  represent the height of the sand barrier and  $H$ , the total water level change during the breach. Let  $B$  represent the breadth of the base of the barrier,  $b$  the breadth of the top of the barrier and  $\beta_1$  and  $\beta_2$ , the downstream and upstream slopes respectively. Let  $W$ , represent the width of the breach and  $Q_P$ , the peak outflow during the breach.

The breach process comprises two main phases - a breach *initiation* phase followed by a breach *formation* phase (Wahl, 1998). During the initiation phase, the over topping flow gradually scours a channel on the downstream face of the barrier while the upstream crest of the barrier remains relatively intact. Upstream water levels do not change significantly during this phase. Once the upstream crest of the barrier starts to erode significantly, it signals the start of the breach formation phase. Outflow and erosion rates increase rapidly during this phase until the head difference, between the impoundment and the downstream outflow, reduces significantly. The velocity of the flow through the breach channel then decreases and the scour in the channel reduces until the breach attains its maximum width and the breach formation phase ends. A breach formation time  $T_F$ , may be defined as:

*The time between initial breaching of the upstream face of the barrier until the breach is fully formed.*

The breach formation time has been defined in various ways by different

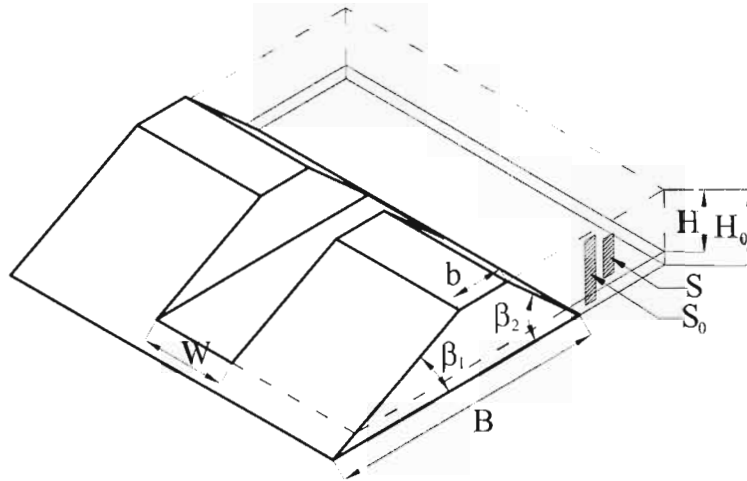


Fig. 2.5: Barrier schematic representing the relevant barrier and breach parameters. The final breach width is denoted  $W$ ,  $H$  is the difference between the initial and final water levels, and  $S$  is the volume of water that has flowed out through the breach.

investigators but, as noted by Wahl (1998), they all essentially refer to the formation phase as described above.

Wahl (2004) reviews the performances of existing dam break models for predicting  $W$ ,  $T_F$  and  $Q_P$  and concludes that Frochlich's 1995a; 1995b predictor equations for  $W$ ,  $T_F$  and  $Q_P$  provide the best overall accuracy.

### 2.4.3 Breach width

Frochlich (1995a) proposed the dimensionally non-homogeneous regression equation as

$$W = 0.1803 K_0 S_0^{0.32} H_0^{0.19}, \quad (2.1)$$

relating the breach width  $W$  (m) to the impounded storage volume  $S_0$  ( $\text{m}^3$ ) and the depth of the water  $H_0$  (m) where  $K_0 = 1.4$  for overtopping induced failures and  $K_0 = 1.0$  for seepage induced failures. Eq. (2.1) lacks generality as this equation cannot be expressed in non-dimensional form and therefore is only applicable to the data from which it was derived.

In an earlier analysis Frochlich (1987) proposed a dimensionally homoge-

neous regression equation for predicting the breach width, namely

$$W/H_0 = 0.47 K_0 \left( S_0/H_0^3 \right)^{1/4}. \quad (2.2)$$

Once again  $K_0 = 1.4$  for overtopping induced failures and  $K_0 = 1.0$  for seepage induced failures. This equation, expressed in non-dimensional form, has a greater range of applicability. Froehlich's equation may be re-arranged to give

$$W/S_0^{1/3} = 0.47 K_0 \left( H_0/S_0^{1/3} \right)^{1/4}. \quad (2.3)$$

It can be seen that expressed in this form, the breach width non-dimensionalised by the length scale  $S_0^{1/3}$  has only a weak dependence on  $H$ .

#### 2.4.4 Breach formation time and peak outflow

Froehlich (1995a) proposed the regression equation

$$T_F = 0.00254 S_0^{0.53} H_0^{-0.90}, \quad (2.4)$$

relating the breach formation time  $T_F$  (hrs) to the impounded storage volume  $S_0$  ( $\text{m}^3$ ) and the depth of the water  $H_0$  (m). If the exponents for  $S_0$  and  $H_0$  in Eq. (2.4) are rounded to 0.5 and  $-1.0$  respectively, and the parameter  $g$  is assumed to be incorporated into the numerical coefficient, then it may be re-written in non-dimensional form as

$$T_F \sim (g/S_0^{1/3})^{-1/2} (H_0/S_0^{1/3})^{-1}. \quad (2.5)$$

In an earlier paper Froehlich (1987) proposed a dimensionally homogeneous regression equation for  $T_F$ . That equation can be expressed in the form of Eq. (2.5) as

$$T_F = 79 (g/S_0^{1/3})^{-1/2} (H_0/S_0^{1/3})^{-0.9}. \quad (2.6)$$

It is evident when Eqs. (2.5) and (2.6) are expressed in a similar form that both equations suggest the same basic scaling for  $T_F$ .

Froehlich (1995b) proposed a regression equation for the peak outflow as

$$Q_P = 0.607 S_0^{0.295} H_0^{1.24}, \quad (2.7)$$

where  $Q_P$  is in  $\text{m}^3\text{s}^{-1}$  and  $S$  and  $H$  are in meters. Using the same data, Webby (1996) suggested an alternative regression equation for the peak outflow

$$Q_P = 0.0443 (g S_0^{5/3})^{1/2} (H_0/S_0^{1/3})^{1.4}. \quad (2.8)$$

Comparing Eqs. (2.7) and (2.8) it is evident that the values of the exponents for  $H$  and  $S$  are similar. Webby (1996) noted that Eq. (2.8) yielded a slightly lower coefficient of determination than Eq. (2.7), but has the desirable feature of dimensional homogeneity.

These regression analyses suggest that the dominant parameters in determining the breach characteristics are  $S_0$  and  $H_0$ .

## 2.5 Existing models for perched TOCEs

Smakhtin (2004) developed a water balance model for perched TOCEs. The model predicts estuarine volumes and water levels which in turn can be used to simulate other parameters such as salinity levels. The aim of the model was to contribute to the development of quantitative knowledge about estuarine ecosystems.

Smakhtin (2004) equated a perched TOCE to a reservoir where the sand bar serves as a dam wall and the estuary mouth as a “spillway”. The width of the spillway is determined as an average of the widths of several previous breaches. When the water level within the impoundment rises above the crest of the berm the impoundment overflows and the rate of outflow is governed by weir hydraulics. During these overflow periods the estuary mouth is assumed to be open. This model requires the observations of several breaches of an estuary to provide input data for the model. Due to the remoteness of some estuaries and the sporadic and infrequent nature of estuary breaches this information is often not readily available. It can also be seen from the discussion in section 2.3 about the natural breach process, that breaching is not well described by this idealized model because when a perched TOCE breaches, the flow does not merely over-top the sand barrier, the flow scours a channel through the sand barrier and the impoundment empties.

Kraus (2003) developed an analytical model to describe the breach growth in a coastal barrier. An idealized breach through a barrier is shown in Fig. 2.6. The model was based on the conservation of mass with the equation

$$B \frac{dz(t)}{dt} \Delta w = \hat{Q}_S(t) \Delta t \quad (2.9)$$

describing the vertical breach growth and

$$B \frac{dw(t)}{dt} \Delta z = \hat{Q}_B(t) \Delta t \quad (2.10)$$

describing the horizontal breach growth, where  $z(t)$  is the depth of the breach channel,  $\Delta w$  is the change in breach width,  $\Delta t$  is the time interval and  $\hat{Q}_S(t)$  and  $\hat{Q}_B(t)$  are the net sediment transport rates along the sides and bottom of the breach channel respectively.

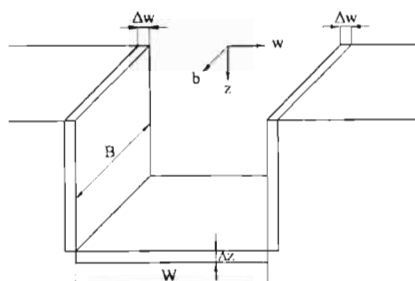


Fig. 2.6: Breach schematic for Eqs. (2.9), (2.10) and (2.11) (adapted from Kraus (2003)).

$\hat{Q}_S$  and  $\hat{Q}_B$  were modeled by

$$\hat{Q}_S = Q_S \left( 1 - \frac{w(t)}{W} \right), \quad \hat{Q}_B = Q_B \left( 1 - \frac{z(t)}{Z} \right) \quad (2.11)$$

where  $Q_S$  and  $Q_B$  are constant maximum transport rates that are not necessarily equal.  $W$  and  $Z$  are the final breach widths and depths respectively.

From this model it is evident that breach growth is influenced by seven parameters, the initial dimensions of the pilot channel  $W_0$  and  $Z_0$ , the final dimensions of the breach channel  $W$  and  $Z$ , the transport rates during the breach  $Q_S$  and  $Q_B$  and the berm breadth  $B$ .

## 2.6 Previous model investigations

Coleman et al. (2002) used a laboratory model to investigate the breaching of a homogeneous earth fill dam under a constant upstream head. This simulates the failure of an embankment with an infinitely large storage reservoir. The aim of the investigation was to predict the breach development with time.

Although perched TOCEs do not breach under a constant head, Coleman et al. (2002) drew several noteworthy conclusions. Firstly the breach initially develops vertically and then horizontally. Secondly the final breach shape is hourglass in plan, with a crescent or half ellipse shaped upstream crest.

Coleman et al. (2002) also describes the observed breach process: the initial overtopping flow erodes a channel into the downstream face of the dam wall. The breach channel slope is initially parallel to the the embankment slope. This is shown in Fig. 2.7 between times  $t_0$  and  $t_1$ . The toe of the breach



Fig. 2.7: Schematic of the breach process as described by Coleman et al. (2002) for a sand barrier under a constant head.

channel erodes upstream along the base until a pivot point is reached, this is shown at time  $t_1$  in Fig. 2.7. The slope then progressively flattens to a terminal value rotating about the pivot point, this is shown in Fig. 2.7 between times  $t_1$  and  $t_2$ . The breach channel widens rapidly by a process of undercutting and collapse similar to the process described in section 2.3.

Kraus (2003) outlines the differences and similarities between an estuary breach and a dike burst. Visser (1998) summarizes the literature on dike breaching in general and recent modeling. Visser (1998) describes a 5 stage model for dike breaching that is driven by the head difference at the dike. The model is specific to dike bursts, however the stages of the breach development may have general applicability. The dike burst process is described by Visser (1998) in five stages as:

- Stage 1: the gradual over topping flow begins to scour a channel into the downstream face. The slope of the channel bed increases as the toe of the embankment is eroded upstream by the turbulence at the toe. The embankment slope continues to increase until a terminal value is reached. This is seen between times  $t_0$  and  $t_1$  in Fig. 2.8.
- Stage 2: the channel bed continues to erode with a constant bed slope. As the erosion continues the channel base erodes parallel to the terminal slope until the lowering of the upstream crest of the dike within the breach channel. This is shown in Fig. 2.8 between times  $t_1$  and  $t_2$ .
- Stage 3: during this stage the lowering of the upstream crest of the dike continues and the breach channel begins to widen by a process of undercutting and collapse, the lowering of the upstream crest is shown between times  $t_2$  and  $t_3$  in Fig. 2.8
- Stage 4: after the complete wash out of the dike in the breach channel,

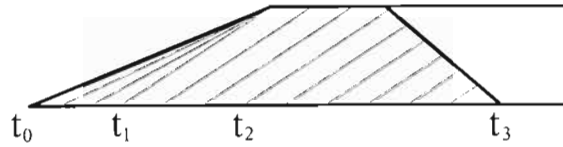


Fig. 2.8: Schematic of the breach process for a dike burst as described by Visser (1998).

the breach continues to grow in the vertical, developing a scour hole and in the horizontal by undercutting and collapse.

- Stage 5: the breach continues to gradually widen until the flow velocities in the breach channel become so small that the breach erosion process stops.

It is evident from the comparison of Figs. 2.7 and 2.8 that there is a difference in the breach process described by Coleman et al. (2002) and Visser (1998). Coleman et al.'s (2002) investigation pertains to dam breaks and Visser's 1998 investigation to dike bursts, although both investigations are for homogeneous embankments under an approximately constant upstream head. This raises an interesting question as to which description most accurately describes the breach process of homogeneous embankments? The present study focuses on the breach process under a falling head, so this question falls outside of the scope of this investigation.

## 2.7 Summary

In this chapter the ecological importance of estuaries and the role that the mouth dynamics play in the functioning of perched TOCEs were discussed. The mechanisms by which coastal sand barriers are built up and breached were reviewed and the observed breach process at natural estuaries was reported.

The conceptual similarities between an estuary breach and dam break lead to a review of the predictive models for the breach parameters of a dam break. The main parameters that influence the breach characteristics of a dam break appear to be related to the storage volume of the impoundment  $S_0$  and the height of the barrier  $H_0$ .



Kraus's (2003) model of the breach development in a coastal barrier was also reviewed. This identified several additional parameters that influenced the breach characteristics of coastal barriers.

The basic question of the scaling of the breach characteristics for perched TOCE however is clearly still unanswered. Several parameters that are likely to have an influence on the breach characteristics of a perched TOCE have been identified and their influence will be further investigated.

Previous model investigations into the breach process were also reviewed and the observations of the researchers were noted. Coleman et al. (2002) investigated the breach process for a homogeneous earth fill dam, under a constant head whilst Visser (1998) investigated the breach process for a homogeneous dike wall, also under a constant head. This investigation focuses on the breach process under a falling head. The investigations by Coleman et al. (2002) and Visser (1998) may be relevant, although a quantitative description of the breach process under a falling head is still lacking.

---

## CHAPTER 3

# METHODOLOGY

---

This investigation was underpinned by dimensional analysis. As described in section 2.4 most investigations into barrier failures have been based on regression analyses of historical data. Many of these regression relationships are dimensionally non-homogeneous and their applicability outside the specific parameter ranges for which they were derived does not give sensible results. Using dimensional analysis to underpin this investigation gives the results more generality making them applicable over a broad range of scales.

### 3.1 Scaling analysis

From Froehlich's breach width predictor equations (Eqs. (2.1) and (2.2)), the only allowance made for the different mechanisms of failure is the  $K_0$  parameter. The  $K_0$  parameter has the effect of increasing the breach width for an over topping type failure. This is because Froehlich's equations related the volume of the impoundment  $S_0$ , to the breach characteristics and the  $K_0$  parameter allows for the additional outflow volume associated with the increased water levels present during an overtopping type failure. It is also noted that Froehlich makes no allowance for different sediment types in his predictor equations.

Following this analysis, it is hypothesized that the dominant parameters influencing the breach characteristics are the outflow storage volume  $S$  and the outflow hydraulic head  $H$ . The barrier breadth  $B$  is also assumed to have some influence. The flow is driven by gravity with  $g$  denoting the body force per unit mass. The influence of the sediment type is assumed negligible. Note that the storage  $S$  can vary independently of  $H$  since the impounded volume may comprise any combination of depth and surface area. Therefore

the breach width  $W$  is assumed to be expressible as

$$W = f_1(S, H, B) \quad (3.1)$$

and the volume of sediment removed from the barrier during a breach  $V_b$ , as

$$V_b = f_2(S, H, B) \quad (3.2)$$

where  $f_1(\cdot)$  and  $f_2(\cdot)$  are unknown functions to be determined empirically.

Similarly the breach formation time  $T_F$  and peak outflow  $Q_P$  are assumed to be given by

$$T_F = f_3(S, H, B, g) \quad (3.3)$$

and

$$Q_P = f_4(S, H, B, g). \quad (3.4)$$

If the storage volume  $S$  is used to define a reference length scale  $S^{1/3}$  (which may be interpreted as the geometric mean of the horizontal and vertical scales of the volume  $S$ ) and some combination of the parameters  $g$ ,  $S$ ,  $H$  and  $B$  is used to define a time scale  $T$  and an outflow scale  $Q$ , then  $W$ ,  $V_b$ ,  $T_F$  and  $Q_P$  can be related to  $H$ ,  $B$  and  $S$  in non-dimensional form as

$$W/S^{1/3} = f_5(H/S^{1/3}, B/S^{1/3}), \quad (3.5)$$

$$V_b/S = f_6(H/S^{1/3}, B/S^{1/3}), \quad (3.6)$$

$$T_F/T = f_7(H/S^{1/3}, B/S^{1/3}) \quad (3.7)$$

and

$$Q_P/Q = f_8(H/S^{1/3}, B/S^{1/3}). \quad (3.8)$$

where  $f_5(\cdot)$ ,  $f_6(\cdot)$ ,  $f_7(\cdot)$  and  $f_8(\cdot)$  are unknown functions (to be determined empirically). Given this frame-work, the aims of this investigation, namely, to investigate the key parameters that influence the breach characteristics, are simple: an experimental study was designed and implemented to investigate the form of the functions  $f_5$ ,  $f_6$ ,  $f_7$  and  $f_8$ .

### 3.1.1 Breach width, $W$ and volume of sediment removed, $V_b$

For the breach width  $W$ , we investigate the form of the function  $f_5$  that relates  $W/S^{1/3}$  to the parameters  $H/S^{1/3}$  and  $B/S^{1/3}$ . If Eq. (3.5) is compared with Froehlich's 1987 breach width predictor equation (Eq. (2.3)) then it implies that

$$f_5 \sim \left(H/S^{1/3}\right)^{1/4}. \quad (3.9)$$

Although a result from this investigation (see section 4) is that the available data is consistent with the simplification

$$f_5 \sim \text{constant}. \quad (3.10)$$

Therefore the breach width may be scaled as

$$W = C_W S^{1/3}. \quad (3.11)$$

where  $C_W$  is a scaling constant and equal to the value of the constant function  $f_5$ .

### 3.1.2 Breach formation time, $T_F$ and peak outflow, $Q_P$

If it is assumed that it is possible to find a representation of the timescale  $T$  in terms of the parameters  $g, H, S$  and  $B$  that gives  $f_7 \simeq \text{constant}$ , then dimensional homogeneity requires that the timescale  $T$  is expressible as a power law of the form

$$T_{\alpha,\gamma} \sim (g/S^{1/3})^{-1/2} (H/S^{1/3})^\alpha (B/S^{1/3})^\gamma, \quad (3.12)$$

and  $T_F$  can then be scaled as

$$T_F = C_T T_{\alpha,\gamma} \quad (3.13)$$

where  $C_T$  is the value of the (assumed constant) function  $f_7$ .

If the above suppositions are reasonable, the duration of the outflow hydrograph should also scale like Eq. (3.12). Therefore a scale for the outflows is  $Q \sim S/T$ , and it follows from Eq. (3.12) that

$$Q_{\alpha,\gamma} \sim (g S^{5/3})^{1/2} (H/S^{1/3})^{-\alpha} (B/S^{1/3})^{-\gamma}. \quad (3.14)$$

The peak outflow  $Q_P$  can then be scaled as

$$Q_P = C_Q Q_{\alpha,\gamma}. \quad (3.15)$$

where  $C_Q$  is the value of the (assumed constant) function  $f_8$ .

Comparing Froehlich's  $T_F$  predictor equations (Eq. (2.5) and (2.6)) with Eq. (3.13), it is evident that Froehlich's analysis supports the form of the proposed scaling and suggests the timescale  $T_{-1,0}$  given by Eq. (3.12) with  $\alpha = -1.0$  and  $\gamma = 0$ .

Webby's  $Q_P$  predictor equation (Eq. (2.8)) is also consistent with the form of the proposed scaling for  $Q_P$  (Eq. (3.15)) but with an outflow scale  $Q_{-1.5,0}$

corresponding approximately to that given by Eq. (3.14) with  $\alpha = -1.5$  and  $\gamma = 0$ .

The scalings proposed by Frochlich for  $T_F$  and Webby for  $Q_P$  suggest that the scales should have different  $\alpha$  and  $\gamma$  values. Although it is clear from the scaling analysis that if the suppositions made are correct, the appropriate scaling for  $T_F$  and  $Q_P$  should have the same  $\alpha$  and  $\gamma$  values.

## 3.2 Pilot study

A crude pilot study was undertaken to size the model and to gauge the sensitivity of the breach width to the parameters  $S$ ,  $H$  and  $B$ .

A trial model was constructed so that the impoundment could drain completely during a breach and there would be no effect on the breach from the downstream tail water. A photo of the pilot study setup is shown in Fig 3.1.

The base of the model was leveled and three side walls were constructed from the earth removed during the leveling of the base. The side walls were roughly triangular in shape, built simply by piling the excavated earth. An impervious plastic membrane was used to line the model and a layer of levelled river sand was placed on top of the plastic membrane. The sand placed on top of the plastic membrane was used to cover the wrinkles in the plastic on the base of the model, so that it would not effect the flow from the impoundment in any way. The river sand was sieved through a 1.5mm sieve to remove any large particles. A sand barrier was hand built out of the sieved sand across the fourth side of the model estuary.

A breach was then triggered by cutting a small channel into the crest of the berm. The initial experiment was repeated several times without changes to the setup in order to check the repeatability of these experiments. The storage area of the impoundment was then doubled to estimate the sensitivity of the final breach dimensions to the change in outflow volume. In subsequent experiments the height of the berm was halved and the berm breadth was doubled so that the effects of these changes on the final breach dimensions could be observed.

Valuable experience was gained from the pilot study. Firstly, triangular side walls made by hand were irregular and the slope of the side walls were difficult to measure. This made estimating the volume of water stored in the impoundment an unnecessarily tedious task. Secondly in order to construct a sand barrier of regular and repeatable dimensions a mold was required. Thirdly if the impoundment was to be filled rapidly, a means was required to stop strong currents from developing in the impoundment that could scour sediment from the upstream face of the barrier. Finally the width of the



Fig. 3.1: Photo of the pilot study experimental setup. The sand barrier is shown on the left with the impoundment on the right. A vertical measuring stick was placed in the impoundment so that the depth of the water could easily be recorded at any time.

breach channel was observed to be relatively insensitive to changes in  $S$ ,  $H$  and  $B$ . Doubling  $S$  did not result in doubling the breach width. Halving  $H$  or doubling  $B$  also did not result in halving the breach width.

### 3.3 Model investigation

#### 3.3.1 Experimental setup

The experiments were designed so that all of the parameters of interest would be systematically varied. Parameter values used in the experiments are given in Table 3.1 these include the impounded storage volume  $S_0$ , barrier height  $H_0$ , and the barrier shape parameters (top & bottom breadths  $b$  and  $B$ , and side slopes  $\beta_1$  and  $\beta_2$ ). A simple rectangular model estuary 2m wide by 4m long was excavated. The bed of the model was leveled, and three sidewalls were built using concrete blocks. The model was lined with a 200 $\mu$ m thick impervious plastic membrane. Fig. 3.2 shows the model under construction.

Sand barriers of various heights and cross-sectional shapes were built across the open side of the model. The sand used for the experiments was

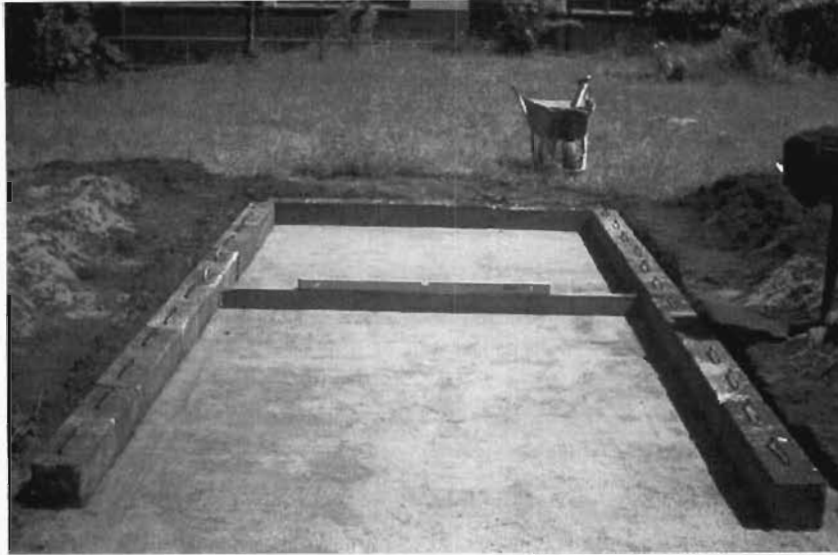


Fig. 3.2: Photo of the leveled base of the model and the three concrete side walls.

not varied and was river sand sieved through a 1.5mm sieve. The sand was uniformly graded with  $d_{50} \simeq 600\mu\text{m}$  and uniformity coefficient  $d_{60}/d_{10} \simeq 3$ . The barriers were positioned at nominal distances of 1, 2, or 3m from the back wall of the model, thereby providing different storage areas for each breaching experiment. The different berm heights combined with the different storage areas created a range of storage volumes for the breaching experiments. The impoundment was filled rapidly by letting the water first enter into a small sub-basin and then overflow into the main impoundment. A breach was initiated using a small ( $\sim 1\text{cm}$  deep) V-notch across the top and centre of the berm.

### 3.3.2 Data acquisition

The depth of the water in the impoundment at the initiation of the breach was recorded using a measuring stick positioned in the impoundment at the beginning of the experiment. The development of the breach to its final dimensions was then observed and recorded with video.

Photographs illustrating the outcome of a typical breaching experiment are shown in Fig. 3.3. It is evident in Fig. 3.3 (a) that the final breach has a venturi or hourglass shape in plan and in Fig. 3.3 (b) that upstream crest

Table 1. Experimental parameters

Barr	Slopes		b (m)	B (m)	H <sub>0</sub> (m)	S <sub>0</sub> (m <sup>3</sup> )	Barrier Shape (Schematic only)	
	$\beta_1$	$\beta_2$					Sea	Estuary
B1	2	3	0	0.40	0.08	0.15 - 0.45	Sea	Estuary
				0.75	0.15	0.30 - 0.90		
B2	2	3	0.1	0.50	0.08	0.15 - 0.45	Sea	Estuary
				0.85	0.15	0.30 - 0.90		
B3	2	3	0.3	0.70	0.08	0.15 - 0.45	Sea	Estuary
				1.05	0.18	0.30 - 0.90		
B4	2	5	0	0.56	0.08	0.15 - 0.45	Sea	Estuary
				1.05	0.15	0.30 - 0.90		

Tab. 3.1: Experimental Parameters.



Fig. 3.3: Photographs showing the outcome of a model breaching experiment (a) An elevation photograph with the sand barrier in the foreground with the storage basin in the background. The hourglass shape of the breach in elevation is evident (b) A plan photograph showing a close up view from upstream showing the curved half ellipse shaped upstream crest of the breach and the irregular sidewalls with small vertical overhangs.

of the breach is a curved, half ellipse shape. This is in accordance with the observations made by Coleman et al. (2002). The breach width therefore varies across the breadth of the barrier. The side-walls of the final breach were usually nearly vertical but could also have unstable vertical overhangs due to under-cutting erosion by the outflow and maintained by cohesion in the saturated sand (see Fig. 3.3 (b)). These factors can make precise, repeatable measurements of a breach width difficult to define. All the breach width measurements reported here were measured at the upstream crest of the barrier. It was observed that the breach width at this location seemed to be reasonably representative of an average over the breadth of the barrier. Vertical overhangs, if present, were ignored when measuring the width.

The upstream half of the breach channel does not scour to the base and



the invert rises slightly towards the curved upstream crest. This prevents the impoundment from draining completely and there is some residual water in the impoundment that can be observed in Fig. 3.3 (a). The water level in the impoundment at the end of the breach was recorded so that the outflow volume could be determined. Seepage flows through the barriers were small relative to the breach outflows and were ignored in estimating the outflow volume.

A video camera was placed upstream of the barrier and recorded the development of the breach and the change in water levels for each experiment.

### 3.4 Summary of experimental procedure

In summary the experimental procedure involved filling the impoundment with water to the top level of the sand barrier. A breach was then initiated through a small pilot channel. The water level at the initiation of the breach was recorded. The development of the breach and change in water levels were recorded by the video camera placed upstream of the sand barrier. At the completion of each breaching event, the final water levels within the impoundment were recorded as well as the final breach width dimension. The experiment was then repeated for different storage volumes, hydraulic heads and barrier shapes.

### 3.5 Data Processing

It was noted that the breach width measured at the upstream crest was a reasonable average of the width across the breach channel, as shown in Fig. 3.3 (a). The breach volume was therefore calculated as the measured breach width  $W$ , multiplied by the cross sectional area of the berm as

$$V_b = WA_{cross\ sectional}. \quad (3.16)$$

Video frames from the camera were extracted at regular time intervals for detailed temporal analysis. Water levels and breach widths were scaled off the video frames by counting pixels and using reference scales in the field of view. The water levels were measured from the crest of the sand barrier and the breach widths were scaled off the images following the guidelines used for measuring the final breach widths. An example of how the water levels and breach widths were scaled from the video images is shown in Fig. 3.4.

The video recordings yielded time-histories for the breach widths  $w(t)$  and water levels  $h(t)$ , for each breaching experiment. The outflow volume

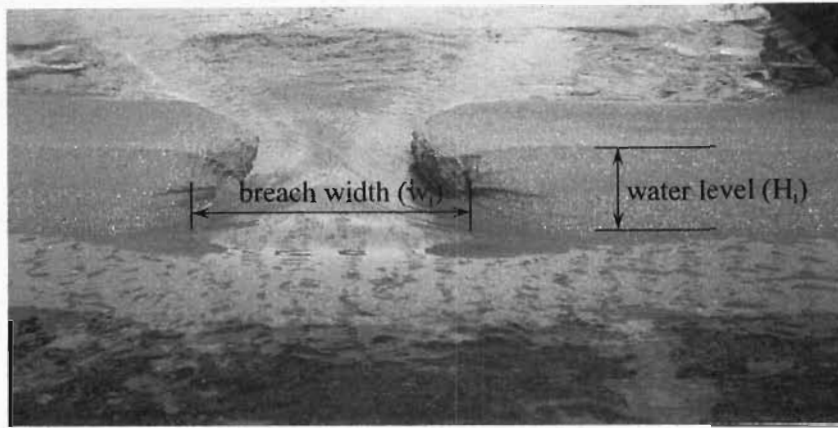


Fig. 3.4: A captured video image showing how and where the water levels and breach widths were obtained for this time step ( $t_i$ ).

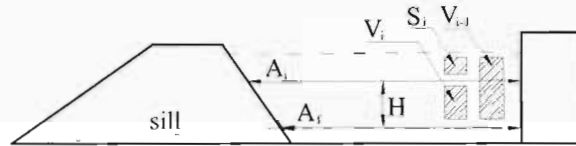


Fig. 3.5: Graphical representation of the parameters  $s_i$ ,  $H_i$ ,  $A_i$  and  $A_f$ .

$s_i$ , at any time step  $t_i$ , was calculated as the difference between the initial volume stored in the impoundment  $V_0$  and the volume  $v_i$  still stored in the impoundment at time  $t_i$  as

$$s_i = V_0 - v_i, \quad (3.17)$$

These parameters are shown graphically in Fig. 3.5. The volume stored in the impoundment at time step  $t_i$  was calculated as

$$v_i = H_i [(A_i + A_f)/2], \quad (3.18)$$

where  $H_i$  is the depth of the water at time  $t_i$ , relative to the final water level in the impoundment,  $A_i$  is the surface area of the impoundment at time  $t_i$  and  $A_f$  is the final surface area in the impoundment. These parameters are also displayed graphically in Fig. 3.5.

The data of  $w(t)$ ,  $h(t)$  and  $s(t)$  were normalized using the final breach width  $W$ , the total water level change  $H$  and the total outflow volume  $S$  re-

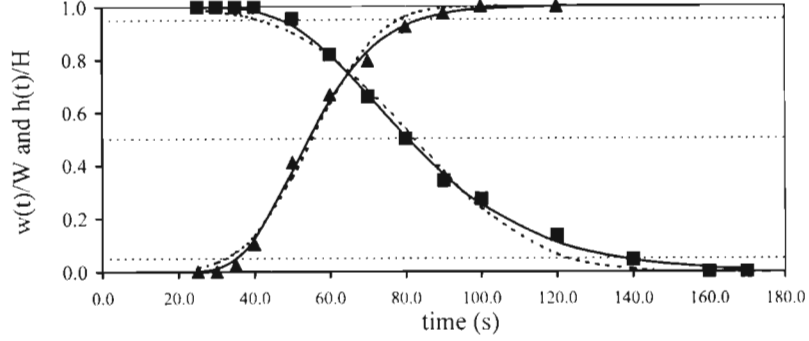


Fig. 3.6: The non-dimensional breach width (solid triangles) and water level (solid squares) data for model  $B2$ ,  $H_0 = 0.15\text{m}$ ,  $S_0 = 0.9\text{m}^3$  fitted with both the Log Normal (solid black line) and Gaussian (dashed black line) sigmoidal curves. The 5<sup>th</sup>, 50<sup>th</sup> and 95<sup>th</sup> percentile levels are shown as horizontal dashed lines for reference.

spectively. The time sequences of normalized data were then fitted with parametric sigmoidal curves using nonlinear least squares optimization. Several sigmoidal curves were tested for their efficiency in describing the temporal developments, including Gaussian, Gamma and Log-Normal (LN) functions.

The normalized breach width ( $w(t)/W$ ) and water level ( $h(t)/H$ ) data for the breaching experiment of  $B2$ ,  $H_0 = 0.15\text{m}$ ,  $S_0 = 0.9\text{m}^3$  are shown in Fig. 3.6. The Gaussian and LN functions are shown fitted to the data. It is evident in Fig. 3.6 that the data have an asymmetry that is not accounted for by the Gaussian function. The corrected Akaike information criterion (Hurvich and Tsai, 1989) was used as a metric to evaluate the most efficient curve-fit to the data. The Log-Normal sigmoid was generally found to be the most efficient fit as it captures the temporal asymmetry in the data and can be characterized by only two parameters: one that fixes the position on the time axis ( $T_{50}$ ) and the other that describes the duration or temporal width ( $T_F$ ). The LN sigmoidal function is given by

$$F(t|T_{50}, T_F) = \frac{1}{2} \left[ 1 + \operatorname{erf} \left( \frac{\ln(t) - T_{50}}{T_F \sqrt{2}} \right) \right] \quad (3.19)$$

where

$$\operatorname{erf}(x) = \frac{2}{\pi} \int_0^x e^{-t^2} .dt. \quad (3.20)$$

The outflow rate at each time step  $q(t)$  was computed by differentiating

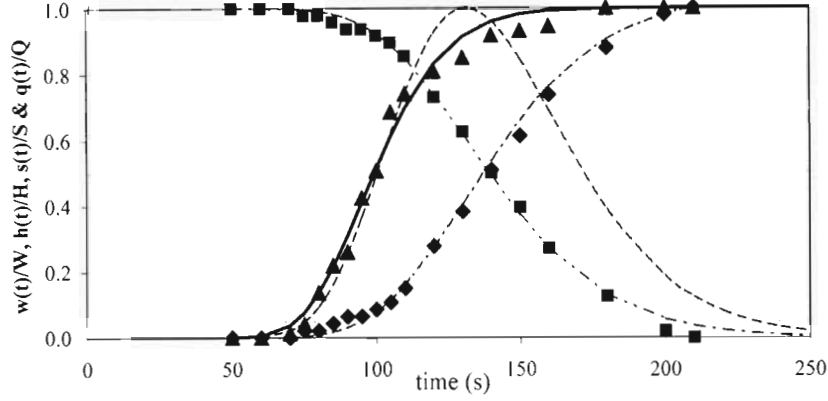


Fig. 3.7: The time history of the non-dimensional breach width (solid triangle), water level (solid squares), outflow volume (solid diamonds) and flow rate (dash dot dash line) data for model  $B2$ ,  $H_0 = 0.15\text{m}$ ,  $S_0 = 0.9\text{m}^3$ . The breach width, water level and outflow volume data are fitted with Log-Normal sigmoidal functions. The 5<sup>th</sup>, 50<sup>th</sup>, and 95<sup>th</sup> percentile levels are shown as horizontal dashed lines for reference.

the outflow volume  $s(t)$  with respect to time

$$q(t) = \frac{ds(t)}{dt}. \quad (3.21)$$

The derivative of the outflow volume  $ds(t)/dt$  was estimated by differentiating the LN curve fitted to the normalized outflow curve  $s(t)/S$ . Therefore,

$$\frac{ds(t)}{dt} = S \frac{1}{t T_F \sqrt{2\pi}} e^{-\frac{(\ln(t) - T_{50})^2}{2T_F^2}}. \quad (3.22)$$

The outflow hydrographs could therefore be plotted and the peak outflows  $Q_P$  obtained. Fig. 3.7 shows the outflow volumes  $s(t)$  and the inferred hydrograph  $q(t)$  non-dimensionalised by  $S$  and  $Q_P$  respectively for the breaching experiment of  $B2$ ,  $H_0 = 0.15\text{m}$ ,  $S_0 = 0.9\text{m}^3$ . Also shown are the data for  $w(t)/W$  and  $h(t)/H$  from Fig. 3.6

The breach formation times were initially visually estimated from the video recordings. These estimates are referred to as  $T_{F_{visual}}$ . There were difficulties in accurately estimating  $T_{F_{visual}}$  since it requires a subjective judgement of the start and end of the breach formation phase (as defined in section 2.4.2).

The start of the breach formation phase is well defined, and its detection

is not subject to large errors, because of the rapid initial changes in the width of the breach channel as is evident in Fig. 3.7. On the other hand, the asymptotic nature of the breach width development at the end of the breach formation phase means that the end of the breach formation phase is difficult to judge accurately. For example, in Fig. 3.7, at the start of the breach formation phase, a 10% change in the breach width occurs over a 10s period. In comparison, at the end of the breach formation phase a 10% change in the breach width occurs over a 40s period. The value of  $T_{F_{visual}}$  for this experiment was estimated to be 60s. It is however evident that errors of say 40% could occur as a result of different subjective judgements for the end of the breach formation phase. Therefore a more objective and robust method of determining the breach formation time was required. The method of fitting the LN sigmoidal function to the data and using the fitted curve to estimate  $T_F$  is considered to provide a more robust estimate.

The fitted LN functions can be characterized by two parameters: one that fixes the position on the time axis and the other that describes the duration or temporal width. The 50<sup>th</sup>-percentile (or median) time  $T_{50}$  was selected as a convenient time reference. Analysis of the video sequences for the breach width development indicated that the difference between the 5<sup>th</sup>-percentile time  $T_{05}$  and the 95<sup>th</sup>-percentile time  $T_{95}$  corresponded closely to subjective visual estimates of the breach formation time. Based on this,  $T_F = (T_{95} - T_{05})$  was used as the estimate of the breach formation time. The times  $T_{05}$  and  $T_{95}$  were obtained from least-squares fitting of the sigmoidal curves to each sequence of breach width measurements. This definition implies that  $T_F$  represents the time required for 90% of the breach width development to occur. A comparison between the visually estimated breach durations, denoted  $T_{F_{visual}}$  and the times  $T_F$  inferred from the fitted sigmoidal curves is shown in Fig. 3.8 where it can be seen that there is a satisfactory correspondence. A large portion of the scatter in the data is due to difficulties in accurately estimating  $T_{F_{visual}}$  since it requires subjective judgement of the start and end of the breach formation phase.

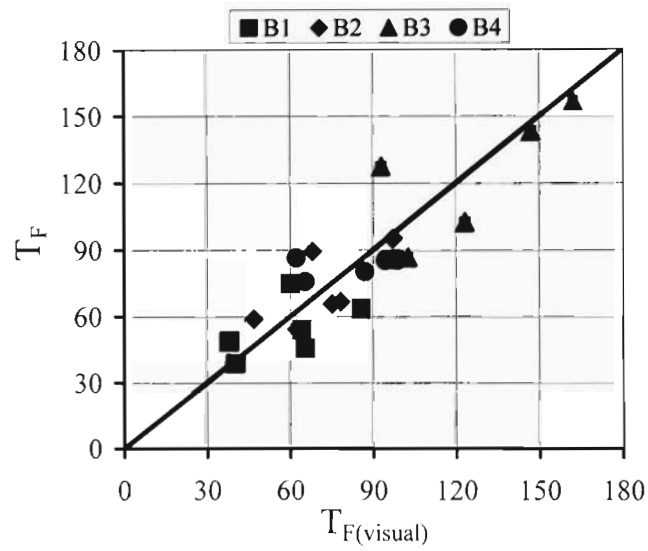


Fig. 3.8: The visually estimated breach formation times,  $T_{F(\text{visual})}$  plotted against the timescale estimated from the fitted LN sigmoidal curves  $T_F = (T_{95} - T_{05})$ . Symbols refer to different barrier shapes (see Table 1).

---

## CHAPTER 4

### RESULTS

---

In section 4.1 the observed breaching process is discussed using a representative sample from the model experiments for illustrative purposes. In section 4.2 the main quantitative results characterizing the breach development are presented. In section 4.3.1 the data from the model experiments are used to investigate the scaling of the breach widths and breach volumes. In section 4.3.4 the model data are used to investigate the scaling of the breach formation times and peak outflows. Finally in sections 4.5.1 and 4.5.2 data from full scale observations are used together with the model data to test the scalings deduced from the laboratory experiments. The results presented in this chapter have been published in the papers by Stretch and Parkinson (2006) and Parkinson and Stretch (2006) which are reproduced in Appendix B.

#### 4.1 Observed breaching process

The breaching process can be broadly considered to comprise two main phases - a breach initiation phase followed by a breach formation phase (Wahl, 1998). During the initiation phase the overtopping flow gradually scours a channel on the downstream face of the barrier while the upstream crest remains relatively intact. The upstream water level does not change significantly during this phase. Once the upstream crest of the barrier begins to erode, it signals the start of the breach formation phase.

As scouring lowers the upstream crest, the volume of water entering the breach channel increases which in turn increases the rate of scour. The size of the breach grows rapidly during this phase, both deepening and widening. Strong velocities and turbulence at the bottom of the downstream face cause the toe of the channel to erode upstream along the base to a pivot point. As the channel bed is eroded about the pivot point, the slope of the channel bed

decreases, as illustrated in Fig. 2.7. The crest of the breach moves upstream as it erodes because of the sloping upstream face of the barrier. The upstream water level decreases as the breach widens and the outflow increases. The falling head causes the velocity of the water in the channel to decrease. The rate of scour decreases with the decreasing velocity of the water and the breach width attains a maximum value. This signals the end of the breach formation phase.

The process described here is qualitatively similar to the breaching of small-scale sand barriers described by Coleman et al. (2002) as discussed in section 2.6.

Fig. 3.7 shows the normalized breach widths, water levels, outflow volumes and hydrograph for the breaching experiments of barrier  $B2$ ,  $H_0 = 0.15\text{m}$ ,  $S_0 = 0.9\text{m}^3$ . It can be seen that the temporal evolution of the breach width, water level and outflow volume all have a sigmoidal shape although they exhibit temporal asymmetry in which the most rapid changes occur during the initial phases of their development. The breach width begins developing first and it develops most rapidly, reaching about 70% of its final value while the water levels and outflow volumes are still within 30% of their initial values. The outflow hydrograph shows that the peak flow occurs during the final stages of the breach development where the breach width already exceeds about 80% of its final value.

Fig. 4.1 gives a corresponding visual record of the same experiment as Fig. 3.7. Figs. 4.1 (a) and (b) show the breach in its *initiation phase*. It can be seen that the overflow is gradually scouring a channel into the downstream face of the barrier while the upstream crest remains intact. This phase corresponds to times between  $t \approx 70\text{s}$  in Fig. 3.7 where it is evident that the outflows at this time are low and that water levels have not yet changed significantly.



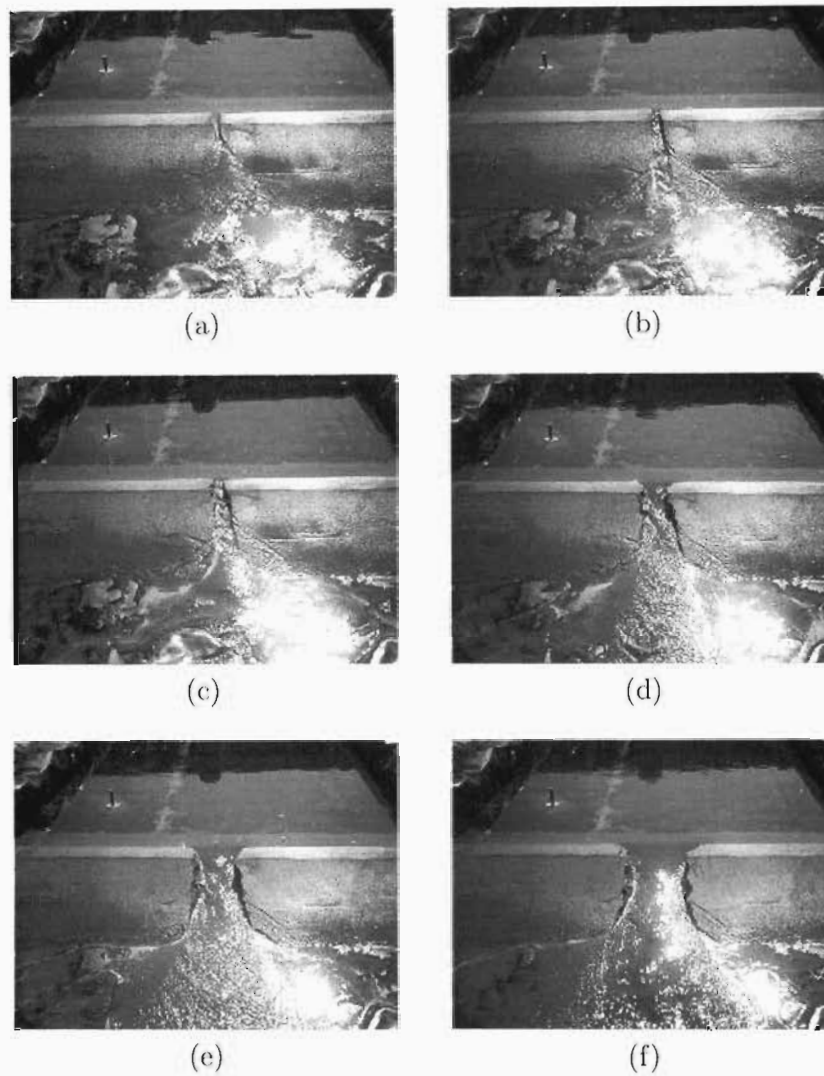


Fig. 4.1: Photo sequence of a breaching experiment (berm B2,  $H_0 = 0.15\text{m}$ , bay area of  $3\text{m} \times 2\text{m}$ ). The berm is in the foreground with the rectangular storage basin behind. (a) and (b) show the breach in its *initiation* phase while (c), (d), (e) and (f) show the breach in its *formation* phase.

Fig. 4.1 (c) shows the breach near the start of its *formation* phase. The upstream crest of the breach channel has begun to erode and the rate of widening and deepening of the channel has increased. This corresponds to time  $t \approx 80$ s in Fig. 3.7 where it is evident that the flow rate and the rate of widening of the breach channel has started to rapidly increase. The additional volume of water entering the channel increases the rate of scour causing it to widen and deepen, allowing more water into the breach. This cycle causes the rapid widening of the breach channel that is evident in Fig. 3.7 between times  $t \approx 80$ s and  $t \approx 130$ s which corresponds to Fig. 4.1 (d),(c) and (f).

As the water level in the storage basin drops, the reduced hydraulic head causes the velocity of the flow through the breach channel to decrease. This in turn reduces the rate of scour. In Fig. 3.7 the rate of widening of the breach channel begins to decrease at  $t \approx 110$ s. Once the breach attains its maximum width the breach formation phase ends. In Fig. 3.7 this occurs at about  $t \approx 150$ s (Fig. 4.2). Therefore, the time period from  $t \approx 80$ s to  $t \approx 150$ s (i.e. an elapsed time of 70s) is the visually estimated breach formation time for this experiment denoted  $T_{F_{visual}}$ .

From Fig. 3.7 it can be seen that approximately 30% of the outflow volume still remains in the impoundment at the end of the breach formation phase. Fig. 4.2 shows the breach at the end of the formation phase. It is evident that there is still a significant amount of water in the impoundment and that there is still significant flow through the breach channel. Fig. 4.2 also shows the hourglass or venturi shape of the breach channel, in plan view, at the end of the breach formation time.

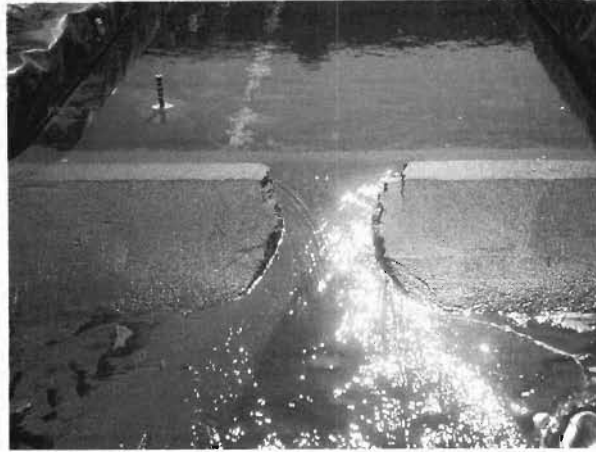


Fig. 4.2: Photo of the berm B2,  $H_0 = 0.15\text{m}$ ,  $S_0 = 0.9\text{m}^3$  at the end of the breach formation phase. The berm is in the foreground with the rectangular storage basin behind.

## 4.2 Quantitative features of the breach process

Fig. 4.3 shows all the breach width development data ( $w(t)$ ) for all the experiments plotted in non-dimensional form. Note that the self-similar nature of the breach width development is evident by the collapse of all the data onto a single curve, despite variations in the barrier shapes and outflow volumes (refer Table 1).

Fig. 4.4 shows all the water level ( $h(t)$ ), outflow measurements ( $s(t)$ ) and hydrographs ( $q(t)$ ) plotted in non-dimensional form. Note that the hydrographs exhibit a temporal asymmetry with the peaks occurring before the median reference times.

A composite picture representing an average of all the data from our experiments is given in Fig. 4.5 so that the temporal relationships between different characteristics of the breaching event can be clearly seen. The  $T_{50}$  time for each breach width development sequence was used as a reference time in the plot, while the average breach formation time  $T_{Average}$  is used to scale the times. The data points (shown previously in Figs. 4.3 and 4.4) have been omitted for clarity. Fig. 4.5 summarizes the main features of the

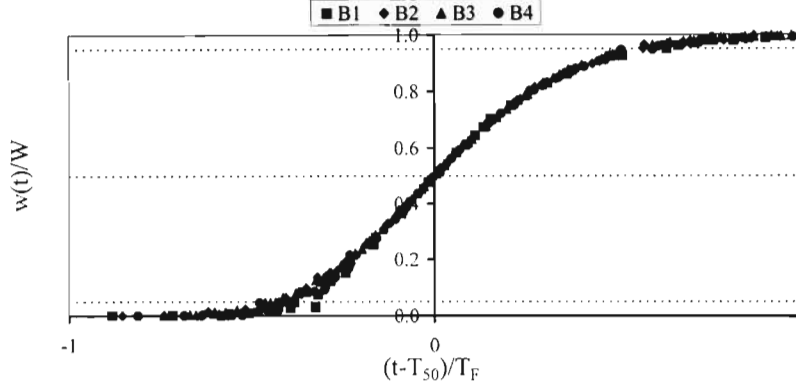


Fig. 4.3: Breach width measurements presented in non-dimensional form: breach widths are normalized by the final breach width, and time is normalized by the breach formation timescale  $T_F = (T_{95} - T_{05})$  with the median time  $T_{50}$  as the time origin. Symbols refer to different barrier shapes as indicated in Table 1. The 5<sup>th</sup>, 50<sup>th</sup> and 95<sup>th</sup> percentile levels are shown as horizontal dashed lines for reference.

breach development, notably

- the temporal asymmetry in the breach development,
- the shorter timescale for the breach width changes compared to that for the water level (or outflow volume) changes - breach widths reach 70% of their final values while water levels and outflow volumes are still within 30% of their initial values,
- the temporal lag between changes in the breach width and the water levels (or outflow volumes) - significant water level changes begin after a time-lag of about  $1/3 T_F$  following the beginning of the breach formation phase,
- the peak outflow occurs late in the development of the breach width, when it is within about 20% of its final equilibrium value,
- a significant proportion of the outflow (about 30%) occurs after the breach width has reached its final equilibrium value.

As observed in Fig. 4.5, the timescale of the breach width changes is significantly shorter than that of the water level changes and/or outflow volumes. The timescales are compared in Fig. 4.6. It can be seen that the

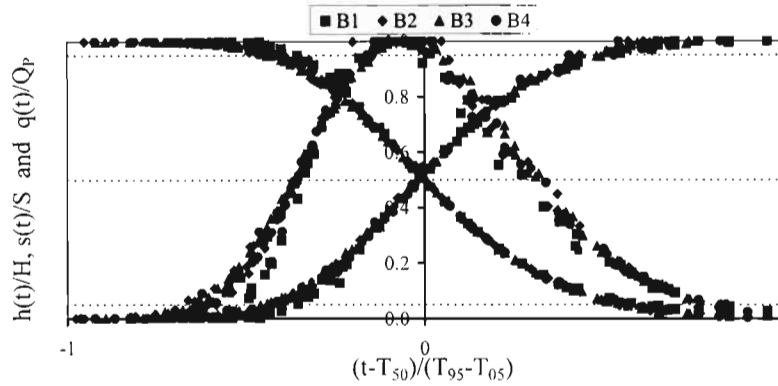


Fig. 4.4: Combined measurements of water levels and outflow volumes for all the experiments, plotted in non-dimensional form. The computed outflow hydrographs are also shown, non-dimensionalised by the peak outflows  $Q_P$ . Time is non-dimensionalised by the timescale  $(T_{95} - T_{05})$  inferred from sigmoidal curves fitted to the outflow volumes. Symbols refer to different barrier shapes as indicated in Table 1. The 5<sup>th</sup>, 50<sup>th</sup> and 95<sup>th</sup> percentile levels are shown as horizontal dashed lines for reference.

duration of the water level changes (or outflows) are on average about 50% longer than that for the breach widths.

We note that the temporal relationships between changes in breach widths, water levels, and outflow volumes may be expected to vary with the morphology of the impounded storage volume. In our model experiments, the storage volume is nearly linearly related to the water depth. This may not be representative of natural estuaries and lagoons implying that some of these results could have limited generality.

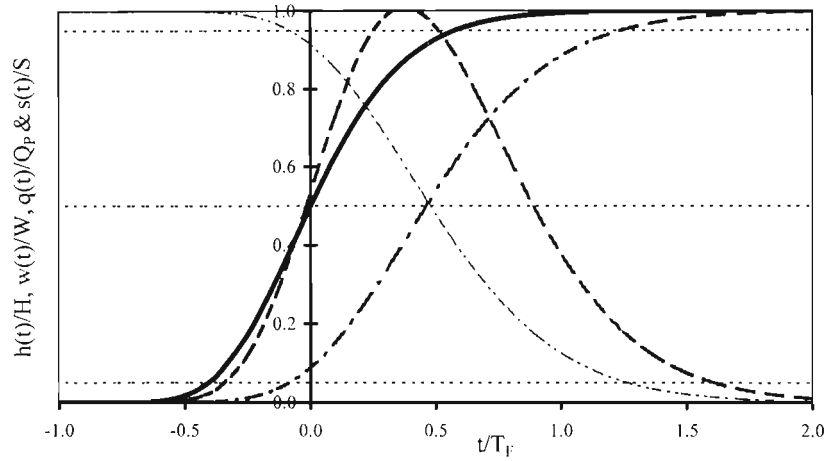


Fig. 4.5: A non-dimensional composite plot constructed from averaging the time-histories of the breach widths (heavy solid line), outflow volumes (dash-dotted line), water levels (dash-dot-dot line), and outflow hydrographs (dashed line). The 5<sup>th</sup>, 50<sup>th</sup> and 95<sup>th</sup> percentile levels are shown as horizontal dashed lines for reference.

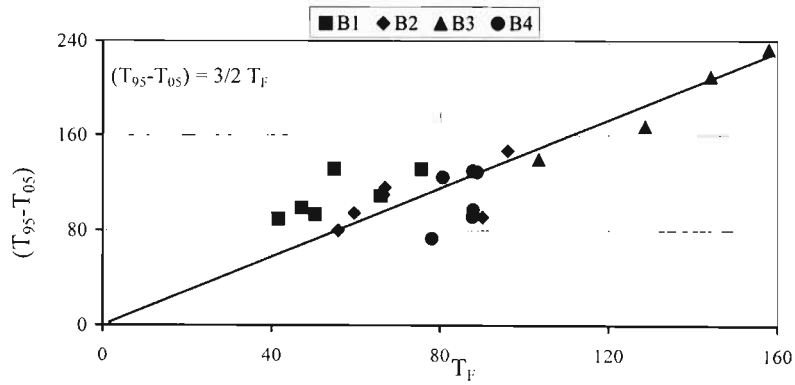


Fig. 4.6: Comparison of the timescales for breach width development  $T_F$  and for the water level variations (or outflow volumes). In both cases the time differences  $(T_{95} - T_{05})$  inferred from the respective fitted sigmoidal curves are used. The line shown has a slope of  $3/2$ .

## 4.3 Scaling results from model data

### 4.3.1 Breach widths

In order to test the scaling relationship given by Eq. (3.5) the measured breach widths  $W$ , non-dimensionalized by the length scale  $S^{1/3}$ , are shown plotted against the non-dimensional hydraulic head  $H/S^{1/3}$  and barrier breadth  $B/S^{1/3}$  in Fig. 4.7 (a) and (b) respectively.

It can be seen in Fig. 4.7 (a) and (b) that the non-dimensional breach width is approximately constant and does not appear to vary with either  $H/S^{1/3}$  or  $B/S^{1/3}$ . The data are scattered around a horizontal line implying that  $W/S^{1/3}$  is independent of  $H/S^{1/3}$  and  $B/S^{1/3}$ . Therefore,  $f_5 \simeq \text{constant}$  (Eq. (3.5)) is a good description of the data.

From these results, it would appear that, for similar barrier shapes and for barrier breadths  $0.5 < B/S^{1/3} < 2.0$  and hydraulic heads  $0.07 < H/S^{1/3} < 0.22$ , the breach width scales approximately on the cube-root of the outflow volume namely

$$W = C_W S^{1/3} \quad (4.1)$$

where  $C_W$  is the scaling constant and equal to  $0.38 \pm 0.05$  ( $\pm$  one standard deviation) i.e., the coefficient of variation was 15%.

This immediately raises the interesting question, does this result apply at intermediate times during the development of the breach? In other words, is the breach width during the breach development in ‘‘equilibrium’’ with the outflow volume that has passed through the breach up to that time?

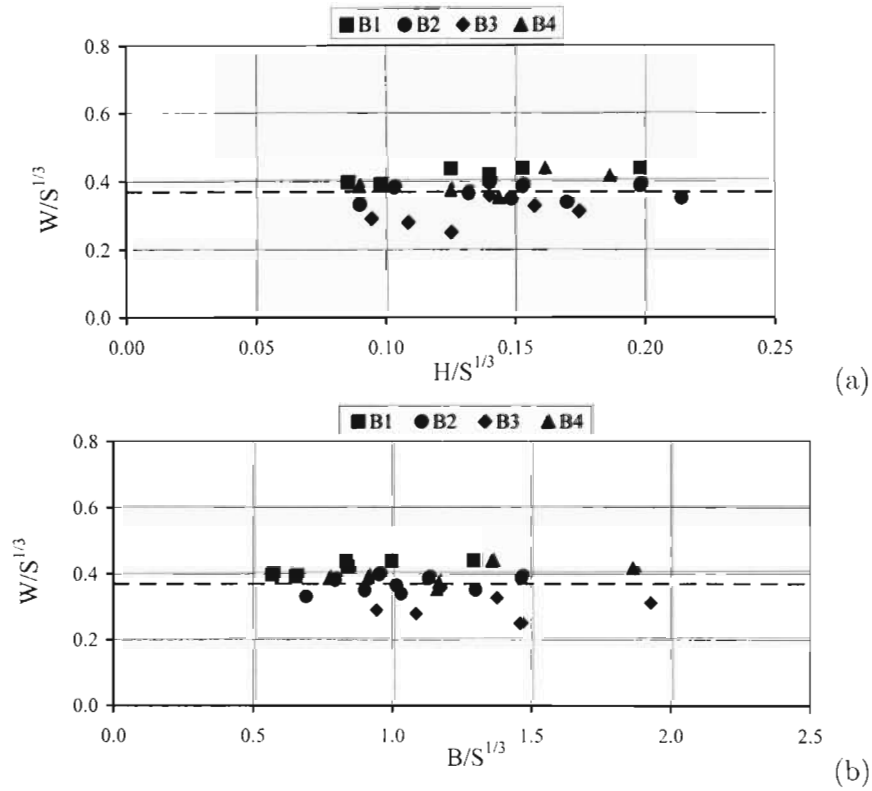


Fig. 4.7: Non-dimensional breach widths from the model experiments, plotted against (a)  $H/S^{1/3}$ , and (b)  $B/S^{1/3}$ . The horizontal dashed line represents the average value of the model data and is equal to the scaling coefficient  $C_W = 0.38$ . The symbols correspond to different berm shapes as listed in Table 1.



### 4.3.2 Breach development with time

Fig. 4.8 shows a normalized plot of the breach width development  $w(t)/W$  against the outflow volume  $s(t)/S$ . It can be seen that the breach channel width is not proportional to the cube root of the outflow volume at intermediate times (as represented by the solid curve in Fig. 4.8), but is generally greater than predicted by this scaling. From Fig. 4.8 it is apparent that the breach width develops in an exponential manner (dashed curve in the figure) and approaches its final value asymptotically. This observation is consistent with the notion that the scouring of the breach channel depends on exceeding a critical velocity (or shear stress). Flow velocities in the breach channel depend on the available hydraulic head which is greatest at inception of the breach formation. In the later stages of the breach formation, when water levels have reduced, the velocities in the breach channel are too low to sustain high scour rates and the rate of change of the breach width approaches zero. This effect is not captured by the cube root scaling which suggests more sustained scour rates in the final stages of the breach development.

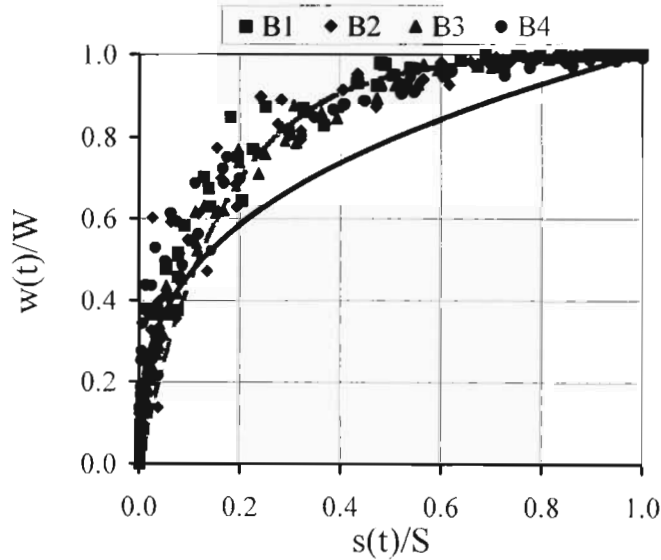


Fig. 4.8: The non-dimensional breach width plotted against the non-dimensional outflow volume. The solid line represents a  $1/3$  power law while the red dashed line is Eq. 4.2 with  $k = 6$ . The symbols correspond to different berm shapes as listed in Table 1.

As shown in Fig. 4.8, the data can be approximated by an exponential

curve

$$w(t)/W = \left(1 - e^{-k\frac{s(t)}{S}}\right), \quad (4.2)$$

with  $k \simeq 6$ . This is a solution to the differential equation

$$dw/ds = k (W/S) (1 - w(t)/W). \quad (4.3)$$

Using the relationship  $ds = q(t) dt$  it follows that

$$dw/dt = k q(t) W/S (1 - w(t)/W). \quad (4.4)$$

This equation has a similar form to the model suggested by Kraus (2003) (Eq. (2.11)) for breach channel growth in coastal barriers.

### 4.3.3 Breach volumes

The non-dimensional breach volumes  $V_b/S$  are shown in Fig. 4.9 (a) and (b) plotted against  $H/S^{1/3}$  and barrier breadth  $B/S^{1/3}$  respectively. It can be seen in Fig. 4.9 that  $V_b$  has an almost linear dependence on both  $H/S^{1/3}$  and  $B/S^{1/3}$ . If both relationships are assumed to be linear then,

$$\frac{V_b}{S} \propto \frac{H}{S^{1/3}} \quad \text{and} \quad \frac{V_b}{S} \propto \frac{B}{S^{1/3}} \quad (4.5)$$

from which it follows that

$$\frac{V_b}{HBS^{1/3}} = \text{constant}. \quad (4.6)$$

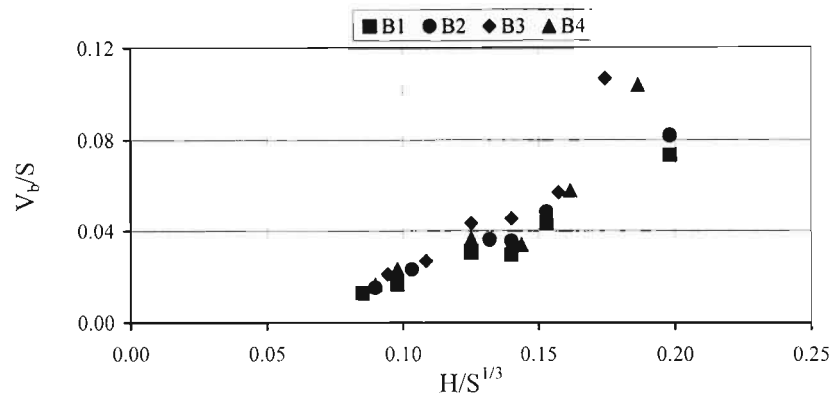
Fig. 4.10 (a) and (b) shows  $V_b/HBS^{1/3}$  plotted against  $H/S^{1/3}$  and  $B/S^{1/3}$  respectively. It is evident in Fig. 4.10 (a) and (b) that  $V_b/HBS^{1/3}$  is approximately constant and independent of  $H/S^{1/3}$  and  $B/S^{1/3}$  respectively. Therefore  $V_b/HBS^{1/3} \simeq \text{constant}$  is a good description of the data.

It is intuitive that the volume of sediment removed from the sand barrier during a breach is proportional to the cross sectional area of the sand barrier and the width of the breach channel,  $V_b \propto HBW$ . From the breach width investigation,  $W$  was found to be proportional to  $S^{1/3}$ . Therefore it would be expected that  $V_b \propto HBS^{1/3}$ . Therefore  $V_b/HBS^{1/3}$  should be independent of other parameters. This is confirmed in Fig. (4.10) (a) and (b) where it is clear that  $V_b/HBS^{1/3}$  does not vary with either  $H/S^{1/3}$  or  $B/S^{1/3}$  respectively.

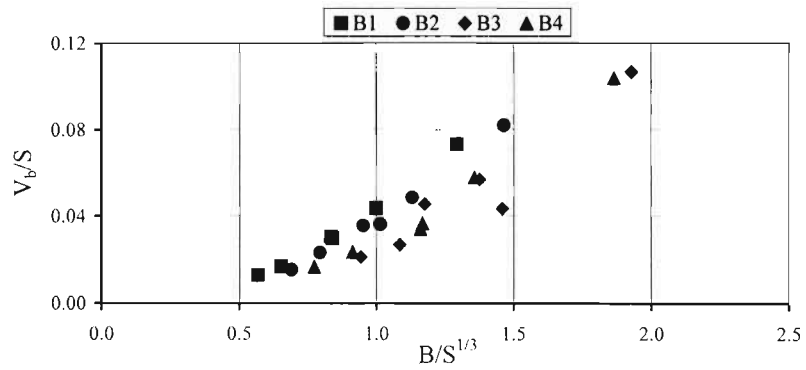
From these results it appears that the breach volume scales approximately on  $HBS^{1/3}$ . Therefore

$$V_b = C_V HBS^{1/3} \quad (4.7)$$

where  $C_V$  is the scaling constant and equal to  $0.26 \pm 0.03$  ( $\pm$  one standard deviation) i.e., the coefficient of variation was 10%.



(a)



(b)

Fig. 4.9: Breach volumes from the model experiments non-dimensionalised by  $S$ , plotted against (a)  $H/S^{1/3}$ , and (b)  $B/S^{1/3}$ . The symbols correspond to different berm shapes as listed in Table 1.

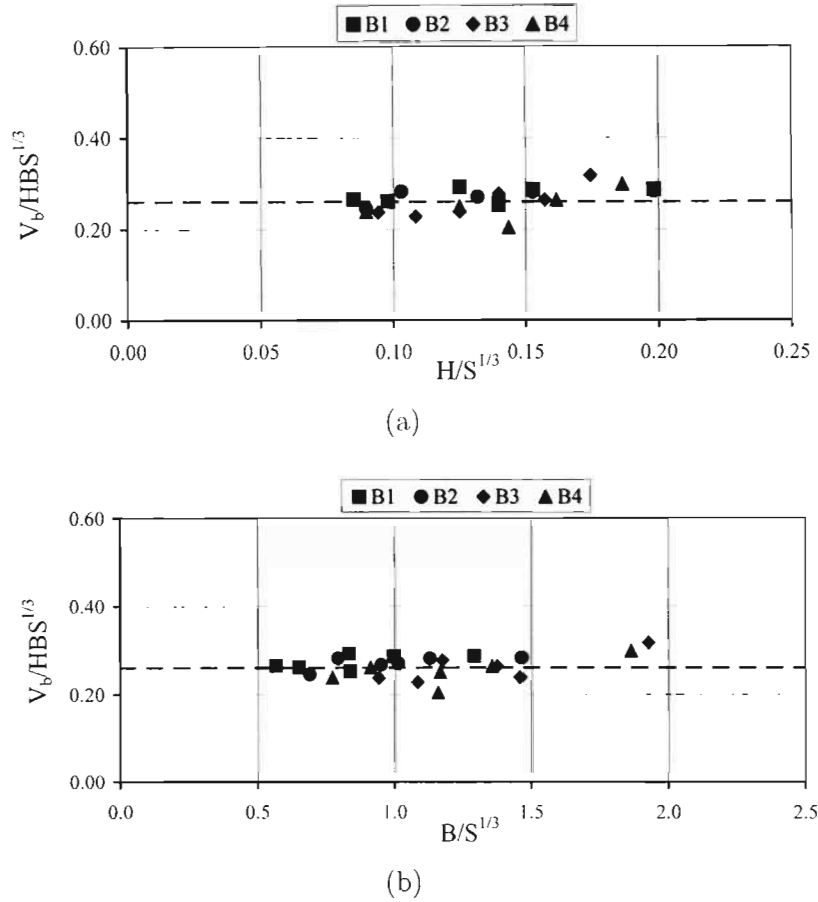


Fig. 4.10: Breach volumes from the model experiments non-dimensionalised by  $HBS^{1/3}$ , plotted against (a)  $H/S^{1/3}$ , and (b)  $B/S^{1/3}$ . The horizontal dashed line represents the average value of the model data and is equal to the scaling co-efficient  $C_v = 0.26$ . The symbols correspond to different berm shapes as listed in Table 1.

### 4.3.4 Breach formation times and peak outflows

Having obtained estimates of the breach formation times  $T_F$  and peak outflows  $Q_P$ , for each breach experiment, the data can be used to test the scaling relationships suggested in section 3.1.

In Fig. 4.11 the breach formation times  $T_F$  are shown non-dimensionalised by the timescale  $T_{-1,0}$  (given by Eq. (3.12) with  $\alpha = -1$  and  $\gamma = 0$ ) plotted against (a)  $H/S^{1/3}$  and (b)  $B/S^{1/3}$ . Similarly, Fig. 4.12 shows the measured peak outflows  $Q_P$  non-dimensionalised by the flow scale  $Q_{-1,0}$  (from Eq. (3.14) with  $\alpha = -1$  and  $\gamma = 0$ ) plotted against (a)  $H/S^{1/3}$  and (b)  $B/S^{1/3}$ . This choice of the parameters  $\alpha$  and  $\gamma$  corresponds approximately to the scaling proposed by Froehlich and Webby (see section 2.4.1).

In Fig. 4.11 there is a trend in the model data, with  $T_F/T_{-1,0}$  increasing with increasing  $H/S^{1/3}$  and  $B/S^{1/3}$ . In particular the trend is evident in Fig. 4.11 (b). This suggests that there is some dependence of  $T_F$  on  $H$  and  $B$  that is not accounted for by the timescale  $T_{-1,0}$ . The average value of  $T_F/T_{-1,0}$  is  $39 \pm 18$ . Therefore the co-efficient of variation is 45%.

In Fig. 4.12 there is a weak trend with  $Q_P/Q_{-1,0}$  decreasing with increasing  $H/S^{1/3}$  and  $B/S^{1/3}$ , once again this trend is more evident in Fig. 4.12 (b). The average value of  $Q_P/Q_{-1,0}$  is  $0.023 \pm 0.008$  therefore the co-efficient of variation is 35%.

By a process of (manual) optimization the values of  $\alpha$  and  $\gamma$  were varied to reduced the coefficient of variation of  $T_F/T_{\alpha,\gamma}$  and  $Q_P/Q_{\alpha,\gamma}$  to a minimum. The values of  $\alpha$  and  $\gamma$  which produced the minimum variation were  $\alpha = -1.5$  and  $\gamma = 1$ .

Fig. 4.13 shows  $T_F/T_{-1.5,1}$  plotted against (a)  $H/S^{1/3}$  and (b)  $B/S^{1/3}$ . In this case the trend that was apparent in Fig. (4.11) has been reduced, particularly in Fig. 4.13 (b). Nearly all the improved correlation is due to the dependence on the barrier breadth  $B$  through the non-zero  $\gamma$  value. The average value for  $T_F/T_{-1.5,1}$  was  $13 \pm 2.9$  and the co-efficient of variation is 23%. The values of the co-efficients of variation for the breach formation timescales have been reproduced in Table 4.1 for comparison.

Fig. 4.14 shows  $Q_P/Q_{-1.5,1}$  plotted against (a)  $H/S^{1/3}$  and (b)  $B/S^{1/3}$ . It is evident that there are no obvious trends in the figure and the average value of  $Q_P/Q_{-1.5,1}$  is  $0.065 \pm 0.017$  and the co-efficient of variation is 26%. The values of the co-efficients of variation, for the peak outflows, have also been reproduced in Table 4.1 for comparison.

These results suggest that breach formation times  $T_F$  and peak outflows  $Q_P$  can be scaled as suggested in section 3.1, and that the values of  $\alpha = -1.5$  and  $\gamma = 1$  for the scales provide good results. The non-zero value for  $\gamma$  suggests a dependence on the barrier breadth  $B$  that should be accounted

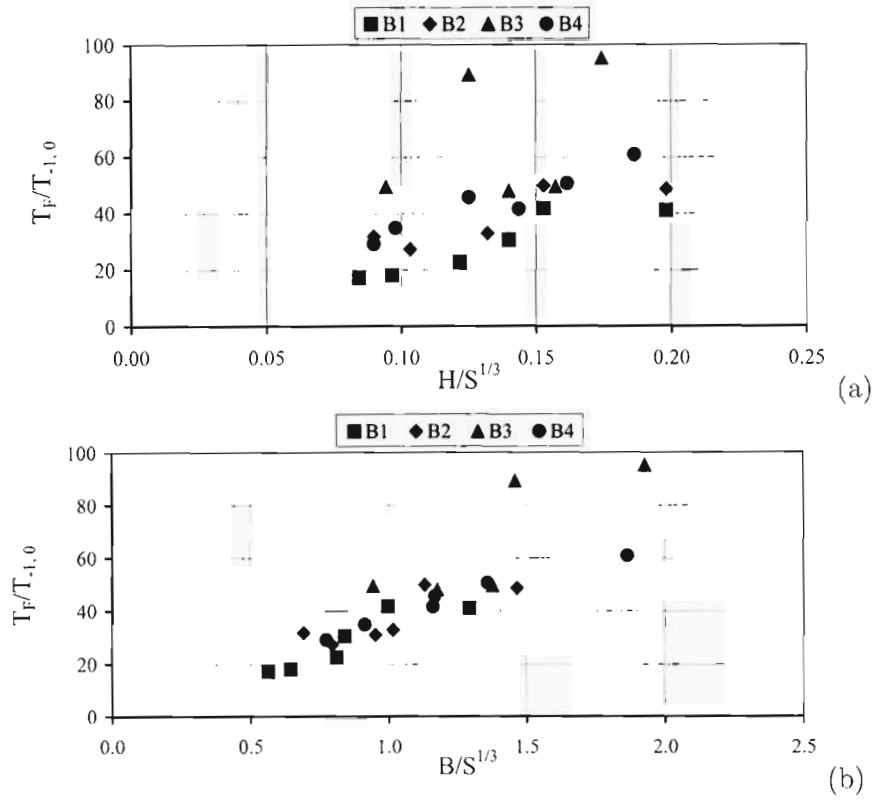


Fig. 4.11: The breach formation times non-dimensionalised by the timescale given by Eq. 3.3 with  $\alpha = -1.0$ ,  $\gamma = 0$  plotted against (a)  $H/S^{1/3}$  and (b)  $B/S^{1/3}$ . The symbols correspond to different berm shapes as listed in Table 1.

for and gives improved results over previously suggested models (Froehlich, 1987, 1995a,b; Webby, 1996).

These scaling results for the breach characteristics will be further tested using full-scale data (from actual estuaries and dam failures) in chapter 5.

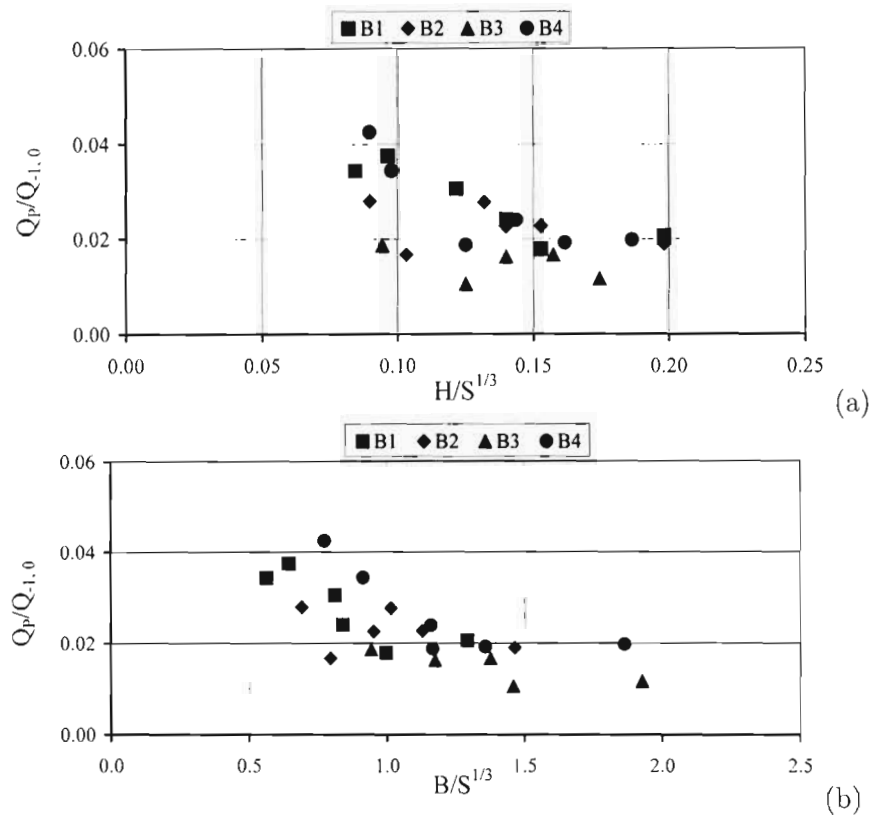


Fig. 4.12: The Peak outflows non-dimensionalised by the outflow scale given by Eq. 3.14 with  $\alpha = -1.0$ ,  $\gamma = 0$  plotted against (a)  $H/S^{1/3}$  and (b)  $B/S^{1/3}$ . The symbols correspond to different berm shapes as listed in Table 1.

Function	Co-efficient of variation
$T_F/T_{-1,0}$	45%
$T_F/T_{-1.5,1}$	23%
$Q_P/Q_{-1,0}$	35%
$Q_P/Q_{-1.5,1}$	26%

Tab. 4.1: Comparison of co-efficients of variation



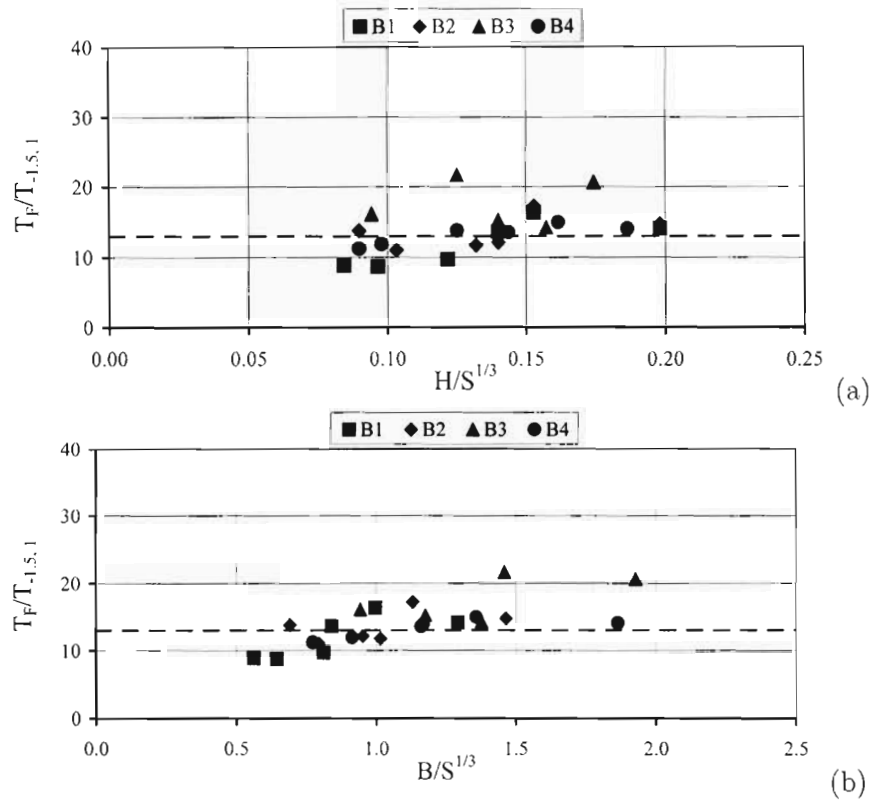


Fig. 4.13: The breach formation times plotted against the timescale given by Eq. 3.12 with  $\alpha = -1.5$ ,  $\gamma = 1$  plotted against (a)  $H/S^{1/3}$  and (b)  $B/S^{1/3}$ . The horizontal dashed line represents the average value of the model data and is equal to the scaling co-efficient  $C_T = 13$ . The symbols correspond to different berm shapes as listed in Table 1.

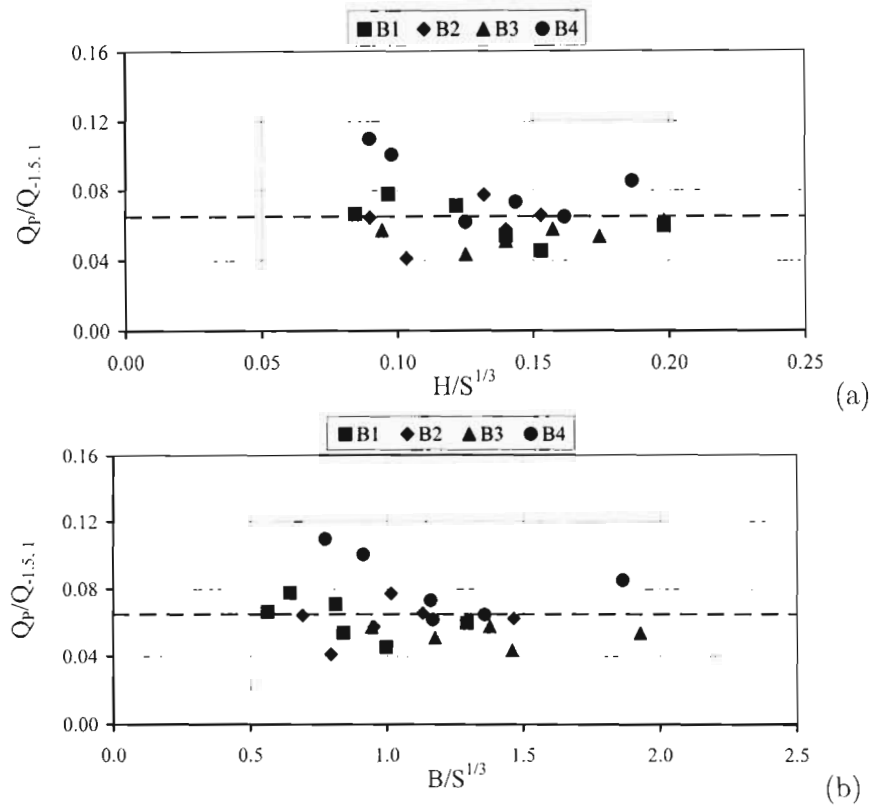


Fig. 4.14: The Peak outflows non-dimensionalised by the outflow scale given by Eq. 3.14 with  $\alpha = -1.5$ ,  $\gamma = 1$  plotted against (a)  $H/S^{1/3}$  and (b)  $B/S^{1/3}$ . The horizontal dashed line represents the average value of the model data and is equal to the scaling co-efficient  $C_Q = 0.067$ . The symbols correspond to different berm shapes as listed in Table 1.

## 4.4 Obtaining full scale data

A rigorous test of the simple scaling relationships suggested by the model breaching experiments requires data from a much broader range of scales than are possible with laboratory experiments alone. The range of scales can be dramatically extended by comparing the model data with data from barrier breaching at full-scale estuaries and from earth dam failures. For dams and estuaries length scales are typically two orders of magnitude larger than for the model experiments and volumes are six orders of magnitude larger.

As discussed in section 2.4 there are some differences between earth fill dams and natural sand barriers but the overall conceptual similarity between the breaching of coastal sand barriers and the failure of earth-fill dams, justifies a comparison between them in terms of the scaling results considered here.

### 4.4.1 Estuary data: breach widths and volumes

Detailed observational data for breach characteristics at actual estuaries or coastal lagoons are rare and usually do not include sufficient information for a comparison with the present model experiments. However, five examples have been obtained and the relevant information is summarized in Table 2. The information for Mhlanga and Mdloti estuaries, situated adjacent to each other on the East coast of South Africa, were obtained from a detailed study reported by Perissinotto et al. (2004), Stretch and Zietsman (2004), and Zietsman (2004). The information for the breaching of the Bot River estuary, situated on the Western coast of South Africa, was obtained from a study reported by van Nickerk et al. (2005). The breaching of the Wamberal Lagoon situated in South Eastern Australia, is reported by Odd et al. (1995). The last example, reported by Kraus et al. (2002), consists of post-breach observations made at Stone Lagoon, in Northern California. Note that the data in Table 4.2 are subject to considerable uncertainty since in some cases (e.g., areas and volumes) they were inferred from secondary information, such as maps and pictures.

### 4.4.2 Estuary Data: breach formation times and peak outflows

The infrequent and irregular occurrences of natural estuary breachings means that direct observations of these events are difficult to make. However, a continuous water level monitor was installed at the Mhlanga estuary during a

Name	Area (ha)	Storage (Mm <sup>3</sup> )	H (m)	Berm breadth (m)	Breach width (m)	Breach volume (m <sup>3</sup> )
Mhlanga	70	0.750	2.5	30	30	1400
Mdloti	80	0.900	2.5	40	30	1500
Stone	300	10.00	3.5	100	90	18000
Wamberai	50	1.375	2.8	70	50	5250
Bot River	1000	31.5	2.7	190	95	23085

Tab. 4.2: Breach parameters for natural lagoons and estuaries

recent field study reported by Perissinotto et al. (2004); Stretch and Zietsman (2004); Zietsman (2004). Water level records for three breaching events were captured by the water level monitor.

In order to estimate a breach formation time for the Mhlanga estuary from the water level records, the data were fitted with Log-Normal sigmoidal curves to estimate  $(T_{95} - T_{05})$  for each breach. The relationship shown in Fig. 3.8 between the time scale for the water level variations and  $T_F$  (based on the model experiments) was then used to estimate a breach formation time for the estuary. This procedure yielded an estimate of  $T_F \simeq 1\frac{1}{2}$  hours. Outflow hydrographs were computed using the same method as for the model experiments. Fig. 4.15 shows a sample of the recorded water levels for one of the Mhlanga estuary breaches and the associated outflow hydrograph, non-dimensionalised by  $H$  and  $Q_P$  respectively. The estimated peak outflow was  $210 \text{ m}^3/\text{s}$ . The same procedure was applied to field data from the Wamberal lagoon (Odd et al., 1995) and  $T_F$  was estimated as  $1\frac{3}{4}$  hours with peak outflow estimated as  $111 \text{ m}^3/\text{s}$ . In this case the outflows were also measured directly as part of the field study and a peak outflow of  $105 \text{ m}^3/\text{s}$  was reported, which corroborates our estimate.

#### 4.4.3 Earth dam data

Wahl (1998) compiled a database of 108 dam failures. The dam failure data comes from a number of sources including those previously compiled by Froehlich (1987, 1995b). Only a subset of the database is useful in this study because the required information is missing in some cases. Furthermore, only failures involving homogeneous earth fill dams (no clay core-walls) were

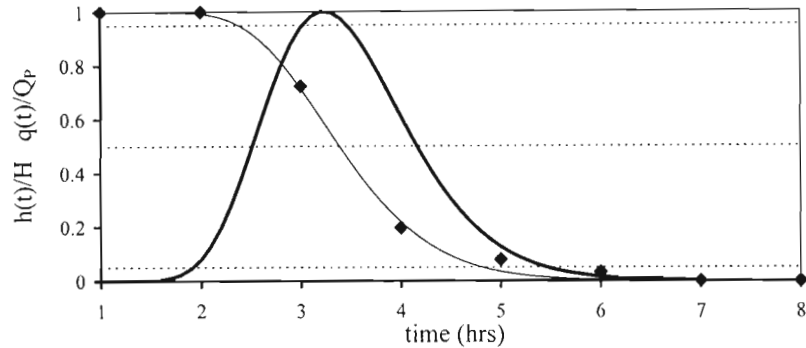


Fig. 4.15: Recorded water levels for a natural breaching event at the Mhlanga estuary, plotted in nondimensional form. The fitted Log-Normal sigmoidal curve is shown (thin solid black line) together with the associated outflow hydrograph (thick solid black line).

considered since they are more similar to coastal sand barriers.

Wahl (1998) cautions that some of the data are probably subject to large errors. For example peak outflows were estimated by various methods, often at some distance downstream of the dam break. Breach formation times were usually obtained from eye witness accounts after the dam break event and it is possible that the observers would not have been able to accurately discern the breach initiation phase from the formation phase. Despite these and other uncertainties the value that the additional range of data adds outweighs these uncertainties.

## 4.5 Scaling results from full scale data

### 4.5.1 Breach widths and volumes

The breach width  $W$  and breach volume  $V_b$  data for earth dams compiled by Wahl (1998) and the full scale estuary data are shown plotted in non-dimensional form in Figs. 4.16 and 4.17 respectively. The model data is also reproduced for comparison. It is evident in the figures that the full scale data are remarkably consistent with the experimental data. This provides strong support for the applicability of the scalings inferred from the model experiments.

In particular, there is no obvious variation in the non-dimensional breach

widths  $W$  and volumes  $V_b$  with the hydraulic head  $H$  and barrier breadth  $B$ . From these results it may be concluded that the breach width  $W$  scales like

$$W = C_W S^{1/3} \quad (4.8)$$

where  $C_W$  for all the data is  $0.33 \pm 0.11$  with a coefficient of variation equal to 35% and breach volume  $V_b$  scales like

$$V_b = C_V HBS^{1/3}. \quad (4.9)$$

where  $C_V$  for all the data is  $0.21 \pm 0.12$  with a coefficient of variation of 54%. It is evident in Fig. 4.17 there is an outlying data point which is largely responsible for the high co-efficient of variation.

Based on the available data, these results are applicable to the breaching of cohesionless sand barriers with parameter ranges  $0.2 < B/S^{1/3} < 2.0$  and  $0.01 < H/S^{1/3} < 0.2$ .

Considering the differences noted previously between the earth dams and model experiments, the degree of consistency is remarkable and strongly supports the supposition that the water volume flowing through the breach is the dominant factor that determines the breach size. Other factors such as sediment characteristics, hydraulic head, and barrier breadth appear to be relatively unimportant. The apparent insensitivity to sediment characteristics is particularly noteworthy, given that the sediment types for the dams are very variable.

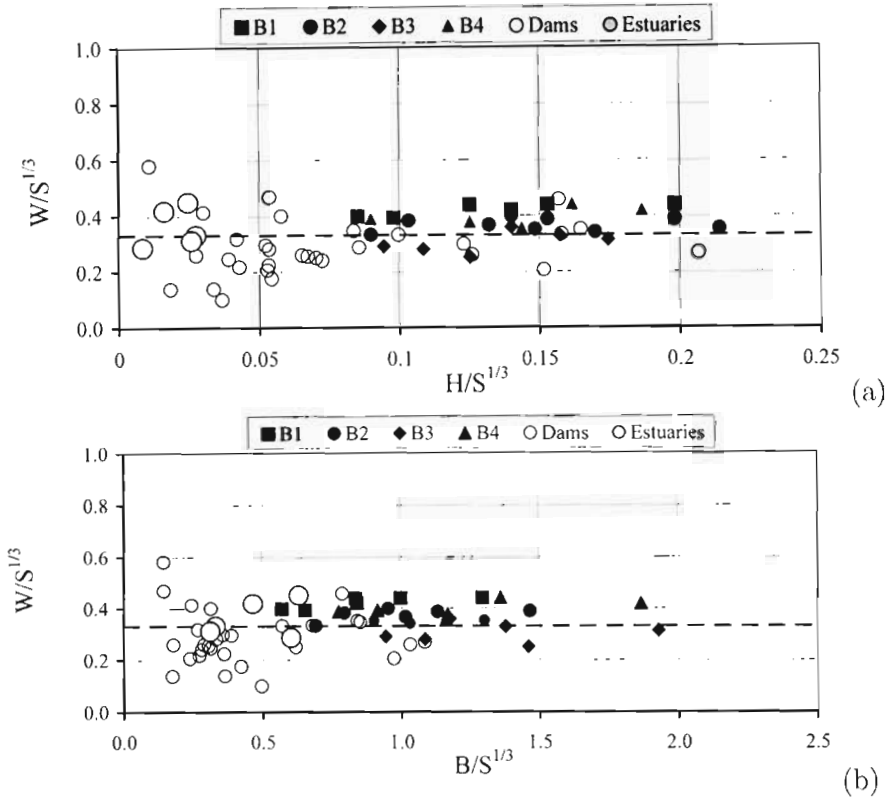


Fig. 4.16: Non-dimensional breach widths plotted against (a) the hydraulic head  $H$ , and (b) the barrier breadth  $B$ . The horizontal dashed line represents the average value of all of the data and is equal to the scaling co-efficient  $C_w = 0.33$ . Data from homogeneous earth dam failures (Wahl, 1998) are plotted as circles. Data from actual estuaries are plotted as large filled circles. Data from the model experiments are shown as solid symbols. The symbols correspond to different berm shapes as listed in Table 1.

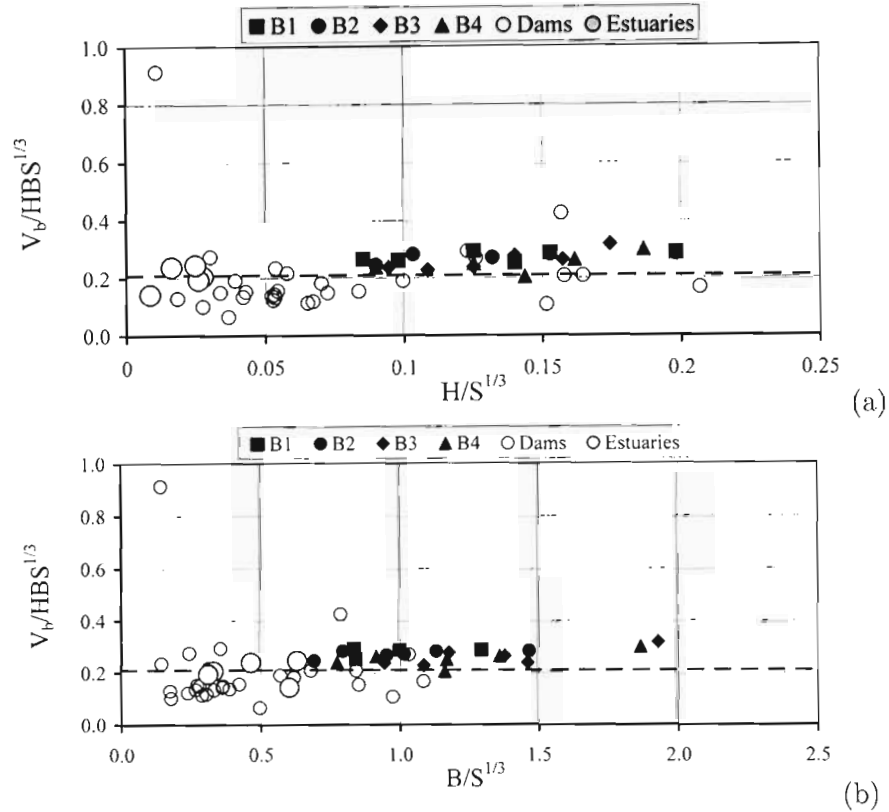


Fig. 4.17: Non-dimensional breach volume plotted against (a) the hydraulic head  $H$ , and (b) the barrier breadth  $B$ . The horizontal dashed line represents the average value for all of the data and is equal to the scaling co-efficient  $C_V = 0.21$ . Data from homogeneous earth dam failures (Wahl, 1998) are plotted as circles. Data from actual estuaries are plotted as large filled circles. Data from the model experiments are shown as solid symbols. The symbols correspond to different berm shapes as listed in Table 1.



### 4.5.2 Breach formation times and peak outflows

Fig. 4.18 (a) and (b) shows the breach formation times  $T_F$ , for the estuary, dam and model data non-dimensionalised by the timescale  $T_{-1.5,1}$  plotted against  $H/S^{1/3}$  and  $B/S^{1/3}$  respectively. In Fig. 4.19 (a) and (b) the peak outflows  $Q_P$  are similarly shown non-dimensionalised by the outflow scale  $Q_{-1.5,1}$ . It can be seen in Fig. 4.18 that there are no obvious trends in the full scale or model data, although the dam data are higher than the model data. This suggests that the breach formation times for the dams are longer than those for the model experiments. Considering the likely errors in the dam data, in particular the likelihood that all or part of the breach initiation time may be included in the reported breach formation times (as discussed in section 4.4.3) the scatter in the data is not unreasonable. A large amount of the scatter may also be attributed to the definition of the breach formation time, which is subject to interpretation.

Similar comparisons have been done for various  $\alpha$  and  $\gamma$  combinations in the ranges  $-2 \leq \alpha \leq 0$  and  $0 \leq \gamma \leq 2$ . Multi-variate linear regression analysis was used to objectively assess the trends in the scaled data by applying a statistical t-test to indicate whether the regression coefficients for  $H$  and  $B$  were significantly different from zero at a 95% confidence level. The tests confirmed that the combination  $\alpha = -\frac{3}{2}$ ,  $\gamma = 1$  provides scaling results with no statistically significant trends, while other combinations (particularly where  $\gamma < 1$ ) do not.

In Fig. 4.19 once again there are no obvious trends in the data and there is good agreement between the model and full scale data, particularly with respect to the full scale estuaries. This provides strong support for the scaling arguments in section 3.1. From these results it may be concluded that the breach formation times  $T_F$  and peak outflows  $Q_P$  scale like

$$T_F \simeq C_T (g/S^{1/3})^{-1/2} (H/S^{1/3})^{-3/2} (B/S^{1/3})^1 \quad (4.10)$$

$$Q_P \simeq C_Q (g S^{5/3})^{-1/2} (H/S^{1/3})^{3/2} (B/S^{1/3})^{-1} \quad (4.11)$$

where the value of scaling constant  $C_T$  is equal to  $16 \pm 5.7$ , i.e. the coefficient of variation is 37%, for all of the data. The value of the scaling constant  $C_Q$  is equal to  $0.058 \pm 0.024$  i.e. the co-efficient of variation is 41% for all of the data. Which, based on the available data, is applicable to the breaching of cohesionless sand barriers with parameters  $0.2 < B/S^{1/3} < 2.0$  and  $0.01 < H/S^{1/3} < 0.2$ . Once again the apparent insensitivity to sediment characteristics is particularly noteworthy.

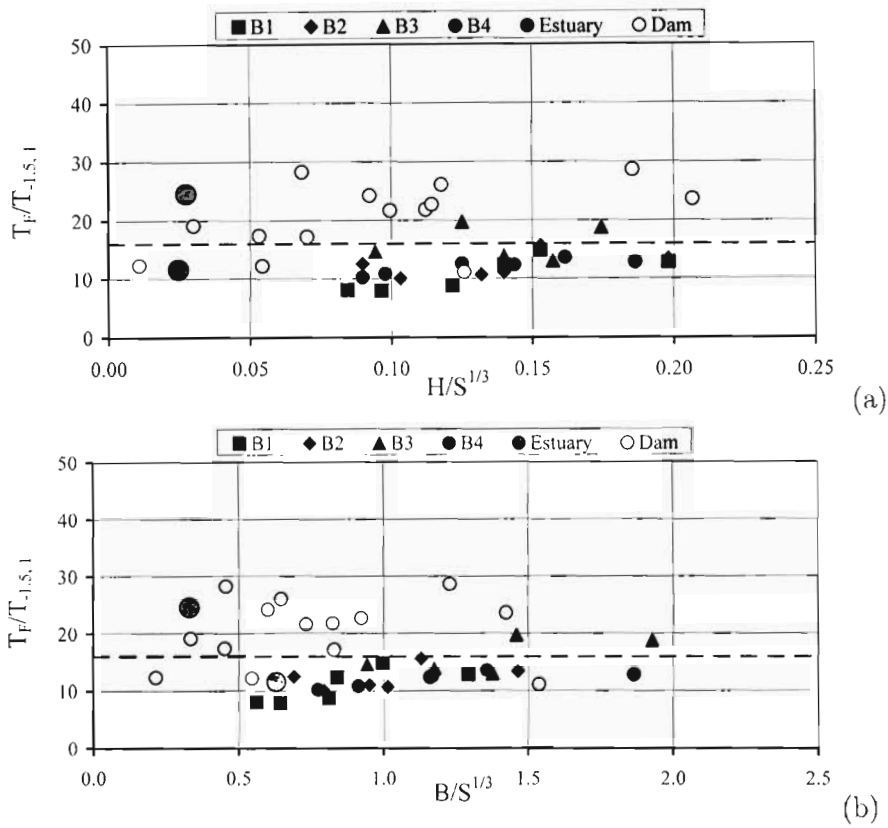


Fig. 4.18: The breach formation times non-dimensionalised by the time scales given by Eq. 3.12 with  $\alpha = -1.5$ ,  $\gamma = 1$  plotted against (a)  $H/S^{1/3}$  and (b)  $B/S^{1/3}$ . The horizontal dashed line represents the average value of all of the data and is equal to the scaling co-efficient  $C_T = 16$ . Data from homogeneous earth dam failures (Wahl, 1998) are plotted as circles. Data from actual estuaries are plotted as large filled circles. Data from the model experiments are shown as solid symbols. The symbols correspond to different berm shapes as listed in Table 1.

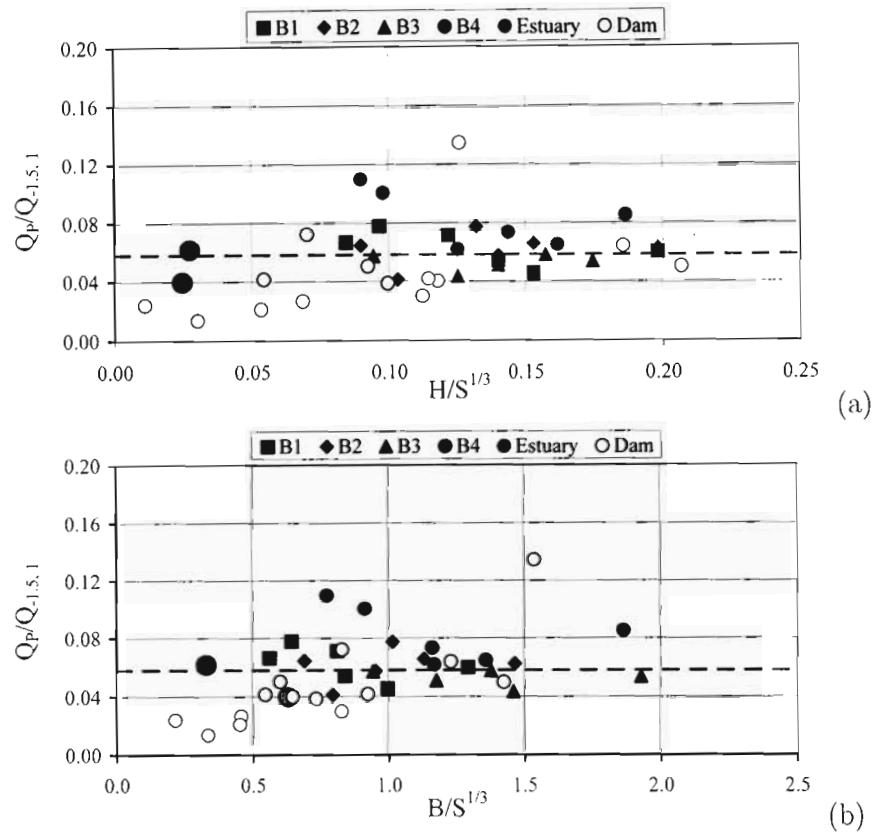


Fig. 4.19: The peak outflows non-dimensionalised by the time scales given by Eq. 3.12 with  $\alpha = -1.5$ ,  $\gamma = 1$  plotted against (a)  $H/S^{1/3}$  and (b)  $B/S^{1/3}$ . The horizontal dashed line represents the average value for all of the data and is equal to the scaling co-efficient  $C_Q = 0.058$ . Data from homogeneous earth dam failures (Wahl, 1998) are plotted as circles. Data from actual estuaries are plotted as large filled circles. Data from the model experiments are shown as solid symbols. The symbols correspond to different berm shapes as listed in Table 1.

## 4.6 Discussion

### 4.6.1 Breach widths and volumes

It is perhaps easy to overlook the power of the scaling result illustrated in non-dimensional form. If the data is re-plotted in dimensional form then the power of these results is more evident. In Fig. 4.20 the measured breach widths  $W$  are plotted against the values predicted by Eq. 4.8 with  $C_W = 0.33$  and in Fig. 4.21 the measured breach volumes  $V_b$  are plotted against predictions from Eq. 4.9 with  $C_V = 0.21$ . It is clear in the plot that there is strong agreement between the measured and predicted values even though the model data are separated from the full scale data by several orders of magnitude.

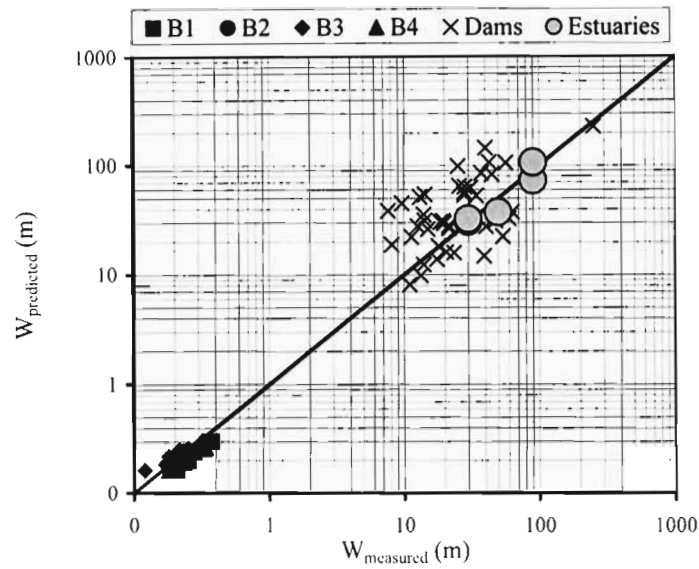


Fig. 4.20: Dimensional plot of the measured breach widths versus the breach widths predicted by Eq. 4.8 with  $C_W = 0.33$ .

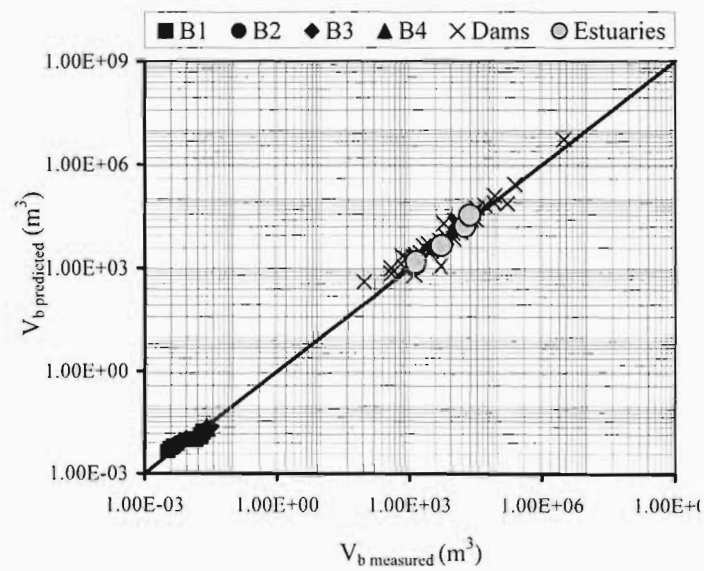


Fig. 4.21: Dimensional plot of the measured breach volumes versus the breach volumes predicted by Eq. 4.9 with  $C_V = 0.21$ .

### 4.6.2 The effects of floods

Overtopping failures of dams or natural coastal barriers are generally associated with floods. The flood-waters add to the volume of water that passes through the breach, and provided the time-scale of the flood inflows is not long compared to the time to drain the storage volume, the effect of the flood would be equivalent to an enlarged impounded storage. This point was noted by Froehlich (1987) and used to explain the slightly higher  $K_0$  values obtained from the regression analysis for overtopping cases (refer section 3.1). Therefore to use the present scaling results to predict breach characteristics at estuaries during floods, allowance must be made for the additional inflow volumes. For large floods, these volumes can exceed the normal storage capacity of a lagoon or estuary by many times over.

An interesting example is a large flood that occurred in the region of the Mdloti/Mhlanga catchments in 1987, with estimated return period of 100 years, with roughly 1000mm of rain during a three-day period. The Mhloti catchment area is about 500 km<sup>2</sup>. Using an estimated average run-off coefficient of say 0.6<sup>1</sup>, this translates into a runoff volume of order 300 million cubic meters, or about 300 times the storage capacity of the lagoon. Using the scaling  $W = C_W S^{1/3}$  with this outflow volume, suggests a breach width exceeding 200m. Archival pictures taken just after the flood confirm that the actual breach was in fact of this order.

### 4.6.3 Breach formation times and peak outflows

In Fig. 4.22 the measured breach formation times  $T_F$ , are plotted against the values predicted by Eq. 4.10 with  $C_T = 16$  and in Fig. 4.23 the measured peak outflows  $Q_P$  are plotted against the values predicted by Eq. 4.11 with  $C_Q = 0.058$ . Once again it is clear that there is good agreement between the predicted values and the measured values with the model data separated from the full scale data by several orders of magnitude. A simple physical explanation of the observed outflow scaling follows by analogy with the hydraulics of broad-crested weirs Coleman et al. (2002). From Fig. 4.5 it is evident that the peak outflow occurs when the breach is nearly fully formed, that is with width  $\simeq W$ , and that the available hydraulic head remains approximately equal to  $H$  at that time. Whence, using the weir analogy

$$Q = C_D \sqrt{gH} W H \quad (4.12)$$

---

<sup>1</sup>A high runoff coefficient is justified here because of the rare combination of long duration and intense rainfall that resulted in a very saturated catchment!

where  $C_D$  is a discharge coefficient. Using the relationship  $W \sim S^{1/3}$  it follows from Eq. 4.12 that

$$Q \sim (g S^{5/3})^{1/2} (H/S^{1/3})^{3/2} \quad (4.13)$$

which is consistent with  $\alpha = -1.5$  in Eq. 3.14.

The influence of the barrier breadth  $B$  on  $T_F$  and  $Q_P$  is more difficult to explain physically. It may reflect energy losses in the breach channel.

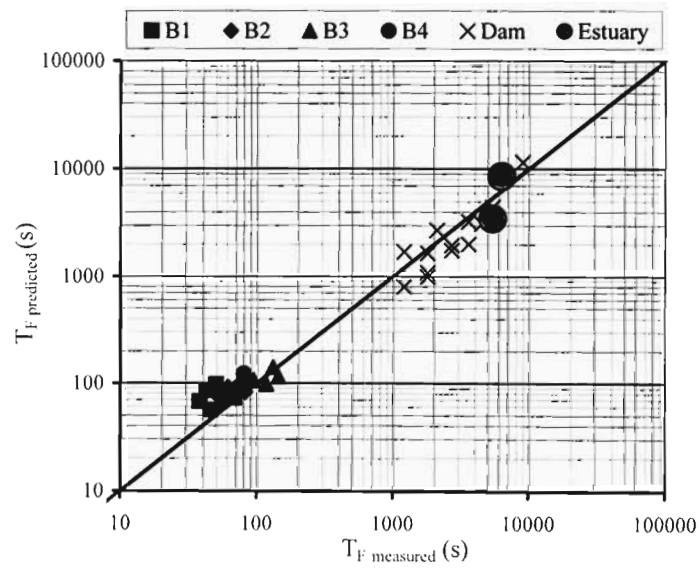


Fig. 4.22: Dimensional plot of the measured breach formation times versus the breach formations times predicted by Eq. 4.10 with  $C_T = 16$ .

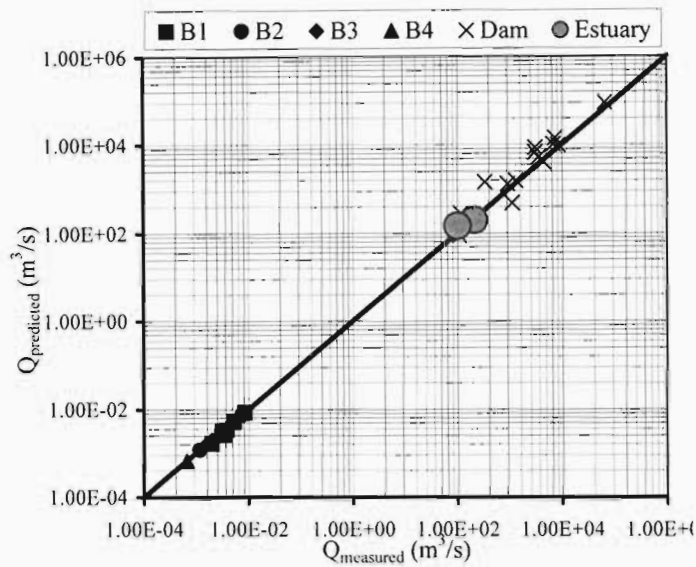


Fig. 4.23: Dimensional plot of the measured peak outflows versus the peak outflows predicted by Eq. 4.11 with  $C_Q = 0.058$ .

#### 4.6.4 Management implications

The artificial breaching of temporary open estuaries is a widely used management intervention. One of the key questions regarding this practice concerns the effects that breaching events have on sedimentation (Beck et al., 2004; Schumann, 2003). The results presented here can be used to quantify sediment transport effects by providing a means to predict the outflow hydrographs and associated peak outflows. Furthermore the results concerning the scaling of the breach formation time can be used to determine the optimal timing and duration of artificial breaching events with respect to tide state.

Breaching events can cause significant scouring of estuarine sediments. To illustrate this, consider the estimated peak outflow of  $210 \text{ m}^3/\text{s}$  for the Mhlanga estuary reported in section 4.4.2. An estimate of the median (2-year return period) flood peak for this catchment is  $36 \text{ m}^3/\text{s}$  (Jezewski et al., 1986). Assuming a Log-Normal probability distribution for annual flood peaks (Pegram, 1994), the peak outflow of  $210 \text{ m}^3/\text{s}$  corresponds approximately to that of a flood with a 25-year return period.

This example indicates that breaching events (both natural or artificial) can produce severe impacts on the estuarine habitat. Historically, this particular estuary was closed for extended periods during dry seasons. However,



more recently, discharges from upstream waste-water treatment facilities have significantly increased the dry-period flows into the estuary. This in turn triggers quasi-periodic breaching every 30 to 40 days even in the absence of rainfall. The system is therefore currently experiencing a peak outflow comparable to that of a 25-year flood at regular and short intervals. The implications concerning the overall functioning of the system are severe, as discussed in detail by Perissinotto et al. (2004) e.g. increased scouring and removal of benthic communities.

---

## CHAPTER 5

### CONCLUSION

---

The breaching of sand barriers plays a key role in the ecological functioning of temporary open closed estuaries (TOCEs). The overall objective of this study was to develop a better understanding of the mouth dynamics of TOCEs for integration into predictive models to be used for management applications.

Analysis of the data obtained from the model experiments has provided insight into the breach process and the temporal features of the breach development. The analysis of the data has also allowed the scaling of the key characteristics of breaching events to be investigated.

The breach was found to develop in a manner similar to that described by Coleman et al. (2002), with the breach channel bed slope decreasing about a pivot point.

The noteworthy features of the temporal development of the breach process include the temporal asymmetry, the shorter time scale for the breach width changes compared to the water levels (or outflows), and the timing of the peak outflow near the end of the breach formation phase.

The results of the scaling investigation indicate that the breach characteristics the breach width  $W$ , volume  $V_b$ , formation time  $T_F$  and peak outflow  $Q_p$  all scale on the breach outflow volume  $S$ , hydraulic head  $H$  and barrier breadth  $B$ . The breach width  $W$  scales like,

$$W = C_W S^{1/3} \quad (5.1)$$

and the breach volume  $V_b$  like

$$V_b = C_V HBS^{1/3} \quad (5.2)$$

where the values of the constants obtained from the model and full scale data are  $C_W = 0.33 \pm 0.11$  and  $C_V = 0.21 \pm 0.12$ . The breach formation times  $T_F$  scale like

$$T_F = C_T (g/S^{1/3})^{-1/2} (H/S^{1/3})^{-3/2} (B/S^{1/3})^1 \quad (5.3)$$

and the peak outflows  $Q_P$  like

$$Q_P = C_Q (g S^{5/3})^{1/2} (H/S^{1/3})^{3/2} (B/S^{1/3})^{-1} \quad (5.4)$$

where the values of the constants obtained from the model and full scale data are  $C_T = 16 \pm 5.7$  and  $C_Q = 0.058 \pm 0.024$ . From the range of values tested the results appear to be applicable to barriers with hydraulic heads  $0.01 < H/S^{1/3} < 0.3$  and barrier breadths  $0.1 < B/S^{1/3} < 2.0$ .

A key assumption in this analysis was that the properties of the sediment could be ignored. The results suggest that this assumption is reasonable, at least for cohesionless sediments. However, further research is recommended to investigate this issue further and to refine the findings of the present study.

These results provide predictive tools that can be incorporated into models for the mouth dynamics of perched intermittently open estuaries. In particular they can be used to guide management interventions, such as artificial breaching. Predictions of the volume of sediment removed from the barrier combined with knowledge of sediment transport rates (Schoonees, 2000) can be used to estimate the length of time that the channel will remain open. Estimates of the breach formation time can be used to predict the optimal timing of an artificial breach with respect to tidal state, whilst predictions of the breach peak outflows can be used to estimate the effect of a breach on the sediment dynamics of an estuary.

---

## REFERENCES

---

- Barnes, R. (1974). *Estuarine Biology*, volume 49 of *The Institute of biology's Studies in Biology*. Edward Arnold.
- Barnes, R. (1977). *The Coastline*. John Wiley and Sons.
- Bascom, W. (1951). The relationship between sand size and beach-face slope. *Transactions, American Geophysical Union*, 32(6):866–874.
- Beck, J., Theron, A., Kemp, A., Huizinga, P., and Basson, G. (2004). Hydraulics of estuarine sediment dynamics in south africa. Technical Report 1257/1/04, Water Rresearch Commission.
- Begg, G. (1978). The estuaries of natal. Technical Report 41, The Natal Town and Regional Planning commission, Pietermaritzburg.
- C.E.M. (2002). Coastal engineering manual. Engineering Manual 1110-2-1100, U.S. Army Corps of Engineers.
- Coleman, S., Andrews, D., and Webby, M. (2002). Overtopping breaching of noncohesive homogeneous embankments. *Journal of Hydraulic Engineering*, 128(9):829–838.
- Cooper, J. (2001). Geomorphological variability among microtidal estuaries from the wave dominated south african coast. *Geomorphology*, 40:99–122.
- Day, J. (1980). What is an estuary? *South African Journal of Science*, (76):198.
- Froehlich, D. (1987). Embankment-dam breach parameters. *Proc. ASCE Conference on Hydraulic Engineering, Williamsburg, Virginia*, pages 570–575.
- Froehlich, D. (1995a). Embankment dam breach parameters revisited. *Proc. ASCE Conference on Water Resources Engineering, San Antonio, Texas*,, pages 887–891.

- Froehlich, D. (1995b). Peak outflow from breached embankment dam. *Journal of Water Resources Planning and Management*, 121(1):90–97.
- Hurvich, C. M. and Tsai, C. (1989). Regression and time series model selection in small samples. *Biometrika*, 76(2):297–307.
- Jezewski, W., Pike, P., and Pike, C. (1986). Estuarine and lake freshwater requirements. Technical report TR 129, SA Dept. Water Affairs and Forestry.
- Kraus, N. and Wamsley, T. (2003). Coastal barrier breaching, part 1: Overview of breaching process. technical note erdc/chl. Technical Report CHETN-IV-56, US Army Corps of Engineers.
- Kraus, N. and Wamsley, T. (2005). Coastal barrier breaching, part 2: Mechanical breaching and breach closure. technical note erdc/chl. Technical Report CHETN-IV-65, US Army Corps of Engineers.
- Kraus, N. C. (2003). Analytical model of incipient breaching of coastal barriers. *Coastal Engineering Journal*, 45(4):511–531.
- Kraus, N. C., Militello, A., and Todoroff, G. (2002). Barrier breaching processes and barrier spit breach, stone lagoon, california. *Shore & Beach*, 70(4):21–28.
- Morant, P. and Quinn, N. (1999). *Influence of Man and management of South African estuaries. In: Estuaries of South Africa. B.R. Allanson and D. Baird (eds)*. Cambridge University Press.
- Odd, N., Roberts, W., and Maddocks, J. (1995). Simulation of lagoon break-out, hydra 2000. *Proc. 26th Congress of the Int. Assoc. for Hydraulic Research*, 3:92–97.
- Parkinson, M. and Stretch, D. (2006). Breaching timescales and peak outflows for perched temporary open estuaries. *Coastal Engineering Journal*, submitted.
- Pegram, G. (1994). Hydrological estimates - guidelines for the hydraulic design and maintenance of river crossings. Technical Report TRH25 (vol 1), Committee of State Road Authorities (CSRA).
- Perissinotto, R., Blair, A., Connell, A., Demetriades, N., Forbes, A., Harrison, T., Iyer, K., Joubert, M., Kibirige, I., Mundree, S., Simpson, H.,

- Stretch, D., Thomas, C., Thwala, X., and Zietsman, I. (2004). Contributions to information requirements for the implementation of resource directed measures for estuaries. Technical Report 1247/2/04, Water Research Commission.
- Ranasinghe, R. and Pattiaratchi, C. (2003). The seasonal closure of tidal inlets: causes and effects. *Coastal Engineering Journal*, 45(4):601–627.
- Ranasinghe, R., Pattiaratchi, C., and Masselink, G. (1999). A morphodynamic model to simulate the seasonal closure of tidal inlets. *Coastal Engineering Journal*, 37(1):1–36.
- Schoonees, K. (2000). Annual variation in net longshore transport. *Coastal Engineering Journal*, 40:141–160.
- Schumann, E. (2003). Towards the management of marine sedimentation in south african estuaries with special reference to the eastern cape. Technical Report 1109/1/03, Water Research Commission.
- Slinger, J. (1996). *Modelling the Physical Dynamics of Estuaries for Management Purposes*. PhD thesis, Department of Mathematics and Applied Mathematics, University of Natal, Durban, South Africa.
- Smakhtin, V. (2004). Simulating the hydrology and mouth conditions of small temporarily closed/open estuaries. *Wetlands*, 24(1):123–132.
- Stretch, D. and Parkinson, M. (2006). The breaching of sand barriers at perched, temporary open/closed estuaries - a model study. *Coastal Engineering Journal*, 48(1):13–30.
- Stretch, D. and Zietsman, I. (2004). The hydrodynamics of mhlanga and mdloti estuaries: Flows, residence times, water levels and mouth dynamics. Hydrodynamics 1247/2/04 - Final Report, Water Research Commission.
- Turner, I. and Leatherman, S. (1997). Beach dewatering as a 'soft' engineering solution to coastal erosion - a history and critical review. *Journal of Coastal Research*, 13(4):1050–1063.
- van Niekerk, L., van der Merwe, J., and Huizinga, P. (2005). The hydrodynamics of the bot river estuary revisited. *Water SA*, 31(1):73–86.
- Visser, P. (1998). Breach growth in sand dikes. Technical Report Report No. 98-1, Delft University of Technology, Hydraulic and Engineering Engineering Division.

- Wahl, T. (1998). Prediction of embankment dam breach parameters - a literature review and needs assessment. Technical Report Dam Safety Report DSO-98-004, US Bureau of Reclamation, Denver, CO.
- Wahl, T. (2004). Uncertainty of predictions of embankment dam breach parameters. *Journal of Hydraulic Engineering*, 130(5):389–397.
- Webby, G. (1996). discussion of peak outflow from breached embankment dam (froehlich, 1995a). *Journal of Water Resources Planning and Management*, 4(122):316–317.
- Whitfield, A. (1980). Available scientific information on individual southern african estuarine systems. Technical Report Report 577/3/00, Water Research Commission.
- Zietsman, I. (2004). The hydrodynamics of temporary open estuaries with case studies of mhlanga and mdloti. Master's thesis, School of Civil Engineering, University of Natal, Durban, South Africa.

---

APPENDIX A

EXPERIMENTAL DATA

---



Barrier	Impoundment Length	H	B	S	W	$V_b$	$T_F$	$Q_P$
	(m)	(m)	(m)	(m <sup>3</sup> )	(m)	(m <sup>3</sup> )	(s)	(m <sup>3</sup> /s)
B1	1	0.115	0.75	0.20	0.255	0.0143	50	0.0033
	2	0.115	0.75	0.43	0.330	0.0186	75	0.0042
	3	0.125	0.75	0.71	0.375	0.0211	66	0.0080
	1	0.060	0.4	0.11	0.210	0.0034	42	0.0020
	2	0.060	0.4	0.23	0.240	0.0038	47	0.0035
	3	0.060	0.4	0.35	0.280	0.0045	55	0.0039
B2	1	0.115	0.85	0.20	0.225	0.0160	60	0.0030
	2	0.115	0.85	0.43	0.290	0.0207	90	0.0053
	3	0.125	0.85	0.71	0.355	0.0253	67	0.0075
	1	0.065	0.5	0.12	0.180	0.0043	56	0.0019
	2	0.065	0.5	0.25	0.240	0.0058	67	0.0017
	3	0.065	0.5	0.38	0.240	0.0058	96	0.0035
B3	1	0.095	1.05	0.16	0.170	0.0172	129	0.0014
	2	0.120	1.05	0.44	0.250	0.0253	88	0.0042
	3	0.125	1.05	0.71	0.320	0.0324	103	0.0054
	1	0.060	0.7	0.11	0.120	0.0048	158	0.0007
	2	0.070	0.7	0.27	0.180	0.0072		
	3	0.070	0.7	0.41	0.215	0.0086	144	0.0026
B4	1	0.105	1.05	0.18	0.235	0.0185	78	0.0027
	2	0.125	1.05	0.46	0.340	0.0268	88	0.0051
	3	0.130	1.05	0.74	0.320	0.0252	88	0.0084
	1	0.060	0.56	0.11	0.180	0.0040	81	0.0012
	2	0.060	0.56	0.23	0.240	0.0054	89	0.0031
	3	0.065	0.56	0.38	0.280	0.0063	88	0.0053

Tab. A.1: Collected experimental data

---

APPENDIX B

JOURNAL ARTICLES

---

## THE BREACHING OF SAND BARRIERS AT PERCHED, TEMPORARY OPEN/CLOSED ESTUARIES — A MODEL STUDY

DEREK STRETCH\* and MICHAEL PARKINSON†

*Centre for Research in Environmental,  
Coastal & Hydrological Engineering,  
School of Civil Engineering,  
University of KwaZulu-Natal, Durban,  
KwaZulu-Natal, 4041, South Africa  
<http://www.ukzn.ac.za/>  
\* [stretchd@ukzn.ac.za](mailto:stretchd@ukzn.ac.za)  
† [parkinsonm@ukzn.ac.za](mailto:parkinsonm@ukzn.ac.za)*

Received 4 March 2005  
Revised 1 December 2005

The mouth dynamics of small temporary open estuaries play a key role in their overall functioning. Intermittent breaching of the sand barriers of these systems leads to large changes in the physico-chemical environment, which in turn triggers major biological responses. The breaching process can also cause significant morphological changes because the strong breach outflows can scour large quantities of accumulated sediments from an estuary. Simple laboratory experiments are reported that aim to understand what determines the size of a breach in the sand barrier. The experiments were specifically designed to test the influence of storage volumes on the breaching process. They suggest a remarkably simple result that the breach width scales on the  $1/3$  power of the total volume of water that flows through the breach. This scaling is shown to be consistent with breaching at actual estuaries (or coastal lagoons) where storage volumes are six orders of magnitude higher than the models. Furthermore, a review of data from earth dam failures also reveals a broad consistency with the scaling deduced from these model tests.

*Keywords:* Breaching; sand-barriers; estuaries; coastal lagoons.

### 1. Introduction

Temporally open/closed estuaries (TOCEs) do not have a permanently open link to the sea. Their inlets are unstable due to a combination of small tidal prism, energetic wave climate (with associated sediment transport), and low or intermittent river inflows. In South Africa, about 70% of estuaries are TOCEs, with most of them

located on the eastern seaboard between the cities of East London and Durban. Similar systems, sometimes referred to as “blind”, “intermittently open”, or “seasonally open” estuaries, are also found in Australia, on the west coast of the USA, South America and India [Ranasinghe *et al.*, 1999; Ranasinghe and Pattiaratchi, 2003; Kraus and Wamsley, 2003]. Perched estuaries are those that have water levels consistently above mean sea level (MSL). They tend to occur on coastlines that have an energetic wave climate with steep beaches and coarse sediments. Steeper beaches are less dissipative and more reflective, which is in turn associated with high wave run-up and beach berms that can reach 2–3 m above MSL, even in the micro-tidal context of South Africa where tidal range is less than 2 m.

Periodic breaching of the sand barriers at perched TOCEs gives rise to large and rapid variations in the physico-chemical environment that in turn triggers major biological responses.<sup>a</sup> This is particularly evident in the case of perched estuaries that are essentially empty when they breach. Furthermore, in these cases, the large outflows that can arise from a sudden breaching of the barrier, can scour significant quantities of accumulated sediments from these estuaries, thereby playing an important role in their morphology. Breaching events are therefore important in the overall functioning and health of these systems.

It is common practice to artificially breach closed estuaries when water levels become high. This is done to prevent flooding of farmlands and/or properties that have encroached into surrounding flood plains, or in some cases to flush the systems from a build-up of contaminants or sediments. Artificial breaching is sometimes viewed as a management strategy to address the effects of reduced inflows due to dams or other abstraction schemes. Reduced inflows can greatly increase the closure periods of TOCEs and artificial breaching attempts to approximately mimic natural mouth dynamics so as to maintain the ecological functioning of the systems. The optimal timing and detailed consequences of such interventions requires an understanding of the breaching and re-closure processes and their impact on the functioning of these ecosystems.

This paper describes simple model experiments that investigated the breaching characteristics of perched estuaries as a function of several key parameters, namely the storage volume in the back-barrier lagoon, the hydraulic head, and the cross-sectional geometry of the sand barrier. The results from the model study are compared with data for two small, perched, temporary open estuaries on the east coast of South Africa [Perissinotto *et al.*, 2004; Stretch and Zietsman, 2004; Zietsman, 2003] and two larger coastal lagoons situated in Australia [Odd *et al.*, 1995] and California [Kraus *et al.*, 2002].

Coleman *et al.* [2002] reported a model study of sand embankment breaching with constant upstream water levels. This corresponds to a special case where the

---

<sup>a</sup>For example breaching usually disrupts the trophic structure that develops during closed phases, and leads to recruitment of new marine organisms from the sea by tide or wave driven inflows.

impounded volume is infinitely large. Although some qualitative features of the initial breach development are similar to the problem addressed here (as discussed in Sec. 4), the focus of the present study was on the final breach characteristics from finite volume releases. This was not included in the Coleman *et al.* [2002] experiments, so a direct quantitative comparison is not possible.

The breaching of sand barriers at TOCEs is conceptually similar to the failure of earth-fill dams and dikes. These failures are of interest because of the associated risks to life and property [Wahl, 1998; 2004; Visser, 1988; 1994; 1998; 2000]. Archival data from historical dam failures have been compiled by Wahl [1998] and were therefore re-analyzed as part of the present study in order to test the scaling results deduced from the model tests.

The aim of this study was to address the following key question concerning the breaching of sand barriers at perched temporary open estuaries:

*What determines the size of a breach and the volume of sediment removed in the process?*

An answer to this question should contribute to a better understanding of the mouth dynamics of TOCEs and be useful for developing models that can accurately mimic the physical dynamics of these systems. For example, if these breach characteristics can be predicted, then the time-scale for re-closure by wave-driven sediment transport can be estimated and used to develop process-based models of the mouth dynamics for management applications.

In Sec. 2, a simple scaling analysis is outlined that provides the background for interpreting the experimental results. In Sec. 3, the experiments are described, followed by a presentation of the results in Sec. 4. In Sec. 5, the experimental results are compared with field observations of breaching at full-scale estuaries, lagoons and earth-fill dams in order to test the scaling results deduced from the experiments.

## 2. Scaling Analysis

Consider the simplified model of a perched estuary, depicted schematically in Fig. 1, comprising a trapezoidal shaped sand barrier of height  $H$ , breadth  $B$ , and upstream and downstream slopes  $\beta_1$  and  $\beta_2$  respectively.

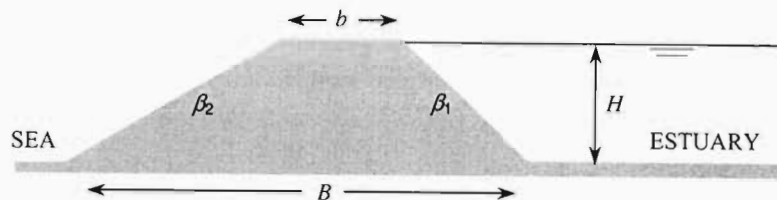


Fig. 1. Schematic representation of a perched, closed estuary separated from the sea by a sand barrier.

We assume that the height  $H$  of the barrier is measured relative to a datum that represents the minimum water level behind the barrier after breaching. In the case of fully perched estuaries this datum is above the average water level downstream of the barrier (mean sea level or MSL).

Our objective is to predict the breach width  $W$  that will occur on failure of the barrier, and the volume of sediment  $V_b$  removed in the process. The type of breaching events that are the focus of this study, typically involve the following processes:

- (1) overtopping of the barrier due to rising water levels in the back-barrier lagoon, resulting in the scouring of a breach channel. This scenario is usually associated with strong inflows (e.g. floods) into the estuary.
- (2) horizontal seepage erosion of the external face of the barrier causing it to collapse and initiate a breach. This scenario does not necessarily require initial overtopping of the barrier to trigger breaching.

Suppose that the dominant parameters controlling the width of a breach are the impounded storage volume  $S$ , the hydraulic head  $H$ , and the breadth of the barrier  $B$ . Since the storage volume  $S$  is assumed to be based on the difference in water level before and after breaching, it may also be interpreted as the total volume of water that flows out through the breach. Note that the storage  $S$  can vary independently of  $H$  since the impounded volume may comprise any combination of depth and surface area.

If the storage volume  $S$  is used to define a reference length scale  $S^{\frac{1}{3}}$  (which may be interpreted as the geometric mean of the horizontal and vertical scales of the volume  $S$ ), then our supposition suggests that the breach width  $W$  can be related to  $H$  and  $B$  in non-dimensional form as

$$W/S^{\frac{1}{3}} = \phi(H/S^{\frac{1}{3}}, B/S^{\frac{1}{3}}) \quad (1)$$

where  $\phi(\cdot)$  is an unknown function to be determined empirically.

The main result of the present investigation (see Secs. 4 and 5) is that the available data is consistent with the simplification  $\phi \simeq \text{constant}$ , so that

$$W/S^{\frac{1}{3}} \simeq C_W \quad (2)$$

where the constant  $C_W \simeq \frac{1}{3}$ . Therefore a simple “rule-of-thumb” for predicting breach width is that it is approximately equal to one third of the cube-root of the volume that flows out through the breach — hereinafter referred to as the “ $\frac{1}{3}$ –rule”.

Froehlich [1987] analysed breach characteristics for approximately 40 earthfill dams and suggested the still widely used regression equation (in our notation)

$$W/H = 0.47K_0(S/H^3)^{\frac{1}{4}} \quad (3)$$

where  $K_0 = 1.4$  for overtopping induced failures and  $K_0 = 1.0$  for seepage induced failures. Froehlich's equation may be re-arranged to give

$$W/S^{\frac{1}{3}} = 0.47K_0(H/S^{\frac{1}{3}})^{\frac{1}{4}} \quad (4)$$

which, when compared with Eq. (1), suggests that

$$\phi \sim (H/S^{\frac{1}{3}})^{\frac{1}{4}}. \quad (5)$$

Froehlich's regression analysis therefore suggests that the function  $\phi$  is independent of the barrier breadth  $B$ , but has a weak dependence on the hydraulic head  $H$ . In Sec. 5, this result will be compared with the simpler  $\frac{1}{3}$  – rule, where  $\phi \simeq \text{constant}$ , as given by Eq. (2).

The scaling analysis of the breach width may be extended to the volume of barrier material  $V_b$  removed during a breach. One possible form of non-dimensional relationship between  $V_b$  and the parameters  $H$ ,  $B$ , and  $S$  may be deduced as

$$V_b/(B.H.S^{1/3}) = \psi(H/S^{\frac{1}{3}}, B/S^{\frac{1}{3}}) \quad (6)$$

where  $\psi(\cdot)$  is an unknown function to be determined empirically.

A secondary result of the present investigation (see Secs. 4 and 5) is that the available data is consistent with the simplification  $\psi \simeq \text{constant}$ , so that

$$V_b/(B.H.S^{1/3}) \simeq C_V \quad (7)$$

where the constant  $C_V \simeq \frac{1}{5}$ . This result is consistent with the  $\frac{1}{3}$  – rule for the breach width  $W$  since simple geometry implies that  $V_b \sim B.H.W$  to within an order unity constant that depends on the detailed three-dimensional shape of the breach. The scaling given by Eq. (7) allows  $V_b$  to be predicted from the parameters  $B$ ,  $H$ , and  $S$ , which are usually known (or can be approximated) for specific case studies.

Another feature of breaching that is of interest is the breach formation time<sup>b</sup>  $T_F$ . In the case of earth dams, this can be used to estimate the outflow hydrograph for risk analysis. In the case of sand-barriers at perched estuaries, the influence of tide and wave action on the breaching process will depend on the ratio of breach formation time to the tidal period. The Froehlich [1987] regression analysis of non-dimensional breach formation times for earth dam failures gave

$$T_F(g/H)^{\frac{1}{2}} = 79(S/H^3)^{0.47} \quad (8)$$

This suggests that the time scale for breach formation is approximately  $(S/gH^2)^{\frac{1}{2}}$ . This scaling will not be tested here, but experiments to investigate this issue are planned for the future.

<sup>b</sup>Defined by c.g. Wahl [1998] as “The time between initial breaching of the upstream face of the barrier until the breach is fully formed.”

### 3. Laboratory Experiments





A simple rectangular model estuary 2 m wide by 4 m long was excavated. The bed of the model was leveled, and three sidewalls were built using concrete blocks. The model was lined with a 200  $\mu\text{m}$  thick impervious plastic membrane.

Sand barriers of various heights and cross-sectional shapes were built across the open side of the model basin. The sand used for the experiments was not varied and was uniformly graded with  $d_{50} \simeq 600 \mu\text{m}$  and uniformity coefficient  $d_{60}/d_{10} \simeq 3$ . The barriers were positioned at nominal distances of 1, 2, or 3 m from the back wall of the model, thereby providing different storage volumes for each breaching experiment. Parameter values used in the experiments are given in Table 1 — include the impounded storage prior to breaching  $S_0$ , hydraulic head  $H$ , and barrier shape parameters (top and bottom breadths  $b$  and  $B$ , and side slopes  $\beta_1$  and  $\beta_2$ ).

The experimental procedure involved filling the impoundment with water to the top level of the sand barrier. A breach was initiated using a small ( $\sim 1$  cm deep) V-notch in the top and center of the barriers. Subsequent development of the breach to its final shape was then observed and recorded with video. The final breach dimensions were noted and the experiment repeated for different storage volumes, hydraulic heads and barrier shapes.

Photographs illustrating the outcome of a typical breaching experiment are shown in Fig. 2. It is evident that the final breach has a venturi shape in plan, with a crescent-shaped upstream crest. The breach width therefore varies across the breadth of the barrier. The side-walls of the final breach were usually nearly vertical (see Fig. 2(b)) but could also have unstable vertical overhangs due to undercutting erosion by the outflow and maintained by cohesion in the saturated sand. These factors can make precise, repeatable measurements of a breach width difficult to define. All breach width measurements reported here were measured at the upstream crest of the barrier. Vertical overhangs, if present, were ignored when measuring the width. It was observed that the breach width at this location seemed

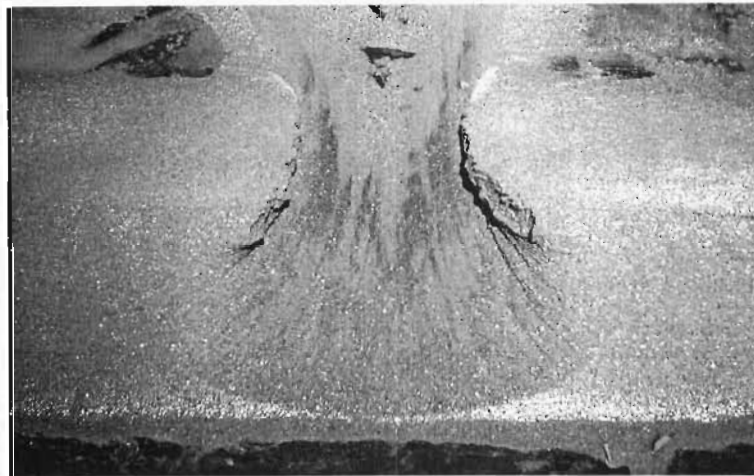
Table 1. Experimental Parameters.

Berm	Slopes		$b$ (cm)	$B$ (cm)	$H$ (cm)	$S_0$ ( $\text{m}^3$ )	Barrier shape (Schematic only)
	$\beta_1$	$\beta_2$					
1	2	3	0	20.0	8	0.15–0.41	
				37.5	15	0.24–0.80	
2	2	3	10	30.0	8	0.15–0.44	
				47.5	15	0.24–0.80	
3	2	3	30	50.0	8	0.16–0.47	
				67.5	15	0.24–0.83	
4	2	5	0	28.0	8	0.15–0.44	
				52.5	15	0.24–0.83	





(a)



(b)

Fig. 2. Photographs showing the outcome of a model breaching experiment. Photo (a) is a view from downstream: the breached sand barrier is visible in the foreground with the storage basin in the background. Photo (b) is a close-up view from upstream showing the crescent-shaped upstream crest of the breach and the irregular sidewalls with small vertical overhangs.

to be reasonably representative of an average over the breadth of the barrier. The breach volumes were not directly measured, but were inferred as the product of the measured breach widths and the cross-sectional areas of the barriers.

It can be seen from Fig. 2(b) that the invert of the breach channel coincides with the impermeable base of the model from about halfway across the barrier. The upstream half of the breach channel does not scour all the way to the base and the invert rises slightly towards the crescent-shaped upstream crest. This prevents the impoundment from draining completely. The residual storage trapped in the lagoon was measured for each experiment and was subtracted from the initial storage  $S_0$  to determine the volume  $S$  that flowed out through the breach. Seepage flows

through the barriers were small relative to the breach outflows and were therefore ignored in estimating the outflow volumes.

No direct hydrodynamic measurements were made. However, the video recordings were archived to allow for the analysis of temporal developments, such as water level variations, from which outflow hydrographs can be deduced. Results from that analysis will be reported elsewhere — here we focus only on the characteristics of the fully developed breach.

The data from all the experiments are tabulated in the appendix of this paper.

## 4. Results and Discussion

### 4.1. *Qualitative features of the breaching process*

The breaching process can be broadly considered to comprise two main phases — a breach initiation phase followed by a breach formation phase. During the initiation phase, the overtopping flow gradually scours a channel on the downstream face of the barrier while the upstream crest remains relatively intact. The upstream water level does not change significantly during this phase. Once the upstream crest of the barrier begins to erode, it signals the start of the main breach formation phase.

As scouring lowers the upstream crest, the volume of water entering the breach channel increases which in turn increases the rate of scour. The size of the breach grows rapidly during this phase, both deepening and widening. Strong velocities and turbulence at the bottom of the downstream face cause the toe of the channel to erode upstream along the base to a pivot point, also observed by Coleman *et al.* [2002]. The crest of the breach moves upstream as it erodes because of the sloping face of the barrier. This causes the slope of the channel to decrease about the pivot point as the channel bed is eroded. The upstream water level decreases as the breach widens and the outflow increases. The falling head causes the velocity of the water in the channel to decrease. The rate of scour also decreases so that the breach width attains a maximum value and the breach formation phase ends.

The process described here is qualitatively similar to the breaching of sand dikes as described by Visser [1998], and the breaching of small-scale sand barriers described by Coleman *et al.* [2002]. However, dike failures differ from estuary breaching in that the upstream water level (due to incoming tides or storm surges) is approximately constant during breaching whereas the downstream water level rises as the polder fills. The model study of Coleman *et al.* [2002] also used constant upstream head conditions, but in that case, the downstream water level was kept low.

### 4.2. *Breach widths and volumes*

The measured breach widths, non-dimensionalized by the cube-root of the outflow volume  $S$ , are shown plotted against the non-dimensional hydraulic head  $H/S^{1/3}$  and barrier breadth  $B/S^{1/3}$  in Fig. 3 in order to test the scaling relationship given by

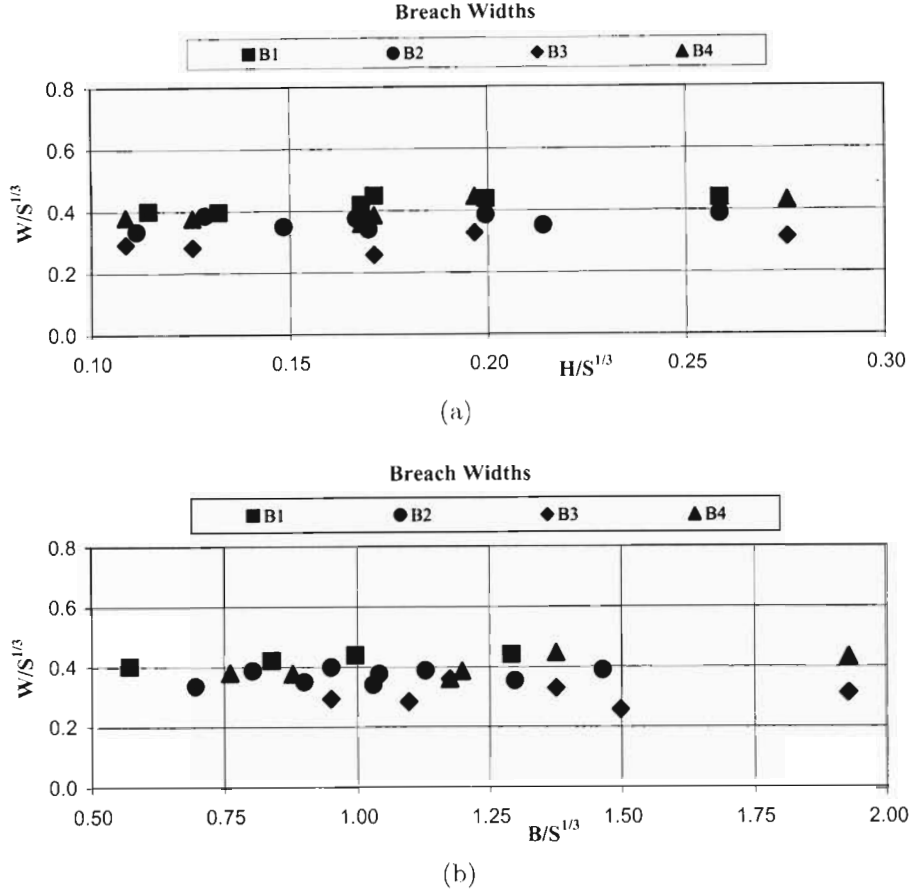


Fig. 3. Non-dimensional breach widths from the model experiments, plotted against (a) the hydraulic head  $H$ , and (b) the barrier breadth  $B$ . The symbols correspond to different berm shapes as listed in Table 1.

Eq. (1). Figures 3(a) and (b) can be interpreted as projections of the function  $\phi(\cdot)$  onto the  $W - H$  and  $W - B$  planes, respectively.

It can be seen from Fig. 3 that the non-dimensional breach width is approximately constant with all the data scattered around a horizontal line. This implies that the simplification  $\phi \simeq \text{constant}$ , as given by Eq. (2) is a good description of the data. The average value of the non-dimensional breach width for all the data was  $0.38 \pm 0.05$  ( $\pm$  one standard deviation), i.e. the coefficient of variation was 15%.

From these results, it seems reasonable to conclude that, for similar barrier shapes and for breadths  $0.5 < B/S^{1/3} < 2.0$  and hydraulic heads  $0.1 < H/S^{1/3} < 0.3$ , the breach width scales approximately on the cube-root of the outflow volume.

The breach volumes  $V_b$  are shown plotted in the non-dimensional form  $V_b/(HBS^{1/3})$  in Fig. 4 in order to test the scaling relationship given by Eq. (6). Figures 4(a) and (b) can be interpreted as projections of the function  $\psi(\cdot)$  onto the  $V_b - H$  and  $V_b - B$  planes, respectively.

As expected from the breach width results presented above, the data suggests that the non-dimensional breach volume is approximately independent of both the

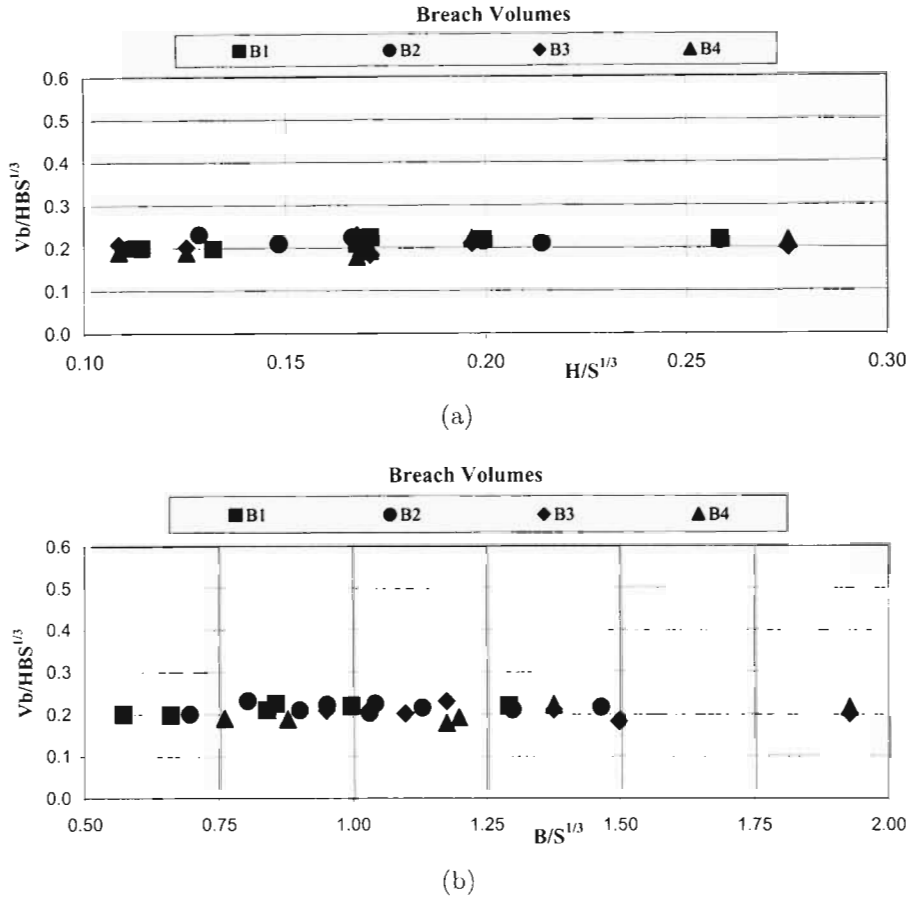


Fig. 4. Non-dimensional breach volumes from the model experiments, plotted against (a) the hydraulic head  $H$ , and (b) the barrier breadth  $B$ . The symbols correspond to different berm shapes as listed in Table 1.

hydraulic head  $H$  and the berm breadth  $B$  for the range of values tested. The simplification  $\psi \simeq \text{constant}$ , as given by Eq. (7) is therefore a good description of the data. The average value of the non-dimensional breach volume for all the data was  $0.21 \pm 0.02$  ( $\pm$  one standard deviation), i.e. the coefficient of variation was 10%.

It is interesting to note that the variance of the breach volume data is smaller than that of the breach widths. A more detailed examination of the data in Fig. 3 reveals a small but consistent reduction in the non-dimensional breach width as the cross-sectional area of the barrier increased. The breach volumes are derived from the product of breach width and barrier cross-sectional area. Therefore, a larger area can compensate for a reduction in breach width to give the same breach volume. This explains the reduced scatter in the data for the non-dimensional breach volumes.

## 5. Comparison with Field Observations

A rigorous test of the simple scaling relationships suggested by the model breaching experiments requires data from a much broader range of scales than are possible with

laboratory experiments alone. The range of scales can be dramatically extended by comparing the model results with data from barrier breaching at full-scale estuaries or from earth dam failures. For the latter, length scales are typically two orders of magnitude larger than the model tests, and volumes are six orders of magnitude larger.

There are some significant differences between earth-fill dams and natural sand barriers that should be noted. For example:

- earth dams typically have a well-defined, regular cross-sectional geometry which is not the case for natural wave-built sand barriers
- earth dams are usually constructed with relatively well-graded sediments, whereas natural coastal sand barriers are uniformly graded due to the sorting action of waves. In some cases, earth dams incorporate cohesive sediments (e.g. in the form of clay core-walls) which are very different from the cohesionless sandy sediments of coastal barriers.
- earth dams typically have a well-defined foundation that is relatively impervious and immobile. Natural sand barriers are more variable and may be founded on additional sandy material that is both pervious and erodible.

Furthermore, the breaching of earth dams is often driven by large hydraulic gradients (due to narrow, high barriers), whereas for coastal breaching these gradients are typically smaller and can vary due to changes in tide and waves. The breaching of coastal barriers may also be affected by longshore and cross-shore sediment transport which are absent in the case of dam failures.<sup>c</sup>

Nevertheless, despite the above-mentioned differences, we suggest that the overall conceptual similarity between the breaching of coastal sand barriers and the failure of earth-fill dams, justifies a comparison between them in terms of the scaling results deduced here.

### **5.1. Breaching of natural coastal barriers**

Detailed observational data for breach characteristics at actual estuaries or coastal lagoons are rare and usually do not include sufficient information for a comparison with the present model experiments. However, four examples have been obtained and the relevant information is summarized in Table 2. The information for Mhlanga and Mdloti estuaries, situated adjacent to each other on the East coast of South Africa, were obtained from a detailed study reported by Perissinotto *et al.* [2004], Stretch and Zietsmann [2004], and Zietsman [2003]. The breaching of the Wamberal Lagoon situated in South Eastern Australia, is reported by Odd *et al.* [1995]. The last example, reported by Kraus *et al.* [2002], consists of post-breach observations made at Stone Lagoon, in Northern California. Note that the data in Table 2 are

---

<sup>c</sup>We are indebted to Nicholas Kraus for pointing out these issues.

Table 2. Breach parameters for natural lagoons &amp; estuaries.

Name	Area (ha)	Storage (Mm <sup>3</sup> )	$H$ (m)	Berm breadth (m)	Breach width (m)	Breach volume (m <sup>3</sup> )	$W/S^{1/3}$	$H/S^{1/3}$	$B/S^{1/3}$	$V_b/HBS^{1/3}$
Mhlanga	70	0.750	2.5	30	30	1400	0.33	0.028	0.33	0.171
Mdloti	80	0.900	2.5	40	30	1500	0.31	0.026	0.41	0.121
Stone	300	10.00	3.5	100	90	18000	0.42	0.016	0.46	0.209
Wamberai	50	1.375	2.8	70	50	5250	0.45	0.015	0.63	0.225

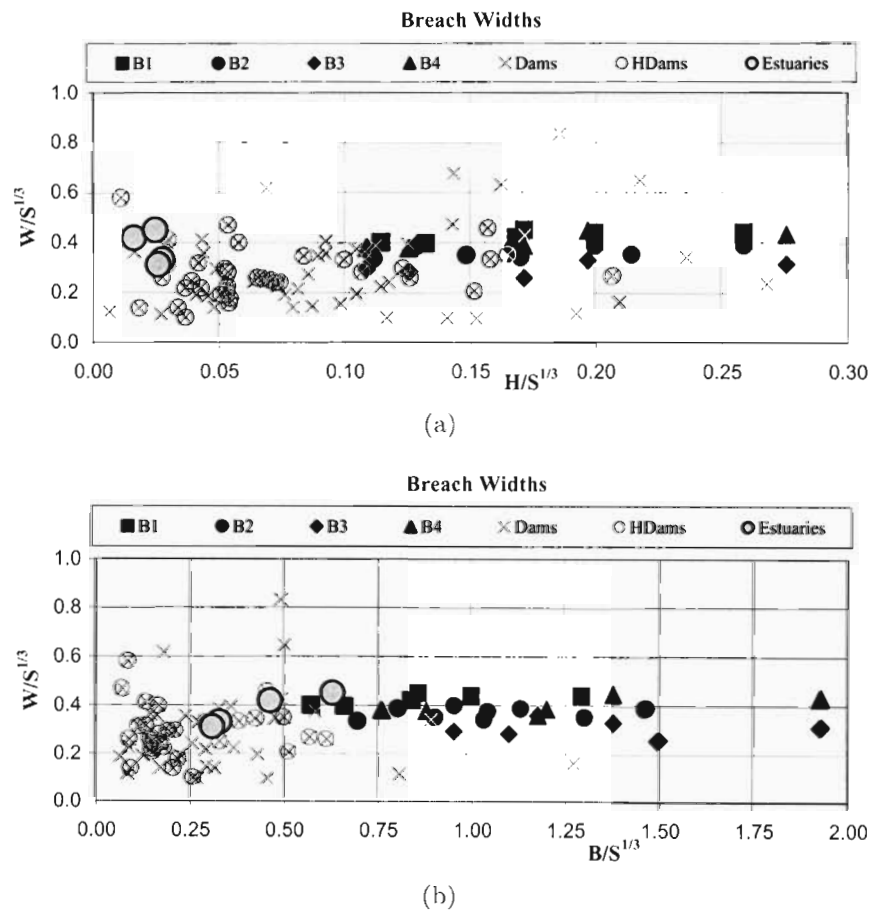


Fig. 5. Non-dimensional breach widths plotted against (a) the hydraulic head  $H$ , and (b) the barrier breadth  $B$ . Data from earth dam failures [Wahl, 1998] are plotted as crosses with homogeneous cases circled (denoted “HDams” in the legend). Data from actual estuaries are plotted as large filled circles. Data from the model experiments are shown as solid symbols (see also Fig. 3). The two dashed lines in (a) are the Froehlich equation (Eq. 4) for  $K_0 = 1.0, 1.4$ .

subject to considerable uncertainty since in some cases (e.g. areas and volumes) they were inferred from secondary information, such as maps and pictures.

The non-dimensional breach characteristics for these estuaries/lagoons are plotted in Figs. 5 and 6 for comparison with the model results. The data are remarkably

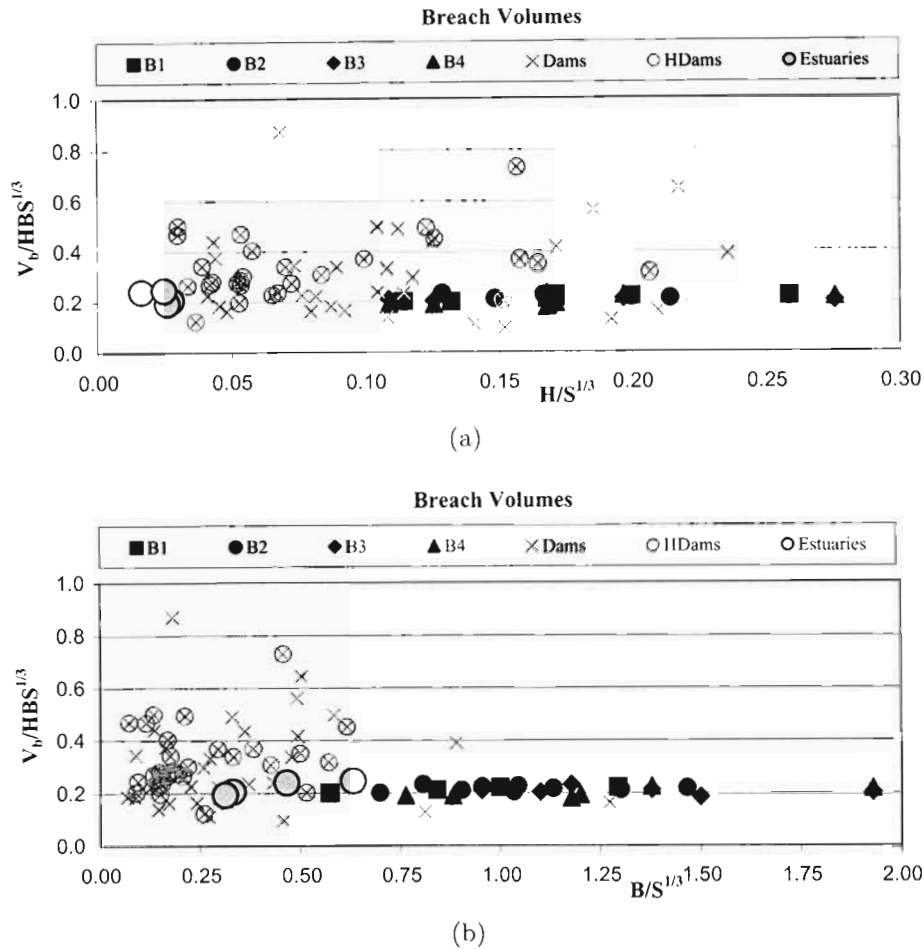


Fig. 6. Non-dimensional breach volumes plotted against (a) the hydraulic head  $H$ , and (b) the barrier breadth  $B$ . Data from earth dam failures [Wahl, 1998] are plotted as crosses with homogeneous cases circled (denoted “HDams” in the legend). Data from actual estuaries are plotted as large filled circles. Data from the model experiments are shown as solid symbols (see also Fig. 4).

consistent with the experimental results and provide strong support for the applicability of the scaling inferred from the model experiments.

It is perhaps easy to overlook the power of the scaling result illustrated in Figs. 5 and 6. Note that if the data for breach widths were re-plotted in dimensional form, the experimental results would be separated from the field data by about two orders of magnitude, while the data for breach volumes would be separated by about six orders of magnitude.

### 5.2. Earth dam failures

The Wahl [1998] compilation of breach data from earth dam failures is also shown plotted in non-dimensional form in Figs. 5 and 6. Dams that were classified as homogeneous earth fill are highlighted in the plot since they are more similar to the type of barriers that are the focus of this study.

There is considerable scatter in the dam-break data, especially if the non-homogeneous cases are included. However it is evident from Figs. 5 and 6 that the breach characteristics of the dams, when scaled as indicated, are generally consistent with the results of the model tests. In particular, there is no obvious variation in the non-dimensional breach widths and volumes with the hydraulic head  $H$  and barrier breadth  $B$ . The average non-dimensional breach width for all the dam failures is 0.31, but with a high coefficient of variation equal to 67%. The average value for the sub-set of homogeneous earth-fill cases is 0.28 with a much lower coefficient of variation equal to 36%.

Considering the differences noted previously, the degree of consistency is remarkable and strongly supports the supposition that the water volume flowing through the breach is the dominant factor that determines the breach size. Other factors such as sediment characteristics, hydraulic head, and barrier breadth appear to be relatively unimportant. The apparent insensitivity to sediment characteristics is particularly noteworthy.

Also shown in Fig. 5(a) is the Froehlich [1987] predictor equation for breach width, appropriately re-scaled into the form used for the present analysis (see Sec. 2). Froehlich obtained this equation from a regression analysis using a sub-set of the dam data shown in Fig. 5. The Froehlich regression equation is also broadly consistent with the model data (Fig. 5(a)). However, the weak dependence of the (non-dimensional) breach width on the hydraulic head that is implied by Froehlich's equation (Eq. (4)) is not clearly supported by the data. The simpler " $\frac{1}{3}$  - rule" with  $\phi \sim \text{constant}$  (Eq. 2) is an adequate description of the data.

It is worth noting that Froehlich [1995] re-visited his earlier analysis of dam break characteristics and proposed a modified regression equation, claiming an improved fit to the data. However, this modified equation is dimensional and does not give sensible results when extrapolated to different scales, such as predicting the results of our experiments.

### 5.3. *The effects of floods*

Overtopping failures of dams or natural coastal barriers are generally associated with floods. The flood-waters add to the volume of water that passes through the breach, and provided the time-scale of the flood inflows which is not long compared to the time to drain the storage volume, the effect of the flood would be equivalent to an enlarged impounded storage. This point was noted by Froehlich [1987] and used to explain the slightly higher  $K_0$  values obtained from the regression analysis for overtopping cases (refer Sec. 2). Therefore, to use the present scaling results to predict breach characteristics at estuaries during floods, allowance must be made for the additional inflow volumes. For large floods, these volumes can exceed the normal storage capacity of a lagoon or estuary by many times over.



An interesting example is a large flood that occurred in the region of the Mdloti/Mhlanga catchments in 1987, with estimated return period of 100 years. Approximately 1000 mm of rain fell over a three-day period. The Mhloti catchment size is about 500 km<sup>2</sup>. With an estimated average run-off coefficient of say 0.6,<sup>d</sup> this translates into a runoff volume of order 300 million cubic metres, or about 300 times the storage capacity of the lagoon. Using the  $\frac{1}{3}$  – rule with this volume suggests a breach width exceeding 200 m. Archival pictures taken just after the flood confirm that the actual breach was in fact of this order.

## 6. Conclusions

The breaching of sand barriers at perched TOCEs plays a key role in the functioning of these systems. The aim of the research presented here was to investigate the scaling of breach characteristics for management applications.

The results of our small-scale lab experiments suggest the remarkably simple scaling that the breach width is approximately proportional to the cube root of the volume that flows out through the breach — i.e.  $W \simeq C_W S^{\frac{1}{3}}$ . Corresponding breach volumes therefore scale like  $V_b \simeq C_V (H.B.S^{\frac{1}{3}})$ . The model experiments and data from full-scale estuaries suggests  $C_W \simeq \frac{1}{3}$  and  $C_V \simeq \frac{1}{5}$ , but these values may vary slightly depending on how breach widths and volumes are defined and measured.

The scaling results from the model experiments have been verified by comparison with breach data from actual estuaries and from earth-dam failures. The comparison covers more than two orders of magnitude in length scales and six orders of magnitude in storage volumes. The results are remarkably good given the uncertainties in the field data, and differences in sediment characteristics. Based on the results in Figs. 5 and 6, the scaling appears to be applicable to barrier breadths in the range  $0.1 < B/S^{\frac{1}{3}} < 2.0$  and hydraulic heads in the range  $0.01 < H/S^{\frac{1}{3}} < 0.3$ . We also expect that it will apply only to barriers comprising cohesionless sediments. However, it is worth noting that the dam failure database includes barriers with a variety of sediment combinations e.g. some of the non-homogeneous cases had core-walls comprising cohesive, clay-type sediments.

To further illustrate the application of the scaling results presented here, all the breach width data are re-plotted in dimensional form in Fig. 7, where they are compared with the simple “ $\frac{1}{3}$  – rule” suggested by our analysis. The extrapolating power of the basic scaling result is evident in this plot, and should provide a useful predictive tool that can be incorporated into models for the mouth dynamics of perched temporary open/closed estuaries or coastal lagoons.

The breaching process involves a complex interaction between unsteady, non-uniform hydraulics and sediment transport. Nevertheless, the observation that the

---

<sup>d</sup>A high runoff coefficient is justified here because of the rare combination of long duration and intense rainfall that resulted in a very saturated catchment!

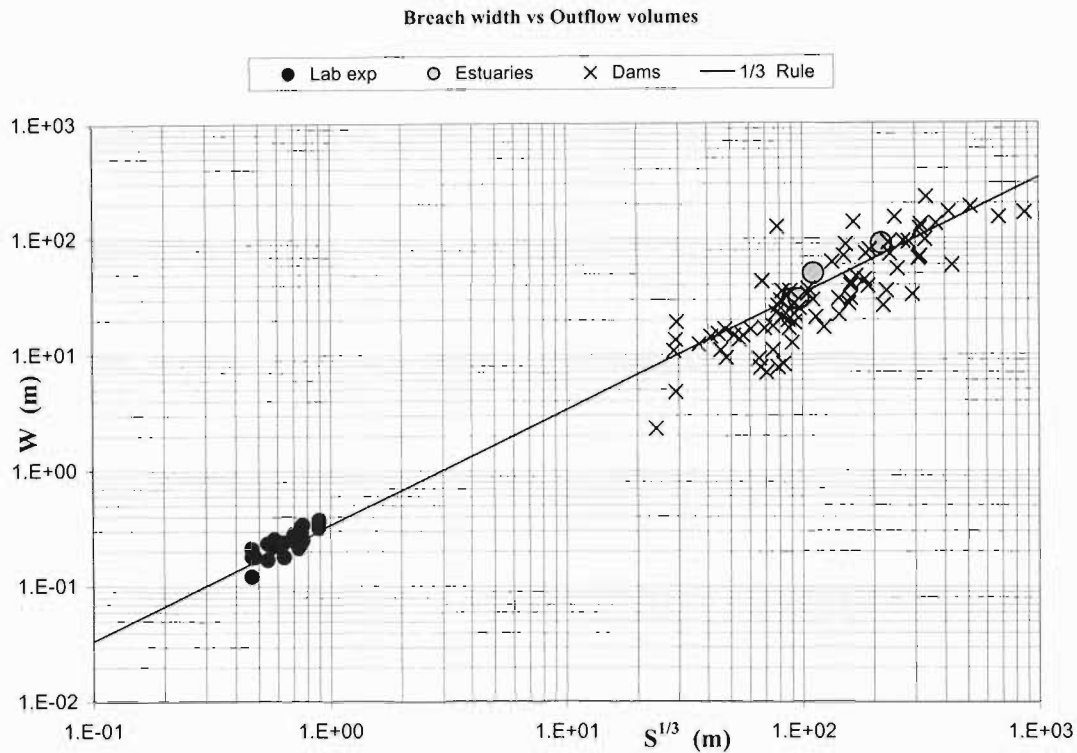


Fig. 7. Breach widths plotted in dimensional form against the cube-root of the estimated outflow volumes. Earth dam failures [Wahl, 1998] are plotted as crosses, actual estuary breaches as large grey circles, and the model experiments as small solid circles. The line is Eq. (2) with  $C_W = \frac{1}{3}$ .

final breach size scales only on the total outflow volume, suggests that there may be a simple physical explanation. One way to investigate this would be to test whether existing breaching models [e.g. Visser, 1988; 1994; 2000] can reproduce the scaling results presented here. Since these models include representations of the physical processes, they may help to explain the scaling.

Finally, we note that the link between breach size and outflow volume is similar to the well-known link between the cross-sectional area of a tidal inlet and its tidal prism [O'Brien, 1931; Jarrett, 1976]. We plan to investigate this further by studying the temporal development of the breach and the characteristics of the outflow hydrograph.

### Acknowledgments

Many helpful discussions with Dr. Cristina Trois are gratefully acknowledged. We are also grateful to Dr. Nicholas Kraus and Dr. Paul Visser for providing copies of their publications on this topic, and for helpful comments on the manuscript. HR Wallingford kindly provided a copy of the paper by Odd *et al.* [1995] on the Wanberal Lagoon in Australia. Funding for MGP was provided by CRECHE and the National Research Foundation, and is gratefully acknowledged.

## Appendix A

Table A.1. Summary of experimental results.

Berm #	$H$ (m)	$B$ (m)	$S_0$ (m <sup>3</sup> )	$S$ (m <sup>3</sup> )	$W$ (m)	$V_b$ (m <sup>3</sup> )	$W/S^{1/3}$	$H/S^{1/3}$	$B/S^{1/3}$	$V_b/(HBS^{1/3})$
B1	0.15	0.75	0.24	0.20	0.26	0.0143	0.44	0.26	1.29	0.22
			0.49	0.43	0.33	0.0186	0.44	0.20	1.00	0.22
			0.80	0.71	0.38	0.0211	0.42	0.17	0.84	0.21
	0.08	0.40	0.41	0.34	0.28	0.0045	0.40	0.11	0.57	0.20
			0.29	0.22	0.24	0.0038	0.40	0.13	0.66	0.20
			0.15	0.10	0.21	0.0034	0.45	0.17	0.86	0.22
B2	0.15	0.85	0.24	0.20	0.23	0.0160	0.39	0.26	1.46	0.22
			0.50	0.43	0.29	0.0207	0.39	0.20	1.13	0.22
			0.80	0.71	0.36	0.0253	0.40	0.17	0.95	0.22
	0.08	0.50	0.44	0.37	0.24	0.0058	0.33	0.11	0.70	0.20
			0.31	0.24	0.24	0.0058	0.39	0.13	0.80	0.23
			0.15	0.11	0.18	0.0043	0.38	0.17	1.04	0.23
B3	0.15	1.05	0.24	0.16	0.17	0.0172	0.31	0.28	1.93	0.20
			0.56	0.44	0.25	0.0253	0.33	0.20	1.38	0.21
			0.83	0.71	0.32	0.0324	0.36	0.17	1.18	0.23
	0.08	0.70	0.47	0.40	0.22	0.0086	0.29	0.11	0.95	0.21
			0.33	0.26	0.18	0.0072	0.28	0.13	1.10	0.20
			0.16	0.10	0.12	0.0048	0.26	0.17	1.50	0.18
B4	0.15	1.05	0.24	0.16	0.24	0.0185	0.43	0.28	1.93	0.22
			0.56	0.44	0.34	0.0268	0.45	0.20	1.38	0.22
			0.83	0.71	0.32	0.0252	0.36	0.17	1.18	0.18
	0.08	0.56	0.44	0.40	0.28	0.0063	0.38	0.11	0.76	0.19
			0.29	0.26	0.24	0.0054	0.38	0.13	0.88	0.19
			0.15	0.10	0.18	0.0040	0.39	0.17	1.20	0.19

## References

- Coleman, S. E., Andrews, D. P. & Webby, M. G. [2002] "Overtopping breaching of noncohesive homogeneous embankments," *J. Hydraulic Engineering* **128**(9), 829-838.
- Froehlich, D. C. [1987] "Embankment-dam breach parameters," in *Proc. ASCE Conference on Hydraulic Engineering*, Williamsburg, Virginia, August 3-7, 1987, pp. 570-575.
- Froehlich, D. C. [1995] "Embankment dam breach parameters revisited," in *Proc. ASCE Conference on Water Resources Engineering*, San Antonio, Texas, August 14-18, 1995, pp. 887-891.
- Jarrett, J. T. [1976] Tidal prism-inlet area relationships. GITI Report 3, US Army Corps of Engineers, Waterways Experiment Station, Vicksburg, Miss, 32pp.
- Kraus, N. C., Militello, A. & Todoroff, G. [2002] "Barrier breaching processes and barrier spit breach," Stone Lagoon, California, *Shore & Beach*, **70**(4), 21-28.

- Kraus, N. C. & Wamsley, T. V. [2003] Coastal barrier breaching, part 1: Overview of breaching process, Technical Notes ERDC/CHL CHETN-IV-56, US Army Corps of Engineers.
- Kraus, N. C. [2003] "Analytical model of incipient breaching of coastal barriers," *Coastal Engineering J.* **45**(4), 511–531.
- O'Brien, M. P. [1969] "Equilibrium flow areas of inlets on sandy coasts," *J. Waterways. & Harbors, Proc. Am. Soc. Civ. Eng.* **95**, 43–52.
- Odd, N. V. M., Roberts, W. & Maddocks, J. [1995] "Simulation of Lagoon Breakout," HYDRA 2000, in *Proc. 26th Congress of the Int. Assoc. for Hydraulic Research*, Vol. 3, pp. 92–97.
- Perissinotto, R., Stretch, D., Forbes, A., Connell, A., Blair, A., Demetriades, N., Kibirige, I., Zietsman, I., Twala, X., Thomas, C., Iyer, K., Simpson, H. & Joubert, M. [2004] "Responses of the biological communities to flow variation and mouth state in two KwaZulu-Natal temporary open/closed estuaries," Water Research Commission Project K5/1247 — Final Report.
- Ranasinghe, R., Pattiaratchi, C. & Masselink, G. [1999] "A morphodynamic model to simulate the seasonal closure of tidal inlets," *Coastal Engineering* **37**, 1–36.
- Ranasinghe, R. & Pattiaratchi, C. [2003] "The seasonal closure of tidal inlets: Causes and effects," *Coastal Engineering Journal* **45**(4), 601–627.
- Stretch, D. D. & Zietsman, I. [2004] The hydrodynamics of Mhlanga and Mdloti estuaries: Flows, residence times, water levels & mouth dynamics, Water Research Commission Project K5/1247 -- Final Report (Hydrodynamics).
- Visser, P. J. [1988] "A model for breach growth in a dike-burst," in *Proc. 21st Coastal Eng. Conf., ASCE*, pp. 1897–1910.
- Visser, P. J., Vrijling, J. K. & Verhagen, H. J. [1990] "A field experiment on breach growth in sand-dikes," in *Proc. 22nd Coastal Eng. Conf., ASCE*, pp. 2087–2100.
- Visser, P. J. [1994] "A model for breach growth in sand-dikes," in *Proc. 24th Coastal Eng. Conf., ASCE*, pp. 2755–2769.
- Visser, P. J., Kraak, A. W., Bakker, W. T., Smit, M. J., Wino Snip, D., Steetzel, H. J. & vd. Graaf, J. [1995] "A large-scale experiment on breaching in sand-dikes," in *Proc. ASCE Conf. Coastal Dynamics*, Gdansk, Poland, pp. 583–594.
- Visser, P. J. [1998] "Breach erosion of sand dikes," in *Proc. 26th Coastal Eng. Conf., ASCE*, pp. 3516–3528.
- Visser, P. J. [2000] "A Model for breach erosion in sand-dikes," in *Proc. 27th Int. Conf. Coastal Eng.*, Sydney, Australia, pp. 3829–3843.
- Wahl, T. L. [1998] Prediction of embankment dam breach parameters — A literature review and needs assessment, US Bureau of Reclamation, Dam Safety Report DSO-98-004, Denver, CO.
- Wahl, T. L. [2004] "Uncertainty of predictions of embankment dam breach parameters," *J. Hydraulic Engineering* **130**(5), 389–397.
- Zietsman, I. [2003] *The Hydrodynamics of Temporary Open Estuaries with Case Studies of Mhlanga and Mdloti*, MScEng dissertation, School of Civil Engineering, University of Natal, Durban, South Africa.

Coastal Engineering Journal  
 © World Scientific Publishing Company and Japan Society of Civil Engineers

## BREACHING TIMESCALES AND PEAK OUTFLOWS FOR PERCHED, TEMPORARY OPEN ESTUARIES

MICHAEL PARKINSON and DEREK STRETCH

*Centre for Research in Environmental, Coastal & Hydrological Engineering  
 School of Civil Engineering, University of KwaZulu-Natal,  
 Durban, KwaZulu-Natal, 4041, South Africa  
 stretchd@ukzn.ac.za ; parkinsonm@ukzn.ac.za  
 http://www.ukzn.ac.za/*

Received (Day Month Year)

Revised (Day Month Year)

Intermittent breaching of sand barriers at temporary open estuaries plays a key role in the functioning of these systems. In addition to their ecological impacts, breaching events can cause significant morphological changes because high breach outflows result in the scouring of significant amounts of accumulated sediments from an estuary. Estimation and modeling of these processes requires insight into the parameters that determine features of the breach such as its size and the timescales for the breach formation. The latter is particularly important for characterizing the outflow hydrograph and for estimating sediment transport effects. Simple laboratory experiments are reported that investigated the temporal evolution of the breach and the scaling of the breach formation time  $T_F$  and peak outflow  $Q_P$ . The experiments were specifically designed to investigate the influence of the outflow volume  $S$ , the hydraulic head  $H$ , and the barrier breadth  $B$ . A scaling is suggested that gives a good description of the experimental data. The scaling is shown to be consistent with observed breach characteristics for actual estuaries (or coastal lagoons) and earth-dam failures where outflow volumes are several orders of magnitude larger than for the models.

*Keywords:* Breaching; sand-barriers; estuaries; coastal lagoons; timescales; peak outflows.

### 1. Introduction

Temporary open/closed estuaries (TOCEs) have unstable inlets due to a combination of small tidal prism, energetic wave climate, and low or intermittent river inflows. In South Africa about 70% of the  $\pm 300$  estuaries are TOCEs with most of them located on the eastern seaboard [Cooper, 2001]. Similar systems are also found in Australia, on the west coast of the USA, South America, India, Sri Lanka and Japan [Ranasinghe *et al.*, 1999; Ranasinghe and Pattiaratchi, 2003; Kraus and Walmsley, 2003].

Perched estuaries have water levels above mean sea level (MSL) and tend to occur on coastlines with steep, reflective beaches where high wave run-up gives rise to sand barriers that are two or more meters above high tide levels. Breaching of

these barriers is a common natural occurrence and can be triggered by overtopping of the barrier or by seepage and liquefaction [Kraus *et al.*, 2002; Kraus and Walmsley, 2003; Kraus, 2003]. During breaching events there is generally a rapid "flushing" of the estuary. This may cause significant morphological changes due to the scouring associated with high peak outflows. It is important to quantify these effects in order to understand the long-term impacts that changes in breaching patterns can have on the system. Breaching also causes large and rapid changes to the estuarine habitat since perched estuaries essentially empty when they breach. Breaching events therefore play an important role in the biological functioning of perched TOCEs.

It is common practice to artificially breach closed estuaries to prevent flooding of adjacent farm-land or to flush out contaminants or sediments. In some cases, artificial breaching is used to mitigate the effects of reduced river inflows caused by the building of dams or other abstraction schemes [Huizinga, 1995; Van Niekerk *et al.*, 2005]. Reduced inflows increase the closed periods of TOCEs and artificial breaching can mitigate negative impacts and help to maintain their ecological functioning. The optimal timing and consequences of these management interventions requires an understanding of breaching and re-closure processes.

Stretch and Parkinson [2006] reported results from model studies to investigate breach size i.e. the final width and volume of the breach. They found that the final breach size is mainly determined by the volume of water that flows through the breach. In this paper we expand on those results by investigating the temporal development and peak outflow of the breach. In particular we focus on breach formation times and outflow hydrographs due to their importance in sediment dynamics.



Fig. 1. Photograph showing a breach of the sand-bar at the Mhlanga estuary, a small perched estuary on the East coast of South Africa.

Coleman *et al.* [2002] reported a model study of sand embankment breaching with constant upstream water levels. Some qualitative features of the initial breach

development are applicable to the problem addressed here. However the present experiments focus on the development of equilibrium breach characteristics from finite volume releases where upstream water levels fall as the reservoir empties. This case was not addressed in the Coleman *et al.* [2002] experiments where no equilibrium state was reached, so a direct quantitative comparison is not possible.

The overall objective of this study is to develop a better understanding of the mouth dynamics of temporary open/closed estuaries. This understanding should lead to improved models for decision support in the management of estuaries.

To establish the generality of results deduced from model experiments, comparisons with full-scale breaching events are necessary. There are few detailed observations of actual estuary breaching events reported in the literature. For this study, data was obtained for several natural breaches of the Mhlanga estuary, a small, perched, temporary open estuary on the east coast of South Africa [Perissinotto *et al.*, 2004; Zietsman, 2003]. The aftermath of a typical breaching event at the Mhlanga estuary is shown in Fig. 1. Observations from artificial breaching of the Bot estuary, a larger South African coastal lagoon [Van Niekerk *et al.*, 2005], and the Wamberal lagoon, situated on the south-east coast of Australia [Odd *et al.*, 1995], are also compared with our results.

Estuary breaching is conceptually similar to the failure of earth-fill dams and dikes. Due to the potentially catastrophic effects of such failures, significant research effort has been invested in their analysis [Wahl, 1998; Visser *et al.*, 1990; Visser *et al.*, 1995; Visser, 1998]. Models to estimate the breach formation time and peak outflow for these situations therefore already exist. Some of these models, and the data on which they are based, are later reviewed and compared with results from our study.

In section 2 a simple scaling analysis is outlined and several existing predictor models are reviewed. In section 3 our experiments are described, followed by a presentation of the results in section 4. In section 4.3 the experimental results are compared with field observations of breaching at full-scale estuaries, lagoons and earth-fill dams in order to test the generality of the scaling results.

## 2. Scaling analysis

### 2.1. Definitions

Consider the simplified model of a perched estuary, depicted schematically in Fig. 2. Suppose that  $S$  is the total volume of water that flows out of the impoundment during a breaching event. The water level at inception of breaching  $H$ , is assumed to be measured relative to a datum that represents the minimum water level behind the barrier after breaching i.e.  $H$  is the total water level change during a breach. In the case of fully perched estuaries this datum is above the average water level downstream of the barrier (mean sea level or MSL) and the estuary essentially empties during a breach. We focus on breaching events driven by overtopping of the barrier so that  $H$  also represents the height of the barrier relative to the datum.

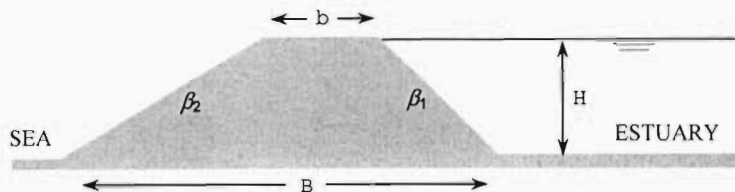


Fig. 2. Schematic of a perched, closed estuary separated from the sea by a sand barrier.

The breaching process comprises two main phases - a breach *initiation* phase followed by a breach *formation* phase [Wahl, 1998; Visser, 1998]. During the initiation phase, the overtopping flow gradually scours a channel on the downstream face of the barrier while the upstream crest remains relatively intact. Upstream water levels do not change significantly during this phase. Once the upstream crest of the barrier starts to erode significantly, it signals the start of the breach formation phase. Outflow and erosion rates increase rapidly during this phase. The upstream face is where the hydraulic control for the overtopping flow is located [Coleman *et al.*, 2002]. As the breach widens and deepens, the outflow through the breach channel increases and the water level in the impoundment drops. The falling hydraulic head causes the velocity of the water in the breach channel to decrease. The rate of erosion in the channel also therefore decreases and the breach approaches a maximum width. When the breach attains its maximum width the breach formation phase ends. Therefore the breach formation time,  $T_F$  may be defined as:

*The time between initial breaching of the upstream face of the barrier until the breach is fully formed.*

The breach formation time has been defined in various ways by different investigators but, as noted by Wahl [1998], they all essentially refer to the formation phase as described above.

In practice, accurately recording the temporal development of a breach is difficult to achieve due to the short timescales involved and to uncertainties in distinguishing the beginning and end of the breach formation phase. An alternative approach that is operationally simpler to implement, is to monitor the water levels in the estuary or lagoon. This information can be then used to infer an outflow hydrograph and a characteristic timescale for the water level variations. In section 4.2 we use our model experiments to investigate the relationship between the timescales for breach formation and those for water level variations behind the barrier.



## 2.2. Scaling Analysis

Following the analysis of Stretch and Parkinson [2006], we suppose that the dominant parameters that control a breach event are the outflow volume  $S$ , the hydraulic head  $H$ , and the breadth of the barrier  $B$  (refer Fig. 2). The flow is driven by gravity with  $g$  denoting the body force per unit mass. Using the volume  $S$  to define a reference length scale  $S^{1/3}$ , our supposition suggests that the breach formation time  $T_F$  can be related to  $H$  and  $B$  in non-dimensional form as

$$T_F/T = \phi\left(H/S^{1/3}, B/S^{1/3}\right), \quad (1)$$

where  $T$  is a timescale formed from the parameters  $g$ ,  $S$ ,  $H$  and  $B$ , and with  $\phi(\cdot)$  an unknown function (to be determined empirically). If we assume that it is possible to find a representation of  $T$  in terms of these four parameters that gives  $\phi \simeq \text{constant}$ , then dimensional homogeneity requires that the timescale  $T$  is expressible as a power law of the form

$$T \sim (g/S^{1/3})^{-1/2} (H/S^{1/3})^\alpha (B/S^{1/3})^\gamma, \quad (2)$$

with

$$T_F = C_T T, \quad (3)$$

where  $C_T$  is the value of the (assumed constant) function  $\phi$ .

Our primary objective is to predict the characteristics of the outflow hydrograph during a breaching event, particularly its duration and peak outflow. If the above suppositions are reasonable, the duration of the outflow hydrograph should also scale like Eq. (2). Therefore a scale for the outflows is  $Q \sim S/T$  and it follows from Eq. (2) that

$$Q \sim (gS^{5/3})^{1/2} (H/S^{1/3})^{-\alpha} (B/S^{1/3})^{-\gamma}. \quad (4)$$

The peak outflows  $Q_P$  can then be scaled as

$$Q_P = C_Q Q. \quad (5)$$

where  $C_Q$  is a constant scaling coefficient.

Testing the above suppositions requires seeking values for the exponents  $\alpha$  and  $\gamma$  that yield a satisfactory combined scaling for  $T_F$  and  $Q_P$  in the form of Eqs. (3) and (5). Of course the generality of this scaling depends on whether the assumptions concerning the parameters that determine  $T_F$  and  $Q_P$  are valid or not. In particular, we note that the properties of the sediment are ignored in the above analysis.

## 2.3. Regression models based on analysis of earth-dam failures

There are a number of existing models for earth dam failures that are based on regression analyses of historical dam break data. Some of these regression relationships are dimensionally non-homogeneous and their application outside the specific

parameter ranges for which they were derived does not give sensible results. Wahl [2004] reviews the performances of existing models in predicting  $T_F$  and  $Q_P$  and concludes that Froehlich's [1995a] regression equation for  $T_F$  and Froehlich's [1995b] regression equation for  $Q_P$  provide the best overall accuracy.

Froehlich [1995a] proposed the regression equation

$$T_F = 0.00254 S^{0.53} H^{-0.90}, \quad (6)$$

relating the breach formation time  $T_F$  (hrs) to the outflow volume  $S$  ( $m^3$ ) and hydraulic head  $H$  (m). If the exponents for  $S$  and  $H$  in Eq. 6 are rounded to 0.5 and  $-1.0$  respectively, and the parameter  $g$  is assumed to be incorporated into the numerical coefficient, then it may be re-written in the form of Eq. (3) as

$$T_F \sim (g/S^{1/3})^{-1/2} (H/S^{1/3})^{-1}, \quad (7)$$

which corresponds to  $\alpha = -1$  and  $\gamma = 0$  in Eq. (2).

In an earlier paper Froehlich [1987] proposed a dimensionally homogeneous regression equation for  $T_F$  which can be expressed in the form of Eq. (3) as

$$T_F = 79 (g/S^{1/3})^{-1/2} (H/S^{1/3})^{-0.9} \quad (8)$$

which corresponds to  $\alpha = -0.9$  and  $\gamma = 0$  in Eq. (2). Comparing Eqs. (7) and (8) it is apparent that both Froehlich models suggest a similar scaling for  $T_F$ . Note that they imply that  $T_F$  is approximately independent of the barrier breadth  $B$ .

Froehlich [1995b] proposed a regression equation for the peak outflow as

$$Q_P = 0.607 S^{0.295} H^{1.24}, \quad (9)$$

where  $Q_P$  is in  $m^3s^{-1}$  and  $S$  and  $H$  are in meters. Using the same data, Webby [1996] suggested an alternative regression equation for the peak outflow

$$Q_P = 0.0443 (g S^{5/3})^{1/2} (H/S^{1/3})^{1.4}, \quad (10)$$

which corresponds to  $\alpha = -1.4$  and  $\gamma = 0$  in Eq. (4). Comparing Eqs. (9) and (10) it is evident that the value of the exponent for  $H$  is similar. Webby noted that Eq. (10) yielded a slightly lower coefficient of determination than Eq. (9), but has the desirable feature of dimensional homogeneity. Both results suggest that the peak outflows are *independent* of the barrier breadth  $B$ .

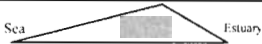
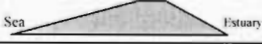
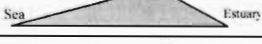
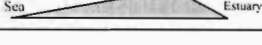
The above-mentioned analyses of Froehlich and Webby support the supposition in section 2.2 regarding the parameterization of the scales  $T$  and  $Q$ . Furthermore they suggest values  $-1.4 \lesssim \alpha \lesssim -0.9$  and  $\gamma \simeq 0$  for the exponents in Eqs. (2) and (4). The scaling of  $T_F$  and  $Q_P$ , and in particular the appropriate values for  $\alpha$  and  $\gamma$ , are explored further in section 4.3 using the results from the present model experiments and observations from actual full-scale breaching events.

### 3. Laboratory experiments

A series of laboratory model experiments was carried out to investigate the characteristics of the breaching process. The experiments are described in this section, and further details are given in Stretch and Parkinson [2006] and Parkinson [2007].

A model estuary basin was constructed with a rectangular shape, two meters wide and four meters long. Three sides of the basin comprised 0.2m high concrete-block walls, while a sand barrier was built across the remaining side. Initial storage volumes were systematically varied by positioning the barrier at nominal distances of one, two and three meters from the opposing wall of the model estuary. The barriers were built with two heights and various cross-sectional shapes : Table 1 lists values for the main experimental parameters including impounded volumes  $S_0$ , height of the barriers  $H_0$ , and geometric parameters of the sand barriers ( $b$ ,  $B$ ,  $\beta_1$  and  $\beta_2$  : refer Fig. 2). A total of twenty-four experiments were performed - further details of each experiment are tabulated in Stretch and Parkinson [2006].

Table 1. Experimental parameters

Berm	Slopes		b (m)	B (m)	$H_0$ (m)	$S_0$ (m <sup>3</sup> )	Barrier Shape (Schematic only)
	$\beta_1$	$\beta_2$					
B1	2	3	0	0.40	0.08	0.15 - 0.45	
				0.75	0.15	0.30 - 0.90	
B2	2	3	0.1	0.50	0.08	0.15 - 0.45	
				0.85	0.15	0.30 - 0.90	
B3	2	3	0.3	0.70	0.08	0.15 - 0.45	
				1.05	0.18	0.30 - 0.90	
B4	2	5	0	0.56	0.08	0.15 - 0.45	
				1.05	0.15	0.30 - 0.90	

The breaching experiments were performed by filling the impounded storage volume with water to the top of the barrier and initiating a breach through a pilot channel across the center of the barrier. The pilot channel was V-shaped and approximately one centimeter deep.

A video camera placed upstream of the barrier was used to record the development of the breach and the change in water levels for each experiment. Video frames were extracted at regular time intervals for detailed temporal analysis. Water levels and breach widths were scaled off the video frames at each time interval by counting pixels and using reference scales in the field of view. Outflow volumes were calculated by multiplying the water level changes by the impoundment surface area during each time interval.

The post-processing of the video recordings yielded time-histories for the breach widths  $w(t)$ , water levels  $h(t)$ , and outflow volumes  $s(t)$  for each breaching experiment. These data were normalized using the final values of the breach width ( $W$ ), total water level change ( $H$ ), and total outflow volume ( $S$ ) respectively. The time sequences of normalized data were then fitted with parametric sigmoidal curves us-

ing nonlinear least squares optimization. Several sigmoidal curves were tested for their efficacy in describing the temporal developments, including Gaussian, Gamma and Log-Normal functions. The corrected Akaike information criterion [Hurvich and Tsai, 1989] was used as a metric to evaluate the most efficient curve-fit to the data. The Log-Normal sigmoid was generally found to be the most efficient and was therefore used for all the results presented herein.

Outflow hydrographs for the experiments were inferred by differentiating the sigmoidal curves fitted to the outflow volumes with respect to time. The peak outflows  $Q_P$  were extracted from these outflow hydrographs.

Breach formation times  $T_F$  were inferred from the characteristics of the sigmoidal curves fitted to the breach width data: details are given in section 4.2.

#### 4. Results and discussion

In section 4.1 we discuss detailed qualitative observations made of the breaching process using a representative sample from our model experiments for illustrative purposes. In section 4.2 we present the main quantitative results characterizing the breach development. Finally in section 4.3 we use the data from the model experiments and from field observations to investigate the scaling of breach formation times and peak outflows.

##### 4.1. Qualitative features of the breach process

Fig. 3 shows the normalized breach widths, water levels and outflow volumes for one of the breaching experiments (barrier  $B2$ ,  $H_0 = 0.15\text{m}$ ,  $S_0 = 0.9\text{m}^3$ : see Table 1). The normalized outflow hydrograph is also shown in Fig. 3.

It can be seen that the temporal evolution of the breach width, water level, and outflow volume all have a sigmoidal shape although they exhibit temporal asymmetry in which the most rapid changes occur during the initial phases of their development. The growth in the breach width is the most rapid, reaching about 70% of its final value while the water levels and outflow volumes are still within 30% of their initial values. The outflow hydrograph shows that the peak flow occurs during the final stages of the breach development where the breach width already exceeds about 80% of its final value.

Fig. 4 gives a corresponding visual record of the same experiment. Figs. 4 (a) and (b) show the breach in its *initiation phase*. The overflow is gradually scouring a channel into the downstream face of the barrier while the upstream crest remains intact. This phase corresponds to times  $t \approx 70\text{s}$  in Fig. 3 where it is evident that the outflows are low and that water levels have not yet changed significantly.

Fig. 4 (c) shows the breach near the start of its *formation phase*. The upstream crest of the breach channel has begun to erode and the rate of widening and deepening of the channel has increased. This corresponds to time  $t \approx 80\text{s}$  in Fig. 3 where it is evident that the flow rate and the rate of widening of the breach channel has

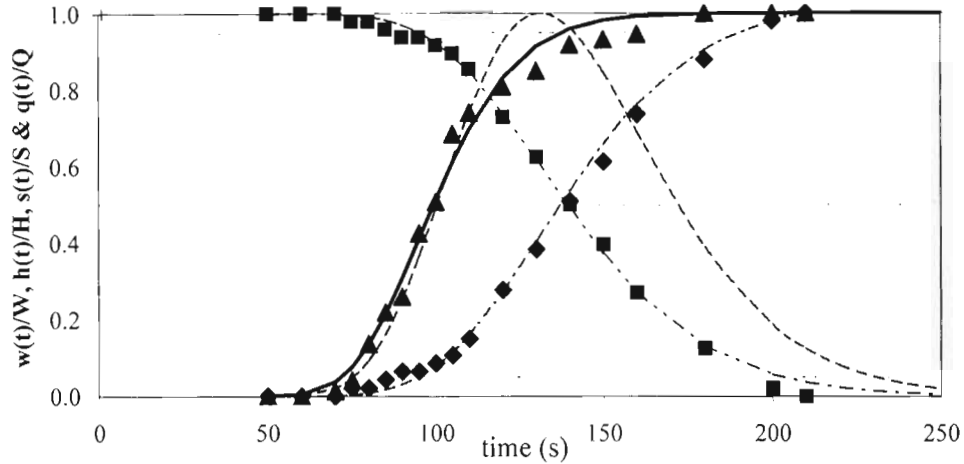


Fig. 3. Time history of the non-dimensional breach width (▲), water level (■), and outflow volume (◆) for model B2,  $H_0 = 0.15\text{m}$ ,  $S_0 = 0.9\text{m}^3$ . Fitted Log-Normal sigmoidal curves are also shown in each case, together with the inferred outflow hydrograph (dashed line). The 5<sup>th</sup>, 50<sup>th</sup> and 95<sup>th</sup> percentile levels are shown as horizontal dashed lines for reference.

started to suddenly increase. The additional volume of water entering the channel increases the rate of scour causing it to widen and deepen, allowing even more water into the breach. This cycle causes the rapid widening of the breach channel that is evident in Fig. 3 for times  $80 \leq t \leq 130\text{s}$ , which corresponds to Fig. 4 (d), (e), (f).

As the water level in the storage basin drops, the reduced hydraulic head causes the velocity of the flow through the breach channel to decrease. This in turn reduces the rate of scour. In Fig. 3 the rate of widening of the breach channel begins to decrease at  $t \approx 110\text{s}$ . Once the breach attains its maximum width the breach formation phase ends. In Fig. 3 this occurs at  $t \approx 150\text{s}$  which corresponds to the state shown in Fig. 4 (g). Therefore, the time period from  $t \approx 80\text{s}$  to  $t \approx 150\text{s}$  (i.e. an elapsed time of 70s) is the estimated breach formation time for this experiment. From Fig. 3 it can be seen that about 30% of the outflow volume occurs after the breach has attained its maximum width. The timescale for the water level variations is therefore significantly longer than that for the breach width development. Furthermore, while the outflow persists, a small amount of sediment may continue to be scoured from the base of the breach channel, but this is difficult to quantify from the video records.

#### 4.2. Quantitative features of the breaching process

As noted in section 3, the Log-Normal (LN) sigmoid was found to provide an efficient fit to the breach width and water level data. It captures the temporal asymmetry that is evident from the example shown in Fig. 3. The fitted LN functions can be

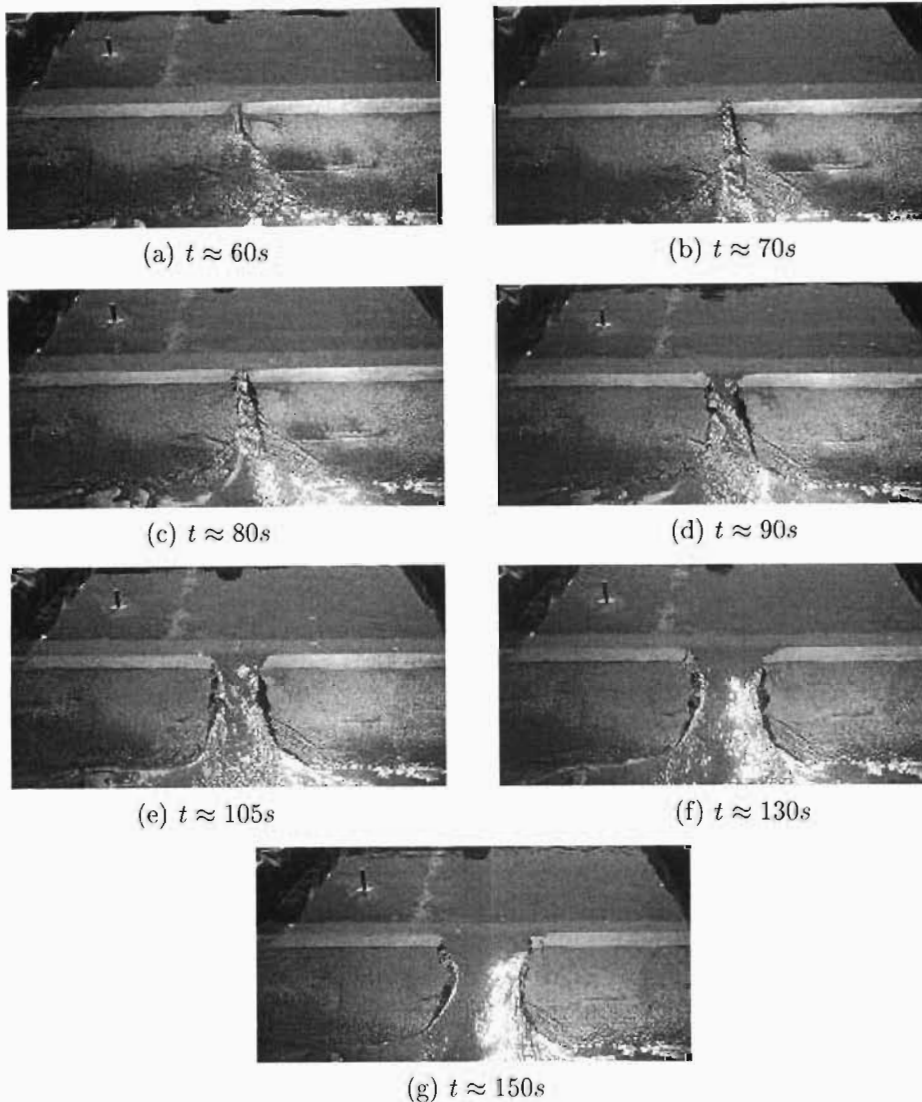


Fig. 4. Photo sequence of a breaching experiment (berm B2,  $H_0 = 0.15\text{m}$ ,  $S_0 = 0.9\text{m}^3$ ). The berm is in the foreground with the rectangular storage basin behind. The approximate times corresponding to Fig. 3 are shown below each photo

characterized by two parameters : one that fixes the position on the time axis and the other that describes the duration (or temporal width). We selected the 50<sup>th</sup>-percentile (or median) time  $T_{50_w}$  as a convenient position reference. Analysis of the video sequences for the breach width development (as in section 4.1) indicated that the difference between the 5<sup>th</sup>-percentile time  $T_{05_w}$  and the 95<sup>th</sup>-percentile time  $T_{95_w}$

corresponded closely to subjective visual estimates of the breach formation time. Therefore we define  $T_F = (T_{95_w} - T_{05_w})$  as our estimate of the breach formation time. The percentiles were estimated from least-squares fitting of the sigmoidal curves to each sequence of breach width measurements. This definition implies that  $T_F$  is the time required for 90% of the breach widening to occur.

The procedure of fitting a sigmoidal function to the data provides a more objective and robust estimate of  $T_F$  than is possible using visual estimates, since the latter requires subjective judgements for the start and end of the breach formation phase. The end of the breach formation phase is particularly difficult to judge because of the asymptotic nature of the breach width development as it approaches its final state.

Fig. 5 shows all the breach width measurements plotted in non-dimensional form. The self-similar nature of the breach width development is evident by the collapse of all the data onto a single curve, despite variations in the shape of the barriers (refer Table 1) and total outflow volumes.

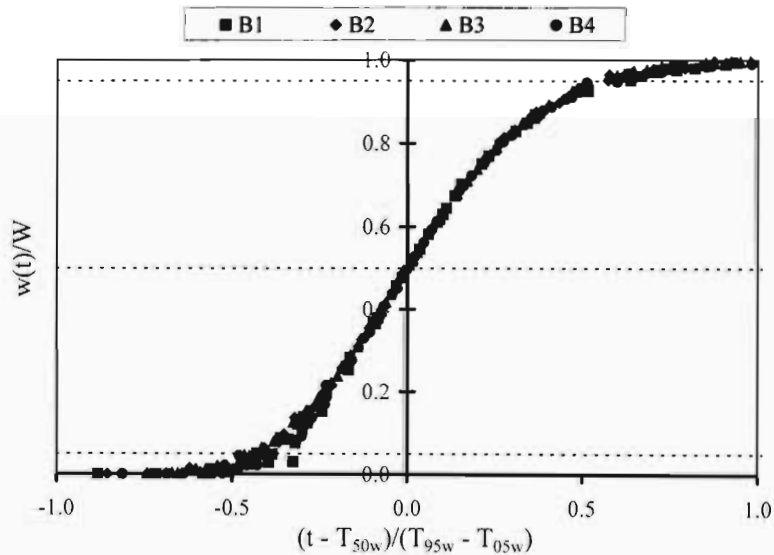


Fig. 5. Breach width measurements presented in non-dimensional form: breach widths are normalized by the final breach width, and time is normalized by the breach formation timescale  $T_F = (T_{95_w} - T_{05_w})$  with the median time  $T_{50_w}$  as the time origin. Symbols refer to different barrier shapes as indicated in Table 1.

Reference times and durations were similarly obtained from sigmoidal curves fitted to the measurements of water levels and outflow volumes. Outflow hydrographs (and peak outflows) were then inferred by differentiating these sigmoidal curves

with respect to time. This procedure reduced the noise inherent in attempting to numerically differentiate discrete-time raw data. Fig. 6 shows all the water level and outflow measurements plotted in non-dimensional form. Note that the hydrographs exhibit a temporal asymmetry with the peak outflows occurring before the median reference times.

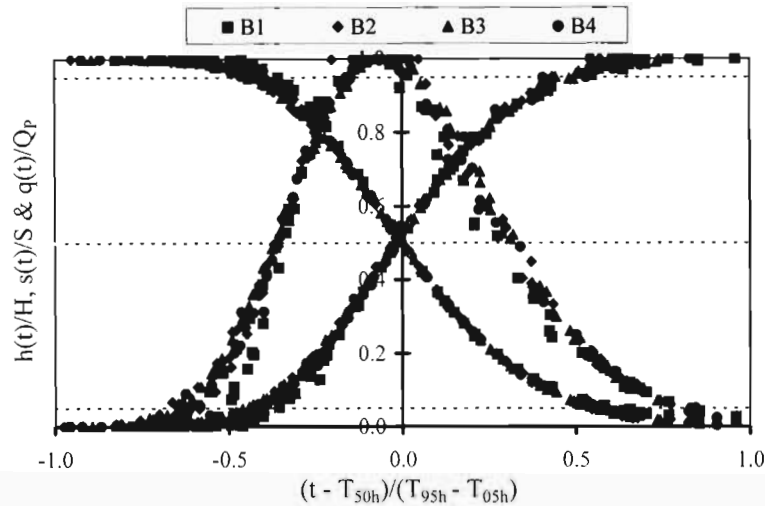


Fig. 6. Combined measurements of water levels and outflow volumes plotted in non-dimensional form. The outflow hydrographs are also shown, normalised by the peak outflows  $Q_P$ . Time is normalized by the duration of the water level changes (between 5<sup>th</sup> and 95<sup>th</sup>-percentiles) with the 50<sup>th</sup>-percentile as the time origin.

A composite plot, representing an average of all the experimental data, is shown in Fig. 7 where the temporal relationships between different characteristics of the breaching event can be clearly seen. The median time for the breach width development is used as the time origin in the plot, while the breach formation time  $T_F$  is used as the reference time scale. The data points (shown previously in Figs. 5 and 6) have been omitted for clarity. Fig. 7 summarizes the main features of the breach development, notably

- the temporal asymmetry in the breach development;
- the shorter timescale for breach width changes compared to that for the water level (or outflow volume) changes e.g. breach widths reach 70% of their final values while water levels are still within 30% of their initial values. The duration of the water level changes (between 5<sup>th</sup> and 95<sup>th</sup> percentiles) is on average about 50% longer than that for the breach widths ( $T_F$ );
- the temporal lag between changes in the breach width and the water lev-



- els/outflow volumes e.g. the 50<sup>th</sup>-percentile for the water level changes occurs on average about  $\frac{1}{2} T_F$  after that for the breach widths;
- the peak outflow occurs late in the development of the breach width i.e. when it is within about 20% of its final equilibrium value;
  - a significant proportion of the outflow (about 30%) occurs after the breach width has essentially reached its final equilibrium value.

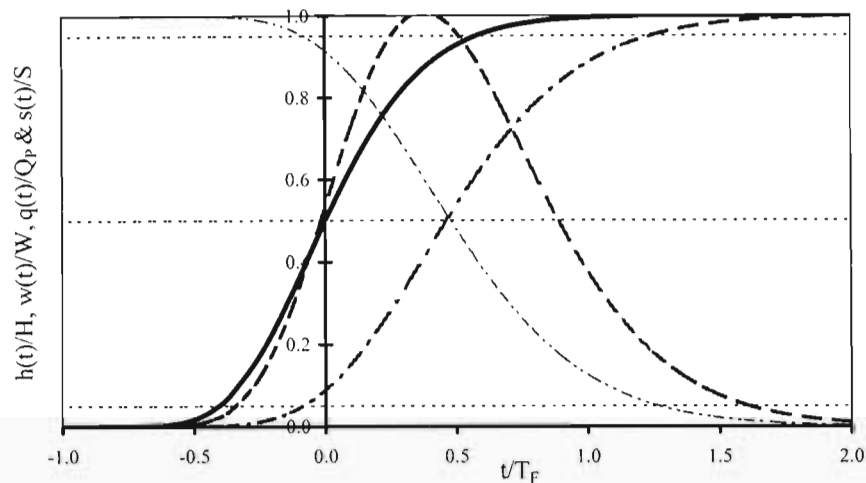


Fig. 7. A non-dimensional composite plot constructed from averaging the time-histories of the breach widths (heavy solid line), outflow volumes (dash-dotted line), water levels (dash-dot-dot line), and outflow hydrographs (dashed line). The 5<sup>th</sup>, 50<sup>th</sup> and 95<sup>th</sup> percentile levels are shown as horizontal dashed lines for reference.

The temporal relationships between changes in breach widths, water levels, and outflow volumes may be expected to vary with the morphology of the impounded storage volume. In our model experiments, the storage volume is nearly linearly related to the water depth. This may not be representative of natural estuaries and lagoons implying that some of these results may have limited generality.

Stretch and Parkinson [2006] found that the final width of the breach channel was proportional to the cube-root of the outflow volume, a relationship termed the “ $\frac{1}{3}$ -rule”. This result raises an interesting question : does the  $\frac{1}{3}$ -rule apply at intermediate times during the development of the breach? In other words, is the breach width at intermediate times in “equilibrium” with the outflow volume that has passed through the breach up to that time?

Fig. 8 shows a normalized plot of the breach widths versus the outflow volumes. It can be seen that the breach width is not consistent with the  $\frac{1}{3}$ -rule at intermediate times, but is generally greater than predicted by this scaling. From Fig. 8 it is

apparent that the breach width develops in an exponential manner and approaches its final value asymptotically. This observation is consistent with the notion that the scouring of the breach channel depends on exceeding a critical velocity (or shear stress). Flow velocities in the breach channel depend on the available hydraulic head which is greatest at inception of the breach formation. In the later stages of the breach formation, when water levels have reduced, the velocities in the breach channel are too low to sustain high scour rates.

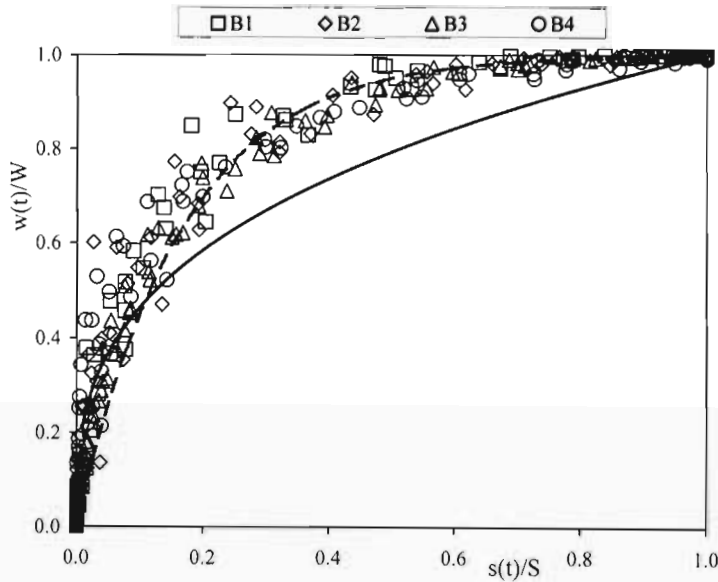


Fig. 8. The non-dimensional breach width plotted against the non-dimensional outflow volume. The solid line represents a  $\frac{1}{3}$  power law while the dashed line is Eq. 11 with  $k = 6$

As shown in Fig. 8, the data can be described by an exponential curve

$$w(t)/W = \left(1 - \exp^{-k \cdot s(t)/S}\right), \quad (11)$$

with  $k \simeq 6$ . This is a solution to the differential equation

$$dw/ds = k (W/S) (1 - w/W). \quad (12)$$

Using the relationship  $ds = q(t) dt$  it follows that

$$dw/dt = k (q(t)W/S) (1 - w/W), \quad (13)$$

which has a similar form to the model suggested by Kraus [2003] for breach growth in coastal barriers.

### 4.3. Scaling of the breach formation times and peak outflows

#### 4.3.1. Preliminaries

In this section the measurements of breach formation times and peak outflows are used to test the scaling analysis presented in section 2.2. Recall that Eqs. (3) and (5) suggest that the non-dimensional breach formation times  $T_F/T$  and peak outflows  $Q_P/Q$  may be constant under certain assumptions. The time and flow scales,  $T$  and  $Q$ , are given by Eqs. (2) and (4) where the appropriate exponents  $\alpha$  and  $\gamma$  are selected so that both  $T_F/T$  and  $Q_P/Q$  are approximately independent of  $H$  and  $B$  i.e. that  $\phi \simeq \text{constant}$  in Eq. (1). As noted in section 2.3, previous work on dam failures has suggested that  $\alpha \simeq -1$  and  $\gamma \simeq 0$ , which provides a starting point for our analysis. Those results were based on regression analyses, but for a scaling analysis to have some generality, it should have a physical justification.

A simple physical argument for scaling the peak outflows follows by analogy with the hydraulics of broad-crested weirs [Coleman *et al.*, 2002]. From Fig. 7 it is evident that the peak outflow occurs when the breach is nearly fully formed i.e. when the width  $\simeq W$ , and that the available hydraulic head remains approximately equal to  $H$  at that time. Whence, using the weir analogy

$$Q = C_D \sqrt{gH} WH \quad (14)$$

where  $C_D$  is a discharge coefficient. Furthermore, using the relationship  $W \sim S^{1/3}$  [Stretch and Parkinson, 2006] it follows from Eq. 14 that

$$Q \sim (g S^{5/3})^{1/2} (H/S^{1/3})^{3/2} \quad (15)$$

which is consistent with  $\alpha = -\frac{3}{2}$  in Eq. (4).

The influence of the barrier breadth  $B$  on  $T_F$  and  $Q_P$  may also be deduced from a simple physical argument. For a given  $H$  and  $S$ , the volume of sediment removed during the breach increases in direct proportion to the barrier breadth [Stretch and Parkinson, 2006]. It is therefore reasonable to expect that  $T_F \sim B$ , and since the duration of the outflow hydrograph should be similarly affected it follows that  $Q_P \sim B^{-1}$ . This argument suggests  $\gamma = 1$  in Eqs. (2) and (4).

#### 4.3.2. Field observations of large scale breaching events

In the context of the present study, the generality of any scaling result deduced from the small scale model experiments must be tested by extrapolating and comparing the predictions with data from field observations of breaching events where time and volume scales are typically several orders of magnitude greater.

Natural estuary breaching events are irregular occurrences and data pertaining to these events are rare. However, during a recent field study of the Mhlanga estuary on the east coast of South Africa [Zietsman, 2003; Perissinotto *et al.*, 2004], several breaching events were captured by an automated water level monitor. To estimate a breach formation time for the Mhlanga estuary, the water level measurements were

fitted with Log-Normal sigmoidal curves to estimate the time between the 5<sup>th</sup> and 95<sup>th</sup> percentiles. The relationship shown in Fig. 7 between the time scale for water level variations and that for the breach formation, was then used to estimate  $T_F$  for the estuary. The procedure yielded  $T_F \simeq 1\frac{1}{2}$  hours while the estimated peak outflow was  $Q_P \simeq 210 \text{ m}^3/\text{s}$ .

The same procedure was applied to water level data from an artificial breach of the Wamberal lagoon [Odd *et al.*, 1995] and yielded estimates  $T_F \simeq 1\frac{3}{4}$  hours and peak outflow  $Q_P \simeq 111 \text{ m}^3/\text{s}$ . The outflow rates were also measured directly as part of the field study by timing floating debris over known distances. A peak outflow of  $105 \text{ m}^3/\text{s}$  was reported, which corroborates our estimate.

Van Niekerk *et al.*, [2005] recently reviewed historical breaching events at the Bot estuary on the east coast of South Africa. This is a large coastal lagoon with breach outflow volumes estimated from bathymetric surveys as  $30 \times 10^6 \text{ m}^3$  and peak outflow rates in the range 254 – 409  $\text{m}^3/\text{s}$ . Water level records during breaching events indicate  $T_F \simeq 20$  hours. The final breach width for this estuary was reported to be in the range 80 – 110m which agrees well with the “ $\frac{1}{3}$ -rule” [Stretch and Parkinson, 2006] that predicts  $W = \frac{1}{3} S^{1/3} = 104\text{m}$ .

Field observations from the breaching of earth-fill dams also provide a source of data for testing the scaling of the breach formation times and peak outflows. Wahl [1998] compiled a database of 108 dam failures. The dam failure data comes from a number of sources including those previously compiled by Froehlich [1987; 1995a; 1995b]. Only a subset of the data is useful to our study because the required information is missing in some cases. Furthermore, only failures involving homogeneous earth fill dams were considered since they are more similar to coastal sand barriers. Wahl [1998] cautions that some of the data is probably subject to large errors. Peak outflows were estimated by various methods, often at some distance downstream of the dam break. Breach formation times were usually obtained from eyewitness accounts after the dam break event and it is possible that the observers would not have been able to accurately discern the breach initiation phase from the formation phase. Despite these and other uncertainties, the successful utilization of this data for comparison with the model experiments by Stretch and Parkinson [2006], provided some confidence for their use in the present context.

The field data for the above-mentioned estuaries are summarized in Table 2, while Fig. 9 shows the range of (non-dimensional)  $H$  and  $B$  values that are represented in the combined data set from both model experiments and field observations. Note that in the case of artificial barriers, which generally have a consistent shape, there is a correlation between  $H$  and  $B$  that is evident in Fig. 9.

#### 4.3.3. *Scaling results*

Fig. 10 shows the scaling results for  $T_F$  and  $Q_P$  where the time and flow scales are obtained using exponents  $\alpha = -1$ ,  $\gamma = 0$  in Eqs. (2) and (4). This corre-

Table 2. Breach observations for estuaries

Estuary	Surface Area (ha)	S (m <sup>3</sup> )	H (m)	B (m)	W (m)	T <sub>F</sub> (hrs)	Q <sub>P</sub> (m <sup>3</sup> /s)
Mhlanga	80	750,000	2.5	30	30	1.5	210
Wamberal	50	1,375,000	2.8	70	50	1.8	105
Bot	1500	30,000,000	2.7	190	95	20	330

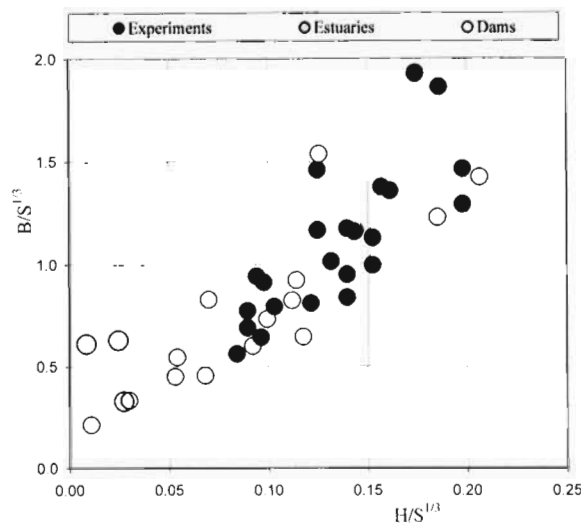


Fig. 9. The non-dimensional hydraulic head  $H$  and barrier breadth  $B$  for all the data used for the scaling analysis. Solid black symbols represent the present model experiments, large grey-filled circles are the estuaries listed in Table 2, and the open circles are from earth-fill dam failures.

sponds approximately to the scaling suggested by Froehlich and Webby (section 2.3). Fig. 11 shows the same data re-scaled using time and flow scales based on exponents  $\alpha = -\frac{3}{2}$ ,  $\gamma = 1$  in Eqs. (2) and (4). This corresponds to the scaling suggested by the physical argument in section 4.3.1. We have used  $HB/S^{2/3}$  as a convenient independent variable in Figs. 10 and 11 since it encapsulates variations in both the hydraulic head  $H$  and barrier breadth  $B$  (refer Fig. 9). Physically, it may be interpreted as a non-dimensional form of the barrier cross-sectional area.

The scaling results shown in Figs. 10 and 11 should be assessed against two criteria. Firstly, the data should not show any trends i.e. should plot along horizontal lines, indicating that the non-dimensionalised  $T_F$  and  $Q_P$  data are constant and independent of  $H$  and  $B$ . Secondly, the scaled  $T_F$  and  $Q_P$  data from the different sources i.e. model experiments and field observations, should collapse together when plotted in this form, even though they come from situations with time and flow scales

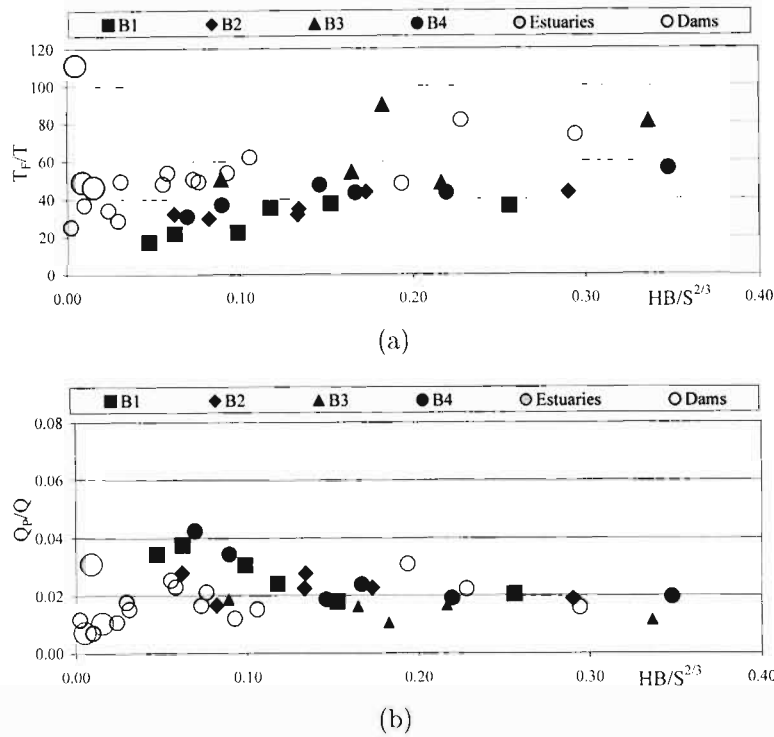


Fig. 10. Scaling results for the breach formation times (a) and peak outflows (b) using the scales given by Eqs. (2) and (4) with exponents  $\alpha = -1$ ,  $\gamma = 0$ .

that differ by several orders of magnitude.

Referring to Fig. 10 it can be seen that the scaling results using  $\alpha = -1$ ,  $\gamma = 0$  are unsatisfactory according to both the above-mentioned criteria. There are discernible trends in the data (particularly evident in the breach formation times), and the scaling is also not entirely effective in collapsing the measurements from the model experiments and field observations. Fig. 11 shows that the scaling results are significantly improved when the exponents are changed to  $\alpha = -\frac{3}{2}$ ,  $\gamma = 1$ , thereby introducing some dependence of the time and flow scales on the barrier breadth  $B$ . The trends are largely removed, while the model data and the estuary field observations are also collapsed to the same values. The  $T_F$  data from dam failures remain about 50% higher, although the trends that can be seen in Fig. 10 have been removed. Given the uncertainties in the field data (as discussed in section 4.3.2) the results of the scaling in this case are satisfactory.

Similar comparisons have been done for various  $\alpha$  and  $\gamma$  combinations in the ranges  $-2 \leq \alpha \leq 0$  and  $0 \leq \gamma \leq 2$ . Multi-variate linear regression analysis was used to objectively assess the trends in the scaled data by applying a statistical t-test to

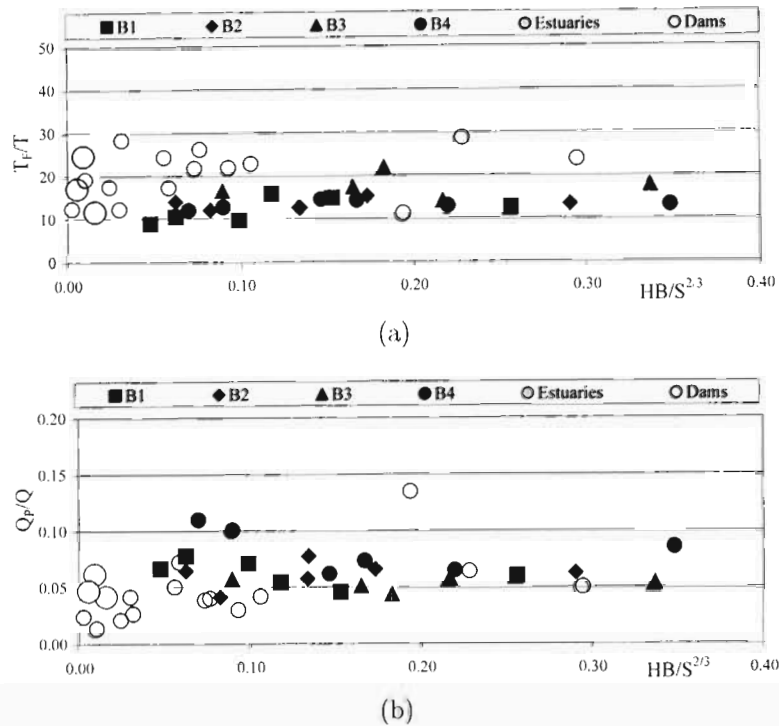


Fig. 11. Scaling results for the breach formation times (a) and peak outflows (b) using the scales given by Eqs. (2) and (4) with exponents  $\alpha = -\frac{3}{2}$ ,  $\gamma = 1$ .

indicate whether the regression coefficients for  $H$  and  $B$  were significantly different from zero at a 95% confidence level. The tests confirmed that the combination  $\alpha = -\frac{3}{2}$ ,  $\gamma = 1$  provides scaling results with no statistically significant trends, while other combinations (particularly where  $\gamma < 1$ ) do not. We note however that no attempt has been made to "fine-tune" the  $\alpha$  and  $\gamma$  parameters, since small changes to their values can be compensated for by changes to the scaling coefficients in Eqs. (3) and (5). Values for these scaling coefficients in the case of  $\alpha = -\frac{3}{2}$ ,  $\gamma = 1$  may be inferred from the data in Fig. 11 as  $C_T \approx 15 \pm 5$  and  $C_Q \approx 0.06 \pm 0.02$ .

The scaling results are further illustrated in Figs. 12 and 13 where all the measurements of breach formation times and peak outflows are plotted in dimensional form against the predicted values from Eqs. (3) and (5). It can be seen that the suggested scaling relationships are approximately valid over the full range of scales covered by the model experiments and field observations. Note that the measurements of  $T_F$  and  $Q_P$  were generally made independently of one another, so that the data provides two independent tests of the scaling.

In summary, the results presented in this section suggest that breach formation

times  $T_F$  and peak outflows  $Q_P$  can be scaled as suggested in section 2.2, and that values  $\alpha = -\frac{3}{2}$  and  $\gamma = 1$  provide good results which are consistent with simple physical arguments. The non-zero  $\gamma$  value indicates that a dependence on the barrier breadth  $B$  should be accounted for and gives improved results over previously suggested models [Froehlich, 1987; Froehlich, 1995a; Froehlich, 1995b; Webby, 1996].

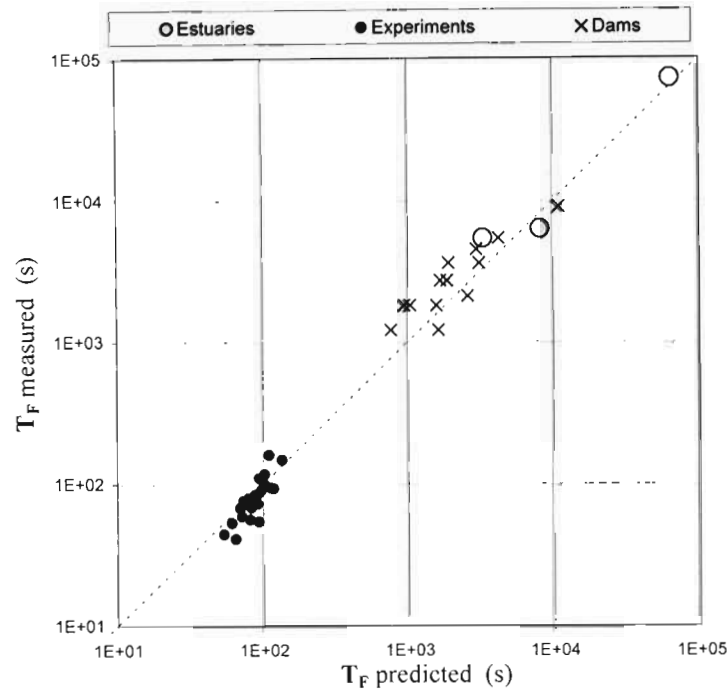


Fig. 12. Measured breach formation times  $T_F$  plotted against the predictions of Eq. 3 with  $C_T = 15$ , and with  $\alpha = -\frac{3}{2}$ ,  $\gamma = 1$  in Eq. 2. The dashed line indicates perfect agreement between measured and predicted values.

## 5. Conclusions

The breaching of sand barriers plays a key role in the functioning of temporary open/closed estuaries (TOCEs). The overall objective of this study was to gain a better understanding of the mouth dynamics of TOCEs for management applications. The focus was on temporal developments and peak outflows during a breach.

A key assumption of our analysis is that the properties of the sediment can be ignored. The results from our small scale lab experiments suggest that this assumption is reasonable, at least for cohesionless sediments, and that the properties of the



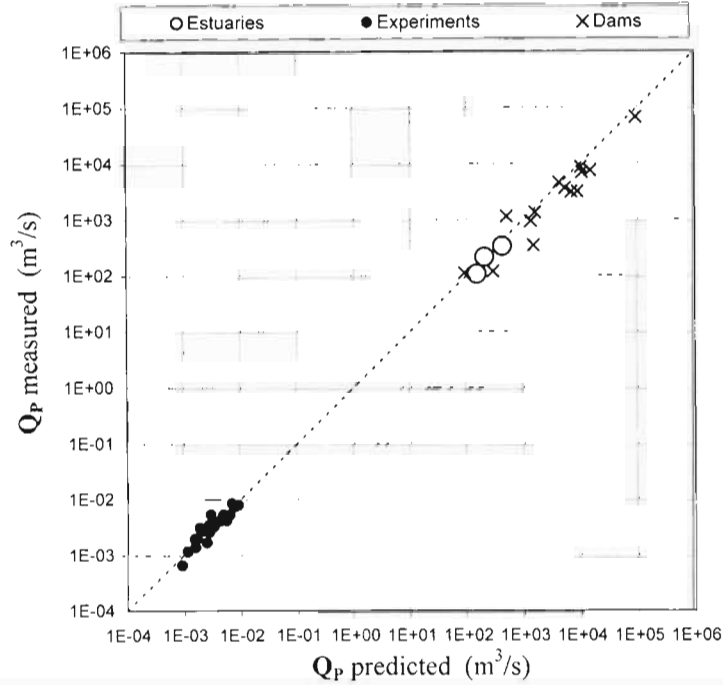


Fig. 13. Measured peak outflows  $Q_P$  plotted against the predictions of Eq. 5 with  $C_Q = 0.06$ , and with  $\alpha = -\frac{3}{2}$ ,  $\gamma = 1$  in Eq. 4. The dashed line indicates perfect agreement between measured and predicted values.

sediment do not play a significant role in the breach development and the associated outflow hydrograph. However the precise range of sediment characteristics for which this is applicable remains to be clarified by further research.

Our model experiments have provided new insights into the temporal features of breach development and associated water level and outflow variations. Key aspects of this include (1) the temporal asymmetry, (2) the shorter timescale for the breach width changes compared to the water levels (or outflows), and (3) the timing of the peak outflow near the end of the breach formation phase.

We have used our experiments to examine the scaling of breach formation times and peak outflows. Our results indicate that they scale like

$$T_F \simeq C_T (g/S^{1/3})^{-1/2} (H/S^{1/3})^{-3/2} (B/S^{1/3})^1$$

$$Q_P \simeq C_Q (g S^{5/3})^{1/2} (H/S^{1/3})^{3/2} (B/S^{1/3})^{-1}$$

with  $C_T \simeq 15 \pm 5$  and  $C_Q \simeq 0.06 \pm 0.02$ . Based on the data we have analysed these results are applicable to the breaching of cohesionless sand barriers with  $0.2 < B/S^{1/3} < 2.0$  and  $0.01 < H/S^{1/3} < 0.2$  (refer Fig. 9).

These results provide simple predictive tools that can be incorporated into models of the mouth dynamics of perched intermittently open estuaries for management applications. For example the artificial breaching of temporary open estuaries is a widely used management intervention, and a key issue regarding this practice concerns the effects that breaching events have on sedimentation [Schumann, 2003; Beck *et al.*, 2004]. The results we have presented here can be used to quantify sediment transport effects by providing a simple means to predict the outflow hydrograph and associated peak outflow. Furthermore our results concerning the scaling of the breach formation time can be used to determine the optimal timing and duration of an artificial breaching event e.g. with respect to tide state.

Breaching events can cause significant scouring of estuarine sediments. To illustrate this, consider the estimated peak outflow of  $210 \text{ m}^3/\text{s}$  for the Mhlanga estuary reported in section 4.3. The median (2 year return period) flood peak for this catchment has been estimated as  $36 \text{ m}^3/\text{s}$  [Jezewski *et al.*, 1986]. Assuming a Log-Normal probability distribution for annual flood peaks [Pegram, 1994], the peak outflow of  $210 \text{ m}^3/\text{s}$  corresponds approximately to that of a flood with a 25-year return period. This example indicates that breaching events (both natural or artificial) can severely impact the estuarine habitat. Historically, this particular estuary was closed for extended periods during dry seasons. However, more recently, discharges from upstream waste-water treatment facilities have significantly increased the dry-period flows into the estuary, which triggers quasi-periodic breaching every 30 to 40 days. The system is therefore currently experiencing a peak outflow comparable to that of a 25-year flood at regular and short intervals. The implications for the overall functioning of the system are severe [Perissinotto *et al.*, 2004].

A limitation of this study is that no measurements of the temporal evolution of the vertical depth profiles in the breach channel were made. Such measurements would require a different experimental technique e.g. adapting that used by Coleman *et al.* [2002]. Depth profiles would allow velocities and shear stresses in the breach channel to be estimated, giving further insights into sediment transport issues, and are therefore recommended for future research. Despite this limitation, our results concerning the outflow hydrographs and breach formation times should be useful for calibrating models that attempt to reproduce the complex mobile-bed hydraulics involved in the breaching process [e.g. Visser, 1988; 1994; 2000].

### Acknowledgements

We thank Dr Nicholas Kraus and Dr Paul Visser for providing copies of their publications on this topic. HR Wallingford kindly provided a copy of the paper by Odd *et al.*, [1995]. Financial support for MGP was provided by CRECHE and the National Research Foundation, and is gratefully acknowledged.

## References

- Beck, J.S., Theron A.T., Kemp, A. Huizinga, P. and Basson, G.R. : Hydraulics of estuarine sediment dynamics in South Africa. Water Research Commission, 1257/1/04, 2004.
- Coleman, S. E., Andrews, D. P. and Webby, M.G. (2002). Overtopping breaching of non-cohesive homogeneous embankments. *J. Hydraulic Engineering*, **128**(9): 829–838.
- Cooper, J. A. G.: Geomorphological variability among microtidal estuaries from the wave dominated South African coast. *Geomorphology*, **40**, 99–122, 2001.
- Froehlich, D. C. : Embankment-Dam Breach Parameters. Proc. ASCE Conference on Hydraulic Engineering, Williamsburg, Virginia, 570–575, 1987.
- Froehlich, D. C. : Embankment Dam Breach Parameters Revisited. Proc. ASCE Conference on Water Resources Engineering, San Antonio, Texas, 887–891, 1995a.
- Froehlich, D. C. : Peak Outflow from Breached Embankment Dam. *J. Water Resources Planning & Management*, **121** (1), 90–97, 1995b.
- Huizinga, P. : River basin management and estuarine needs: the Great Brak case study. *Water Sci. & Technology*, **32**(5-6), 87–93, 1995.
- Hurvich, C. M. and Tsai, C. : Regression and time series model selection in small samples. *Biometrika* **76** (2), 297–307, 1989.
- Jezewski, W.A., Pike, P.D. and Roberts, C.P.R. : Estuarine and lake freshwater requirements. Technical report TR 129, SA Dept. Water Affairs & Forestry, 1986.
- Kraus, N. C., Militello, A. and Todoroff, G. : Barrier breaching processes and barrier spit breach, Stone Lagoon, California. *Shore & Beach*, **70**(4), 21–28, 2002.
- Kraus, N. C. and Wamsley, T. V. : Coastal Barrier Breaching, Part 1: Overview of breaching process. Technical Note ERDC/CHL CHETN-IV-56, US Army Corps of Engineers, 2003.
- Kraus, N. C. : Analytical model of incipient breaching of coastal barriers. *Coastal Engineering J.*, **45**(4), 511–531, 2003.
- Odd, N. V. M., Roberts, W. and Maddocks, J. : Simulation of Lagoon Breakout. HYDRA 2000 - Proc. 26<sup>th</sup> Congress Int. Assoc. for Hydraulic Research, 3, 92–97, 1995.
- Parkinson, M.G. : The Breaching of Temporary Open/Closed Estuaries. MScEng dissertation, School of Civil Engineering, University of KwaZulu-Natal, South Africa, 2007.
- Pegram, G.G.S. : Hydrological Estimates - Guidelines for the hydraulic design and maintenance of river crossings: TRH25, Committee of State Road Authorities (CSRA), South Africa, 1994.
- Perissinotto, R., Stretch, D., Forbes, A., Connell, A., Blair, A., Demetriades, N., Kibirige, I., Zietsman, I., Twala, X., Thomas, C., Iyer, K., Simpson, H., and Joubert, M. : Responses of the biological communities to flow variation and mouth state in two KwaZulu-Natal temporary open/closed estuaries. Water Research Commission - Final Report 1247/2/04, 2004.
- Ranasinghe, R., Pattiaratchi, C. and Masselink, G. : A morphodynamic model to simulate the seasonal closure of tidal inlets. *Coastal Engineering*, **37**, 1–36, 1999.
- Ranasinghe, R. and Pattiaratchi, C. : The seasonal closure of tidal inlets: causes and effects. *Coastal Engineering Journal*, **45**(4), 601–627, 2003.
- Schumann, E.H. (ed) : Towards the management of marine sedimentation in South African estuaries with special reference to the Eastern Cape. Water Research Commission, 1109/1/03, 2003.
- Stretch, D.D. and Parkinson, M.G. : The Breaching Of Sand Barriers at Perched, Temporary Open/Closed Estuaries - A Model Study. *Coastal Engineering J.*, **48**(1), 13–30, 2006.
- Van Niekerk, L., van der Merwe, J. H. and Huizinga, P. : The hydrodynamics of the Bot River Estuary revisited. *Water SA*, **31**(1), 73–85, 2005.
- Visser, P. J. (1988). A model for breach growth in a dike-burst. Proc. 21st Coastal Eng. Conf., ASCE: 1897–1910.
- Visser, P. J., Vrijling, J. K. and Verhagen, H. J. : A field experiment on breach growth in sand-dikes. Proc. 22<sup>nd</sup> ASCE Coastal Eng. Conf., 2087–2100, 1990.
- Visser, P. J. (1994). A model for breach growth in sand-dikes. Proc. 24th Coastal Eng. Conf., ASCE: 2755–2769.
- Visser, P. J., Kraak, A. W., Bakker, W. T., Smit, M. J., Wino Snip, D., Steetzel, H. J. and vd. Graaf, J. : A large-scale experiment on breaching in sand-dikes. Proc. ASCE Conf. Coastal

- Dynamics, Gdansk, Poland, 583-594, 1995.
- Visser, P. J. : Breach erosion of sand dikes, Proc. 26<sup>th</sup> ASCE Coastal Eng. Conf., 3516-3528, 1998.
- Visser, P. J. (2000). A Model for breach erosion in sand-dikes. Proc 27th Int Conf Coastal Eng, Sydney, Australia: 3829-3843.
- Wahl, T. L. : Prediction of Embankment Dam Breach Parameters - A Literature Review and Needs Assessment. USBR Dam Safety Report DSO-98-004, Denver, CO, 1998.
- Wahl, T. L. : Uncertainty of predictions of embankment dam breach parameters. J. Hydraulic Engineering, 130(5), 389-397, 2004.
- Webby, G. M. : discussion of Peak Outflow from Breached Embankment Dam (Froehlich, 1995a). Journal of Water Resources Planning and Management, 122(4), 316-317, 1996.
- Zietsman, I. : The Hydrodynamics of Temporary Open Estuaries with case studies of Mhlanga and Mdloti. MScEng dissertation, School of Civil Engineering, University of Natal, South Africa, 2003.